

5-2013

Accurate Hyperfine Coupling Calculations of Radiation Induced DNA Constituent Radicals Using Density Functional Theory.

Xiqiao Wang

East Tennessee State University

Follow this and additional works at: <https://dc.etsu.edu/honors>



Part of the [Astrophysics and Astronomy Commons](#)

Recommended Citation

Wang, Xiqiao, "Accurate Hyperfine Coupling Calculations of Radiation Induced DNA Constituent Radicals Using Density Functional Theory." (2013). *Undergraduate Honors Theses*. Paper 59. <https://dc.etsu.edu/honors/59>

This Honors Thesis - Open Access is brought to you for free and open access by the Student Works at Digital Commons @ East Tennessee State University. It has been accepted for inclusion in Undergraduate Honors Theses by an authorized administrator of Digital Commons @ East Tennessee State University. For more information, please contact digilib@etsu.edu.

**Accurate Hyperfine Coupling Calculations of Radiation Induced DNA
Constituent Radicals Using Density Functional Theory**

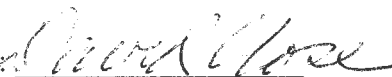
Thesis

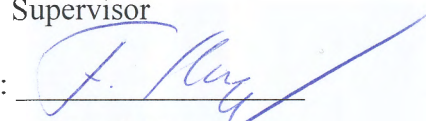
Presented in Partial Fulfillment of the Requirements for the Bachelor's Degree of Science
in the Honors College of East Tennessee State University


By

Xiqiao Wang

Department of Physics and Astronomy
East Tennessee State University
March 2013

Approved: 
Dr. David Close
Supervisor

Approved: 
Dr. Frank Hagelberg
Examiner

Approved: 
Dr. Scott Kirkby
Reader

Date: 3/29/2013

Copyright

by

Xiqiao Wang

2013

Acknowledgements

I would like to thank Dr. David Close for his mentoring in hyperfine coupling calculations and in experimental details of radiation induced DNA constituent radicals. I would also like to thank Dr. Frank Hagelberg for enlightening discussions on computational physics and *ab-initio* calculations. I greatly appreciate the continuous support of all the faculty and friends in the Department of Physics and Astronomy at East Tennessee State University for creating an enjoyable academic atmosphere.

Abstract

Previous density functional theory (DFT) calculations of hyperfine coupling constants (HFCC) on single nucleic acid base radicals agree well with the EPR/ENDOR experiments' values on radiation induced nucleic acid constituents radicals, except for four problem cases,¹ namely the N1-deprotonated cytosine cation radical, the native guanine cation radical, the N3-deprotonated 5'-dCMP cation radical and the N7-H, O6-H protonated 5'-GMP anion. The main effort of the present work is to address these four discrepancies by using the highly parameterized density functional M05/6-2X and by including the crystalline environment's H-bonding effects in the calculations. The geometries of the four model radicals are optimized within their single crystal environment using ONIOM technique. Then the spin density distributions and HFCCs of the radicals are examined within various scales of cluster models. The results obtained by including H-bonding environment are in strong agreement with the experimental values. The calculations show advantages of using the M05/62X functional rather than the B3LYP functional in obtaining more satisfactory HFCC results. However, the delocalization errors are encountered with both M05/6-2X and B3LYP functionals. Further development in eliminating delocalization errors in practical DFT approximations is suggested.

Contents

Acknowledgements.....	1
Abstract.....	2
Introduction and background	5
1.1. An Introduction to Kohn-Sham density functional theory.....	5
1.1.1. Hartree-Fock Theory.....	5
1.1.2. Hohenberg-Kohn theorems and Kohn-Sham equations.....	7
1.1.3. Basis set and exchange-correlation functional approximations.....	10
1.1.4. Delocalization error and static correlation error.....	12
1.2. An introduction to isotropic hyperfine coupling constant calculations.....	17
1.2.1. Isotropic Hyperfine coupling constant.....	17
1.2.2. Some considerations of Accurate Spin Density Calculations.....	19
2. An Introduction to the present work.....	21
2.1. Previous density functional theory calculations on hyperfine coupling constants.....	21
2.2. The four problematic cases in previous hyperfine coupling calculations using density functional theory.....	23
3. Methods.....	29
4. Results and Discussions.....	32
4.1. N1-deprotonated cytosine cation radical in cytosine monohydrate single crystal.....	32
4.2. Native guanine cation radical in Guanine Hydrochloride Monohydrate single crystal.....	57
4.2.1. HFCCs for Gm-Opt-1 Optimized Geometry.....	59
4.2.2. HFCCs for Gm-Opt-2 Optimized Geometry.....	65
4.3. N3-deprotonated 5'-dCMP cation radical in 5'-dGMP Monohydrate Single Crystal	87
4.3.1. H-bonds parameters in optimized geometries.....	88
4.3.2. Spin density and HFCC calculations.....	93
4.4. N7-H, O6-H protonated 5'-GMP anion in 5'-GMP single crystal	
5. Conclusions.....	115

6. References.....117

Introduction

The thesis is composed of five chapters. Chapter 1 briefly introduces the Kohn-Sham density functional theory (DFT), the delocalization error and static correlation error of DFT approximations, and the theoretical calculation of hyperfine coupling constants. Chapter 2 introduces the four problem cases of previous HFCC calculations. Chapter 3 describes the computational methods. Chapter 4 gives detailed results and discussions of the calculations. Chapter 5 summarizes the conclusions. Currently, the calculations on N7-H, O6-H protonated 5'-GMP anion are not included in this report due to the limitation of computational resources at this point.

Chapter 1 Introduction and Background

1.1. An Introduction to Kohn-Sham Density Functional Theory

Density functional theory (DFT) is an exact theory for electronic structures, which is an alternative to Wave Function Theory (WFT). The main charm of DFT in practice is that it incorporates correlation interactions, but still remains a favorable scaling factor with the size of the system. DFT has been widely used in materials science for decades and has thrived in quantum chemistry for the recent twenty years due to its improvements in functional approximations.

1.1.1. Hartree-Fock Theory

In order to understand the basics of density functional theory, one has to begin with understanding the Hartree-Fock (HF) theory, to which the Kohn-Sham density functional theory bears a striking resemblance when deriving the Kohn-Sham equations. Hartree-Fock theory works under the assumption that each electron may be described as being in a single electron orbital by treating its interactions with the other electrons as a mean potential field. In other words, the single electron's motion does not depend on the instantaneous motion of the other

electrons. HF theory is often a good starting point for more elaborate approximations in solving the electronic Schrödinger equation, like the Møller–Plesset perturbation theory and single-reference configuration interaction theory.

The antisymmetry principle states that a wave function describing multiple fermions must be antisymmetric with respect to the interchange of any set of space-spin coordinates. The Slater determinant, which is a determinant of spin orbitals, satisfies the antisymmetric constraint and is used to describe the system's wave function.

$$\Psi = |\phi_1\phi_2 \cdots \phi_N\rangle = \frac{1}{\sqrt{N!}} \begin{vmatrix} \phi_1(x_1) & \phi_2(x_1) & \cdots & \phi_N(x_1) \\ \phi_1(x_2) & \phi_2(x_2) & \cdots & \phi_N(x_2) \\ \vdots & \vdots & \ddots & \vdots \\ \phi_1(x_N) & \phi_2(x_N) & \cdots & \phi_N(x_N) \end{vmatrix}$$

Where x_i stands for the single-spin coordinate of the i 'th electron, and ϕ_i is the i 'th single electron spin orbital. The electrons are all indistinguishable here, and each electron is associated with every spin orbital. It turns out that the assumption that a wave function can be written in terms of a Slater determinant is equivalent to the assumption that each electron moves independently of the other electrons except that it feels the Coulomb repulsion due to the average position of all the other electrons. This also means that each electron under consideration does not interact with itself in HF theory. We should notice that the Hamiltonian of Hartree-Fock theory is the same with that of configuration interaction theory. It is the restriction of the wave function to a single Slater determinant that causes the averaging of inter-electron repulsions.

The Hamiltonian for a time-independent non-relativistic Schrödinger equation under the Born-Oppenheimer approximation can be written as

$$\hat{H} = \sum_i \hat{h}(\phi_i) + \sum_{i<j} \hat{v}(\phi_i, \phi_j) + V_{NN}$$

where the one-electron operator for an electron's kinetic energy and its potential energy within external potentials is defined as

$$\hat{h}(\phi_i) = -\frac{1}{2}\nabla_i^2 - \sum_A \frac{Z_A}{r_{iA}}$$

And the two-electron operator for electron-electron interaction is defined as

$$\hat{v}(\phi_i, \phi_j) = \frac{1}{r_{ij}}$$

Here V_{NN} is a constant for interactions among nuclei. It can be ignored since it does not change the eigenfunctions and only shifts the eigenvalues.

Under the assumption that a wave function can be approximated by a single Slater determinant, the energy of this system, Hartree-Fock energy, can be expressed as follows, where the wave function ϕ_i is denoted as i ,

$$E_{HF} = \langle \Psi | \hat{H} | \Psi \rangle = \sum_i \langle i | \hat{h} | i \rangle + \frac{1}{2} \sum_{ij} (\langle ii | \hat{h} | jj \rangle - \langle ij | \hat{h} | ji \rangle)$$

In this expression, the one-electron and two-electron operator integrals are denoted as

$$\langle i | \hat{h} | j \rangle = \int \phi_i^*(x_1) \hat{h}(x_1) \phi_j(x_1) dx_1$$

and

$$\langle ij | \hat{h} | kl \rangle = \int \phi_i^*(x_1) \phi_j^*(x_2) \frac{1}{r_{12}} \phi_k(x_1) \phi_l(x_2) dx_1 dx_2$$

The Variational Theorem states that the expectation value of the Hamiltonian, computed with any trial wave function, is always higher or equal than the energy of the ground state. By applying the Lagrange's method of undetermined multipliers, we can achieve the ground state wave function which minimize the Hartree-Fock energy. The Lagrange, which is a functional of all the single-electron spin orbitals, is defined as

$$\mathcal{L}[\{\phi_i\}] = E_{HF}[\{\phi_i\}] - \sum_{ij} \epsilon_{ij} (\langle i | j \rangle - \delta_{ij})$$

where ϵ_{ij} are the undetermined Lagrange multipliers and $\langle i | j \rangle$ is the overlap between spin orbitals i and j , i.e.,

$$\langle i | j \rangle = \int \phi_i^*(x) \phi_j(x) dx$$

By setting the first variation of the Lagrange to be zero, $\frac{\delta\mathcal{L}}{\delta\{\phi_i\}} = 0$, we arrive at the Hartree-Fock equations, which defines each spin orbital in the ground state wave function.

$$h(x_1)\phi_i(x_1) + \sum_{j \neq i} \left[\int dx_2 |\phi_j(x_2)|^2 r_{12}^{-1} \right] \phi_i(x_1) - \sum_{j \neq i} \left[\int dx_2 \phi_j^*(x_2) \phi_i(x_2) r_{12}^{-1} \right] \phi_j(x_1) = \epsilon_i \phi_i(x_1)$$

The Hartree-Fock equation can be solved numerically, where an educated initial guess for the spin orbitals is needed. Then the orbital guess is refined iteratively, and this is the reason why HF method is called a self-consistent field (SCF) approach. The second term on the left-hand side of the HF equation describes the Coulomb interaction between the electron within spin orbital ϕ_i and the mean distribution of the other electrons. The third term of the HF equation arises from the asymmetry requirement of the wave function, and it is called the *exchange term*.

1.1.2. The Hohenberg-Kohn Theorems and Kohn-Sham Equations

Density functional theory is made possible by the two Hohenberg-Kohn theorems proposed by Hohenberg and Kohn in 1964.

Theorem I

The external potential is a unique functional of the electron density.

Since the Hamiltonian of the Schrödinger equation is determined by the external potential and the number of electrons N , and N is the integration of electron density over all space, it immediately follows that the Hamiltonian is uniquely determined by the given density function. Thus the system over all spectrum (ground and excited state wave functions) can be derived, and hence all the properties of the system. However, the electron density cannot be uniquely determined by a given Hamiltonian.

Theorem II

A universal functional for the energy $E(\rho)$ can be defined in terms of the density. The exact ground state is the global minimum value of this functional.

From the second theorem, it can be seen that for any system of a given external potential, the ground state density is uniquely determined. This second theorem restricts most of the DFT applications to the study of the ground state.

To obtain the ground state density which minimizes the total energy under a constraint of the total electron number N , the variation of Lagrange is set to zero,

$$\frac{\delta[E(\rho) - \mu(\int \rho(\vec{r})d\vec{r})]}{\delta\rho} = 0$$

The Lagrange multiplier of this constraint is the electronic chemical potential μ . The total energy functional of the system can be written as

$$E(\rho) = V_{ext}(\rho) + F(\rho) = V_{ext}(\rho) + T(\rho) + V_{ee}(\rho)$$

The format of functional $F(\rho)$ is unknown, but it is an universal functional of electron density $\rho(\vec{r})$ for all many-body systems and is independent from the external potential. It is usually written as a sum of the kinetic energy functional, $T(\rho)$, and the electron-electron interaction energy functional, $V_{ee}(\rho)$. Since the non-interacting kinetic energy functional $T_s(\rho)$ and Hartree potential energy functional $V_H(\rho)$ are known, the total energy functional can be written as

$$E(\rho) = V_{ext}(\rho) + T_s(\rho) + V_H(\rho) + V_{xc}(\rho)$$

Where

$$V_{xc}(\rho) = T(\rho) - T_s(\rho) + V_{ee}(\rho) - V_H(\rho)$$

$V_{xc}(\rho)$ is defined as the exchange-correlation energy.

Kohn and Sham introduced a fictitious system of N non-interacting electrons which can be described by a single Slater determinant wave function. In this condition, the electron density of the system can be expressed as the sum of electron density from each single electron spin orbital.

$$\rho = \sum_{i=1}^N \phi_i^2$$

The energy functional of this fictitious system can be expressed in terms of the non-interacting kinetic energy functional $T_s(\rho)$ and an effective external potential energy functional $V_{s,ext}(\rho)$,

$$E_s(\rho) = T_s(\rho) + V_{s,ext}(\rho) = T_s(\rho) + V_{ext}(\rho) + V_H(\rho) + V_{xc}(\rho) = E(\rho)$$

If the effective potential energy functional is chosen so that the total energy expressions of the non-interacting system and the real system are the same, then by plugging the same energy

expression into the Lagrange equation, it will come to the same ground state density. Because the density is an expression of spin orbitals, solving the Lagrange equation gives the Kohn-Sham (KS) equations,

$$\left[-\frac{1}{2}\nabla^2 + v_{ext}(\vec{r}) + \int \frac{\rho(\vec{r}')}{|\vec{r} - \vec{r}'|} d\vec{r}' + v_{xc}(\vec{r}) \right] \phi_i(\vec{r}) = \epsilon_i \phi_i(\vec{r})$$

Where the exchange-correlation potential is

$$v_{xc} = \frac{\delta E_{xc}}{\delta \rho}$$

Since the E_{xc} contains a component from the kinetic energy, it is not the sum of the exchange energy and correlation energy in the sense of Hartree-Fock theory and correlated wave function theories. Each of the Kohn-Sham equations is a Schrodinger equation in the form of

$$(\hat{T}_s + \hat{V}_{s,ext})\varphi_i = \epsilon_i \varphi_i$$

and it may be solved numerically using the SCF approach. An initial guess of the Kohn-Sham spin orbitals are used for SCF iterations. Then the ground state density of the real system can be obtained from these spin orbitals, and the real system's ground state energy may be given from this ground state density. The eigenvalues of KS equations do not have physical meanings for the real system except for the frontier KS eigenvalues. If the total energy functional is explicit, then $\epsilon_N = -I, \epsilon_{N+1} = -A$, where I is the first ionizing energy of the N-body system and A is the electron affinity of the same N-body system. In many cases, the Kohn-Sham orbitals generated from density functional theory are taken as an approximation to the true spin orbitals. Under this presumption, it is reasonable to use the Hartree-Fock converged spin orbitals as the initial Kohn-Sham orbitals in their SCF calculations because the electron correlation energy correction is small, and the lack of correlation components in Hartree-Fock theory should only result in small amount of energy deviation from the energy of the electrons in true orbitals. So, a common way to evaluate the quality of Kohn-Sham orbitals in resembling the true orbitals is to compare them with the Hartree-Fock spin orbitals. If the calculated Kohn-Sham orbitals are very different from the Hartree-Fock orbitals (for example, energetically reversed for orbitals with given symmetry states), then cautions should be taken in seeking for physical explanations from these Kohn-Sham orbitals.

1.1.3. Basis Set and Exchange-Correlation Functional Approximations

Approximations of practical DFT calculations mainly come from two aspects, the first one is the adopted basis set, and the second one is the approximated exchange-correlation functional. Though DFT is an exact theory, unlike wavefunction theory (WFT), it does not provide a systematic way to construct the exact XC functional.

Basis set

In practice, the numerical solution of each KS equation for a single spin orbital is distained by expanding the spin orbital using a suitable set of functions and solving for the expansion coefficients. The expansion of each of the spin orbital corresponds to the expansion in the number of KS equations to be solved.

In quantum chemistry, Slater type orbitals (STO) and Gaussian type orbitals (GTO) are two types of commonly used basis set functions. STO decay exponentially as the distance increases from the nuclear center. GTO has a Gaussian type behavior. STO resembles the true spin orbital behavior better than GTO because it has a cusp behavior at the nucleus position. However, due to the Gaussian Product Theorem, which guarantees that the product of two GTOs centered on two different atoms is a finite sum of Gaussians centered on a point along the axis connecting the two atoms, GTO brings great computational savings in practical calculations. So, the so-called “contracted basis functions,” where a STO is approximated by a linear expansion of GTOs, are commonly used as a compromise between accuracy and computational savings. Starting from this point, extended basis sets come to play important roles in computational chemistry, like the multi-zeta basis sets, Pople split valence basis sets, and the correlational-consistent split-valence basis sets by Dunning which are designed to converge systematically to the complete-basis-set (CBS) limit using empirical extrapolation techniques. For better orbital approximations, polarization and diffuse components are added to basis sets. The polarized basis set is to account for the fact that sometimes orbitals share qualities of both 's' and 'p' orbitals or both 'p' and 'd', etc. and not necessarily have characteristics of only one or the other. As atoms are brought close together, their charge distribution causes a polarization effect which distorts the shape of the atomic orbitals. Because the properties of the valence electrons or the loosely bound electrons in cases of anions or excited states are mainly described by the tail region of the approximated orbitals, the diffuse functions are added, which utilize very small exponents to clarify the

properties of the tail region.

Local Density Approximations (LDA)

In the local density approximation of exchange-correlation (XC) functional, the real system with inhomogeneous electron density $\rho(\vec{r})$ and potential $v(\vec{r})$ distributions is divided into small cells where the $\rho(\vec{r})$ and $v(\vec{r})$ are considered constant. The XC energy of each homogeneously interacting cell is approximated; and the total XC energy is an integral over all homogeneous cells.

$$E_{xc}(\rho) \approx E_{xc}^{LDA}(\rho) = \int d^3r e_{xc}^{homo}(\rho)$$

The systematic underestimations of E_c and overestimations of E_x result in the success of LDA in many fields. An interesting philosophy² behind the DFT of LDA approximation is that it adopts the XC energy density, which yields from spatially homogeneous interacting problem, to spatially inhomogeneous non-interacting KS equations to yield the electron density. LDA is very popular in solid state physics but not in chemistry because of its inadequacy in meeting the chemical accuracy (error within 1 kcal/mol).

General Gradient Approximation (GGA)

General gradient approximation includes the information from the gradient of electron density to make corrections on the LDA XC functional. The word “general” here means that the corrections do not have to follow a systematic gradient expansion from the first order gradient to the higher orders in order to reach higher accuracy. Such kind of functionals that generally include density gradient components can be denoted as follows,

$$E_{xc}^{GGA} = \int dr^3 f(\rho, \nabla\rho)$$

Currently, the most popular GGAs are the PBE for extended systems (materials) and BLYP in chemistry.

Meta-GGA, Hybrid Approximation and Beyond

The Meta-GGA does not only include the density and its gradient, but also includes the Kohn-Sham kinetic energy density $\tau(\vec{r})$ in its XC functional.

$$\tau(\vec{r}) = \frac{\hbar^2}{2m} \sum_i |\nabla\phi_i(\vec{r})|^2$$

Where $\phi_i(\vec{r})$ is the spin orbital in KS equations.

The currently most popular functional in chemistry is B3LYP,³ which is a hybrid functional that combines the LYP GGA for correlation with Becke's three parameter hybrid functional B3 for exchange. The M05/6-2X functional was used to conduct the hyperfine coupling calculations in the present work. It is a part of the Minnesota functionals developed by Truhlar and coworkers and is a highly parameterized hybrid meta-GGA functional, whose performance is optimized by dozens of parameters that are trained by experimental databases. Significant progress in DFT functionals has been made in recent years in the simulation of excited state, Van der Waals interactions, strongly correlated systems, etc.

1.1.4. Delocalization Error and Static Correlation Error

It was recently proposed by Yang's group⁴ upon examining the DFT calculated energies of the stretched H_2^+ radical and H_2 molecule, that delocalization error and static correlation error are the two major systematic errors in commonly used DFT approximations. As pointed out by Yang and coworkers,⁵ the delocalization error accounts for DFT calculation's underestimation of the barriers of chemical reactions, the band gaps of materials, the energies of dissociating molecular ions, and charge transfer excitation energies. It also overestimates the binding energies of charge transfer complexes and the response to an electric field in molecules and materials. On the other hand, the static correlation error accounts for DFT calculation's failure in describing degenerate or near-degenerate states, such as those in transition metal systems, the breaking of chemical bonds, and strongly correlated materials.

Delocalization Error

Massive errors were found on stretching odd-number electrons systems when calculated with LDA and GGA DFT approximations. This well-known problem has been commonly attributed to the self-interaction error (SIE) which is the unphysical interactions of an electron with itself. One way to solve the SIE problem is to include the Hartree-Fock exchange component, which is free from self-interaction error, into the approximation functional. Since

DFT's practical success is to a large extent due to its error cancellation between exchange and correlation approximations, and the exact correlation functional is unknown, a high proportion of HF exchange component may lead to worse performance. Nevertheless, there exist several self-interaction correction (SIC) approaches that provide partial remedies for SIE problem. Since the SIE for many-body system is hard to formulate mathematically, Yang and coworkers provide a different insight into the SIE from the nonlinearity behavior of approximation functional with fractional charges.

In principle, the energy of a system with a fractional number, $N + \delta$, $0 < \delta < 1$, of electrons is known exactly as

$$E(N + \delta) = E(N) + \delta * (E(N + 1) - E(N))$$

The fundamental band gap in solids, or the chemical hardness in molecules, is defined as the difference between the ionization energy and electron affinity, and from the expression of the exact energy of fractional number electron system above, it is also equal to the difference between the energy derivatives of a fractional system from right to left of the electron number N . And these two derivatives, physically, stands for the chemical potentials of an N -electron system and a $(N-1)$ -electron system, $\mu(N)$ and $\mu(N - 1)$.

$$\begin{aligned} E_{gap}(N) &= I - A = [E(N - 1) - E(N)] - [E(N) - E(N + 1)] \\ &= \frac{\delta E}{\delta N} \Big|_{N+\delta} - \frac{\delta E}{\delta N} \Big|_{N-\delta} = \mu(N) - \mu(N - 1) \end{aligned}$$

where I is the first ionizing energy of the N -body system and A is the electron affinity of the same N -body system. The exact chemical potential demonstrates a discontinuity across an integer electron number. The lack of this discontinuity resides at the root of delocalization error. According to Yang *et al.*⁴, commonly used approximate functionals deviate from the exact linearity condition for fractional charges with a convex behavior. This convex behavior means approximate functionals will give lower energies for a delocalized charge distribution, and/or tend to favor fractional charges or delocalized charge distributions over the integer or localized ones. On the contrary, the Hartree-Fock functional of electron density demonstrates a concave behavior for fractional charges and arise the energy for delocalized charge distribution. It will result a so-called localized error. Figure 1. And 2. cited from Yang *et al.*⁴ clearly illustrate the idea of delocalization errors. Figure 1. shows the behavior of the energy of a carbon atom with between five and seven electrons. And Figure 2. shows the hole density distribution of an ionized

He cluster of an 8×8 square of He atoms separated by 2 \AA . The CCSD gives a good discretion of ρ_{hole} . The PBE with GGA functional gives a overdelocalized ρ_{hole} , while HF theory gives a overlocalizd ρ_{hole} . The hybrid functional M062x does not adequately describe ρ_{hole} .

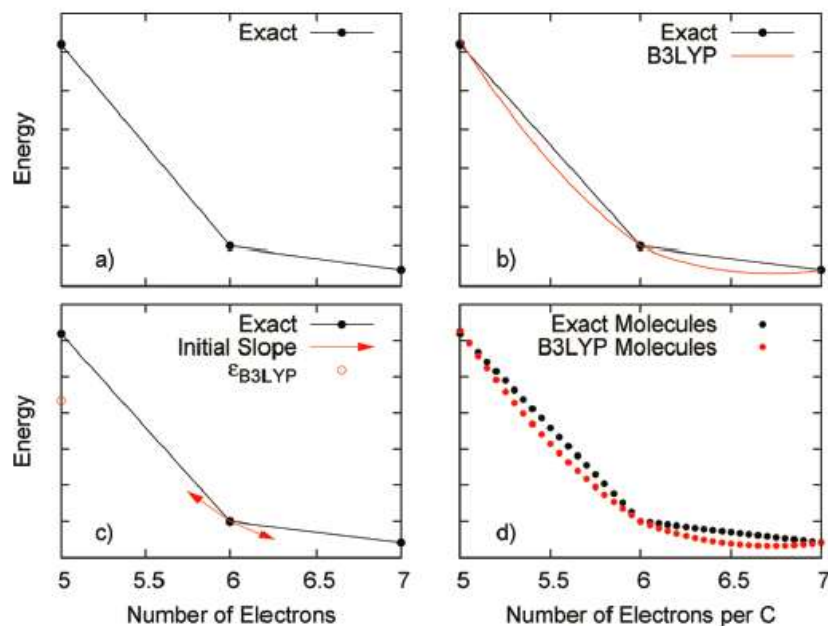


Figure 1. Delocalization error of B3LYP functional for fractional charge. (a) The exact fractional charge behavior of the carbon atom. (b) B3LYP give accurate energy at the intergers but fails for the energy of fractional charges. (c) the initial slope of the B3LYP at $N=6$ does not give an eigenvalue that agrees with the ionization energy. (d) B3LYP gives too low energies for real stretched molecules.⁴

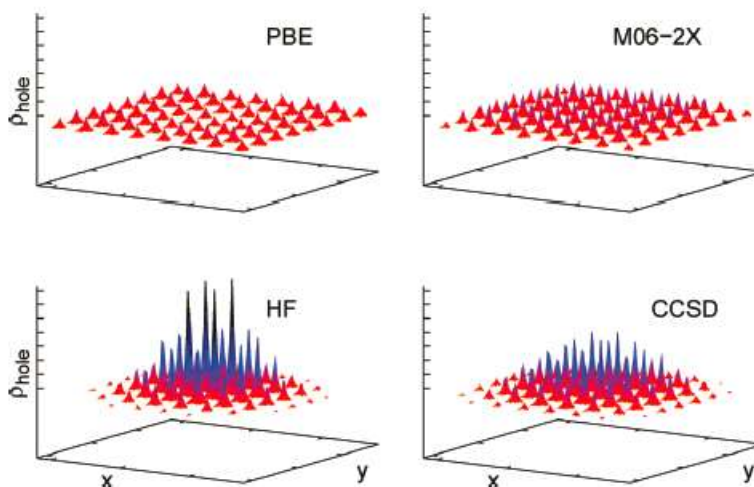


Figure 2. The visualization of delocalization error: the density of the hole, ρ_{hole} , for the

ionization process $He_{64} \rightarrow He_{64}^+$ is shown for four different methods.

So we should pay seek explanation of calculated electron density distribution from both the underlying physics and the functional approximation errors. CCSD (Coupled-cluster Singles and Doubles) gives a good description of ρ_{hole} in this system. A GGA functional, PBE, overdelocalizes ρ_{hole} , whereas Hartree-Fock overlocalizes ρ_{hole} . A hybrid functional, M06-2X, which has quite a large amount of exchange (54%), still does not adequately describe ρ_{hole} .⁴

Static Correlation Error

In Hartree-Fock theory, an N-electron Slater determinant is employed to approximate the wave function of an N-electron system. Each N-electron Slater determinant is formed by N single electron spin orbitals, and this set of orbital occupancies of N electrons is referred to as a configuration. A solution of HF theory is a Slater determinant that approximates the ground state of the system. It is referred to as the Hartree-Fock reference determinant. More generally, an arbitrary wave function can be expressed exactly as a linear combination of all possible N-electron Slater determinants formed from a complete set of spin orbitals $[\phi_i(x)]$. If we denote the N-electron Slater determinant as $|\phi_i\rangle$, and the eigenvectors of a wave function $|\Psi\rangle$ as $|\Psi_j\rangle$, then

$$|\Psi\rangle = \sum_i c_{ij} |\Psi_j\rangle = c_0 |\phi_0\rangle + \sum_{ar} c_a^r |\phi_a^r\rangle + \sum_{a<b,r<s} c_{ab}^{rs} |\phi_{ab}^{rs}\rangle + \dots$$

A complete set of spin orbital ϕ_i has infinite number of one electron functions, thus they will form an infinite number of N-electron Slater determinants, or configurations. $|\phi_a^r\rangle$ stands for a Slater determinant which is formed by replacing the spin-orbital a in the reference determinant $|\phi_0\rangle$ by another spin-orbital r . It is referred to as an excitation from the reference configuration. This is the essence of the Configuration Interaction (CI) theory to solve the Schrödinger equation in the form of a full wave function expansion. In practice, the one-electron-functions set $[\phi_i(x)]$ is always incomplete and the approximations of CI can be evaluated by the fraction of correlation energy they recover. Commonly used CI approximations, such as CISD, truncate the wave function expansion to single or double excitations relative to the reference state. Since the Hamiltonian operator includes only one- and two-electron terms, only singly and doubly excited configurations can interact directly with the reference, and they typically account for about 95% of the correlation energy in small molecules at their equilibrium geometries.⁶ The use of more

than one reference configuration (multi-reference configuration interaction method) means a better description of the electron correlation and will give a lower energy. The truncated CI methods have problems of size-inconsistency, and it cannot be solved by adopting multireference configurations.

The correlation energy is usually defined as the energy difference between the exact non-relativistic energy eigenvalue of the electron Schrödinger equation under the Born-Oppenheimer approximation and the basis limit energy from Hartree-Fock theory.

$$E_{corr} = E_{exact} - E_{HF}$$

E_{corr} is always negative since E_{HF} is an upper bound of the exact energy due to the variational principle. The correlation energy can be further divided into two components, the dynamic correlation energy and the non-dynamic, or static, correlation energy. The dynamic correlation energy is recovered by fully considering the repulsive interaction between electrons, and the mean field approximation of HF theory is not a good description of this interaction. The dynamic correlation energy arises mainly with “tight pairs.”⁷ As a system is geometrically stretched, the magnitude of electron repulsion will decrease. The static correlation energy arises from the lowering of energy through the interaction among degenerate ground state configurations, if any, and between the ground state and the low-lying excited state configurations, which are known as quasi-degeneracy states. The inability of a single reference configuration in CI approximations to describe this kind of interaction introduces static correlation errors. Or, as Yang described, the static correlation “corresponds to a situation that is inherently multideterminantal, and single determinant approaches will fail.”⁴ Multi-configurational methods, such as CASSCF and CASDFT, have been developed to resolve this problem.

Yang and coworkers provide a different view on the static correlation error in DFT. In principle, for an exact exchange-correlation functional, the ground state total energy of a system whose ground state is g -fold degenerate should obey the constancy condition for fractional spins,

$$E\left[\sum_{i=1}^g C_i \rho_i\right] = E(\rho_j) = E_0(N), \quad j = 1, 2, \dots, g$$

Which means any combination of the degenerate ground states should give the same ground state energy. The so-called fractional spins are introduced by the combination of degenerate states. The DFT’s violation of the constancy constraint of energy on degenerate states leads to the same static correlation problem. According to Yang,⁴ this idea can be extended to cases of near-

degeneracy or degenerate cases which are calculated as near-degenerate due to exchange-correlation functional approximations.

1.2. An Introduction to Isotropic Hyperfine Coupling Constant Calculations

1.2.1. Isotropic Hyperfine Coupling Constant

In a free radical, the interaction among the electron spin S , the magnetic nucleus of spin I and external magnetic field \mathbf{B} can be described as a spin Hamiltonian H_S

$$H_S = \mu_B \mathbf{S} \cdot \mathbf{H} \cdot \mathbf{g} + \mathbf{S} \cdot \mathbf{A} \cdot \mathbf{I} - g_N \beta_N \mathbf{H} \cdot \mathbf{I} + \text{small terms}$$

The first term is the Zeeman term describing the interaction between the electron spin and the external magnetic field, through the Bohr magneton μ_B and the \mathbf{g} tensor. The second term describes the hyperfine interaction between the electron spin and the nuclear spin through the hyperfine coupling tensor \mathbf{A} . The third term is the Zeeman coupling of the nuclear magnetic moments (approximately 1/1000 of the magnitude of electronic Zeeman coupling). The small terms correspond to higher order interactions, such as the magnetic interactions among electron orbital, electron spin, and nuclear spin, and nuclear quadrupole resonance. The \mathbf{A} tensor can be decomposed into two terms, the contact term, which is due to Fermi contact, and the dipolar term, which describes the interaction between the dipole components of the electron spin and the nuclear spin. The coefficient of the first contribution is the isotropic hyperfine coupling constant (iHFCC), and the coefficient of the second contribution is the anisotropic hyperfine coupling constant. The iHFCC is related to the spin density at the nucleus located at \vec{r}_N , which can be calculated as

$$A_{iso}(N) = \frac{8\pi}{3} \frac{g_e}{g_0} g_N \beta_N \Delta\rho_N$$

$$\Delta\rho_N = \sum_{\mu,v} P_{\mu,v}^{\alpha-\beta} \langle \phi_\mu(\vec{r}) | \delta(\vec{r} - \vec{r}_N) | \phi_v(\vec{r}) \rangle$$

where $P^{\alpha-\beta}$ is the difference between the density matrices for electrons with α and β spins, it is also known as the spin density matrix. δ is the Dirac delta function. This delta formulation indicates that the calculation of iHFCC depends on the local quality of the wave functions at the nuclei. On the other hand, the dipolar interaction depends on the spin density in the vicinity of

\vec{r}_N . It is worth noting to distinguish the difference between two related quantities. The unpaired electron density, or spin density, $\Delta\rho_N$, at some point in space, such as at the nucleus, is a probability density which is measured in *electron/Angstrom*³. The spin density or spin population, in an orbital, ρ_H , is a number that represents the fractional population of unpaired electrons on an atom.⁸

Different mechanisms give rise to the spin density at the nucleus. Firstly, the direct contribution, also known as delocalization contribution, arises from the orbital at the nucleus that contains unpaired electrons. It is the main contribution of spin density at the nucleus for a σ radical. However, it gives no contribution for a π radical since π orbitals have nodes at the nucleus. Secondly, the spin polarization contribution comes from the exchange interaction of the unpaired electron with the two electrons in a spin-paired bond or an inner shell. The exchange interaction only arises between electrons with parallel spins. As a result, the electron whose spin is parallel with the unpaired electron has a shorter average distance to the unpaired electron than does the electron with antiparallel spin. For a π radical, this will introduce antiparallel spin density at the hydrogen atom within the nodal plane of the unpaired electron's orbital. And this will dominate the spin density at the nucleus with the absence of the direct contribution. The other higher order spin density contributions arise from electron correlation interactions. The absence of correlation interactions in HF theory often leads to 100% error in iHFCC calculations.⁹

The computation of iHFCC is very sensitive to errors in the spin density at the nucleus. A review article by Improta et al.¹⁰ reminds us that one should be cautious when trying to rationalize the iHFCC calculations referring to the spin population from Mulliken population analysis. Because the Mulliken spin population assigned on each atom is a quantity of integration over all space. But we should also notice that the empirical model, McConnell's relation, which is adopted in EPR experiment, takes the spin density at the nucleus to be proportional to the populations of unpaired electrons in the neighboring π atomic orbital,¹¹ which partially supports the use of Mulliken spin population to analyze iHFCC calculations. Below are some common considerations for accurate spin density calculations.

1.2.2. Some Considerations of Accurate Spin Density Calculations

Both solvent and vibrational effects can influence the calculated spin density values. Besides, for non-vibrating gas phase conditions, geometry, XC approximations, and one-electron basis set all affect the accuracy of spin density calculations.

It is known that basis sets of triple-zeta quality plus multiple polarization functions and diffuse functions are required for accurate spin density calculation.¹² There are two major problems with “contracted STO” for accurate spin density calculations at the nucleus.⁹ The first major problem relates to the GTO’s inability to correctly describe the cusp structure at the nucleus. The introduction of additional very tight (i.e., short range, large exponent) Gaussian functions into the contraction of s-type orbital will strongly remove this deficiency by moving the turning point of the orbital closer to the nucleus. Another argument by Chipman about this is that the cusp condition at the nucleus relates to the derivative of a wave function. However, the derivative is not a constraint of the spin density at the nucleus. By proper design of Gaussian functions, it is possible to artificially let the Gaussian functions to give correct amplitude at the nucleus.¹¹ The second major problem with the basis set is that commonly used “contracted STOs” are designed for the evaluation of energies. These basis sets are optimized to allow great flexibility in chemically important valence regions. Because the spin density at the nucleus is strongly correlated to the contraction coefficients and exponentials of Gaussian functions at core region, more flexibility should be allowed for basis set functions of inner shell orbitals. EPR-II/III basis sets developed by Barone¹³ are optimized for the calculations of hyperfine coupling constants by DFT methods (particularly B3LYP). EPR-II is a double-zeta basis set with a single set of polarization functions, while EPR-III is a triple-zeta basis set with diffuse functions and additional polarization functions. Their s functions are enhanced for core region, and all their polarization functions are taken from the correlation-consistent basis set developed by Dunning. Currently, EPR-II/III basis sets are applicable to systems containing only H, B, C, N, O and F atoms in Gaussian 09 program package.

While the implementation of the delta operator is relatively easy in spin density calculations, it is very sensitive to errors of spin densities at the nucleus, and hence to the basis set approximations. A non-local operator, HSF operator, is developed by Hiller, Sucher, and Feinberg (HSF),¹⁴ which samples the wave functions at all points in space, to overcome the problems of the delta operator. However, HSF has problems like incorrect long-range asymptotic behavior of the density with most approximate wave functions and is computationally

demanding.¹² Another alternative operator, the RC operator, developed by Rassolov and Chipman,¹⁵ improves upon many of the drawbacks of both the delta operator and HSF operator.

Chapter 2 An Introduction to the Present Work

2.1. Previous Density Functional Theory Calculations on Hyperfine Coupling Constants

In order to understand the effects of ionizing radiation on DNA, it is important to understand the free radical chemistry of the nucleic acid constituents. The results of detailed electron paramagnetic resonance/electron nuclear double resonance (EPR/ENDOR) experiments on nucleic acid constituents have played a major role in understanding the primary effects (radical cations and radical anions) produced by the ionizing radiation.

To aid in understanding the experimental results, theoretical calculations on single nucleic acid bases have been performed using DFT to compute accurate hyperfine couplings. A series of papers by Wetmore, Boyd and Eriksson¹⁶⁻¹⁹ report theoretical calculations including the estimations of spin densities and isotropic and anisotropic hyperfine couplings on the primary oxidation and reduction products observed in nucleobases. Comparisons of these calculations with experimental results have been summarized in a review article by Close.²⁰ Table 1 from this review article is included below, which summarizes and rates the DFT calculated hyperfine coupling constants (HFCC) results in comparison with their experimental values, based on how well the DFT computational results reproduce the experimental values at the primary and secondary sites of HFCC. In Table 1, while the calculations generally agree nicely with the HFCCs derived from the experimental data, there are four cases of prominent discrepancies in this list, namely the N1-deprotonated cation in Cytosine:H₂O system, the N3-deprotonated cation in 5'dCMP system, the native cation in G:HCl:H₂O system, and the N7-H C6-OH protonated anion in GMP crystal system. The goal of the present work is to address these four problem cases by including H-bonding effects and using the recently developed Minnesota functionals developed by Truhlar and coworkers.²¹⁻²³

Table X: Summary of Calculated Results				
Crystal System	Radical	Computational Results		Overall Rating
		Prim. Sites	Sec. Sites	
Cytosine:H ₂ O	N3-protonated anion (Fig. 1)	+	+	Good
1-MeCytosine	N3-protonated anion R1	+		Fair
Cytosine:H ₂ O	N1-deprotonated cation R2	-		Poor
5'-dCMP	N3-deprotonated cation R3	-		Fair
Cytosine	Amino deprotonated cation R4	+		Good
Thy. anhyd.	C4-OH protonated anion R5	+	+	Good
Thymine	Native anion	-	+	Fair
1-MeThymine	C4-OH prot. anion (Fig. 2)	+	+	Good
TdR	Allyl-like radical R6	+	+	Excellent
Thymine	N1-H deprotonated cation R7	+	+	Good
1-MeThymine	N3-H deprotonated cation R8	+	+	Good
5'-dGMP	Native anion (Fig. 4)	-		Poor
5'-dGMP	C6-OH protonated anion	+	0	Good
GMP	N7-H C6-OH prot. anion (Fig. 5)	-	+	Fair
G:HCl:H ₂ O	Native cation	-		Poor
5'-dGMP	N2-H deprotonated cation R9	+	+	Good
AR	N3-H protonated anion R10	+	0	Good
A:HCl:1/2H ₂ O	Native cation	+	0	Excellent
Adenosine	N6-H deprotonated cation R11	+	0	Excellent

Table 1. Summary of the DFT calculated HFCC results in comparison with the experimental values. The performances of the calculation are rated base on how well they reproduce the experimental HFCC values at the primary and secondary sites of the examined radicals.²⁰

The theoretical calculations in Close's review were performed on gas phase molecules, whereas the experimental values were detected from the radicals formed in the solid state, mainly in single crystals. The DFT calculations omit the electrostatic environment of the radicals, particularly the intricate hydrogen bonding structure in which the free radicals are imbedded. Pauwels and coworkers²⁴ have carried out B3LYP studies with single molecule, cluster model and periodic space model calculations on the reproduction of the hyperfine coupling constants and the principal directions of the hyperfine tensor of radiation-induced +NH₃-•CH-CO₂⁻ glycine radical in solid state. Their work shows best agreement of these two features with the cluster model approach when compared with the single molecule model and periodic space model. In their cluster space model, incorporating the explicit molecular

environment of the cluster model reproduces good EPR parameters, while using the single radical that is optimized in the cluster model only gives poor isotropic hyperfine couplings. Their work indicates the important role played by correct description of hydrogen bond interactions in EPR calculations. A case study of the influence of Hydrogen bonding on hyperfine couplings at the hybrid density functional theory was also presented by O'Malley.²⁵ In our present work, we further test the cluster space model in nucleus acid component crystal system. It is shown that, though the including of the electrostatic environment in theoretical calculations can lead to hyperfine couplings that agree much better with the experimental results, B3LYP functional does not always satisfy this prediction in our calculation. We present the advantages of the highly parameterized Minnesota functionals, specifically, M05/6-2X, over the B3LYP functional in EPR calculations.

2.2. The Four Problematic Cases in Previous Hyperfine Coupling Calculations Using Density Functional Theory

2.2.1. N1-deprotonated Cytosine Cation Radical

In solid state of cytosine monohydrate, the cytosine molecules are hydrogen-bonded through N3H \cdots N1 and N6H \cdots O into parallel ribbons, and the neighboring ribbons further forms complex hydrogen bond network though water molecules.²⁶ Sagstuen et al.²⁷ assigned the primary radiation products as the N1-deprotonated cytosine cation and N3-protonated cytosine anion from ENDOR experiment. It is known from the ENDOR experiment that $\rho(\text{C5})=0.57$ and $\rho(\text{N1})=0.3$, and there are two small exchangeable N-H couplings whose angular variations correlate well with the exo-cyclic N4-H's.²⁰ Experiment also indicates the nitrogen π -spin density at N4 is about 0.17.²⁸ Wetmore et al.¹⁷ reported gas phase DFT calculations on four different deprotonated cations of cytosine. Their computed isotropic hyperfine coupling on the radical center C-5 is -31.5 MHz rather than the experimentally observed -41.5 MHz. Besides, their other calculated isotropic and anisotropic hyperfine couplings are also poorly matched with experimental data. These along with the lack of N4 hyperfine coupling in a N4-C4 amino bond rotation scan lead Wetmore et al to reject the N1-deprotonated cation model, despite the fact that their calculation showed this model is energetically the most stable and has unpaired spin density distributions ($\rho(\text{C5})=0.94$, $\rho(\text{N1})=0.29$, $\rho(\text{O2})=0.35$) best fitting the experimental results among their four different models. Therefore, the agreement of theoretical and experimental

results on the N1-deprotonated cytosine cation is rated as poor in Close's review. Table 2 shows a detailed HFCC comparison between the calculated and experimental values of the N1 deprotonated cytosine cation. The experiment was conducted with cytosine monohydrate (Cm) single crystal.

According to McConnell, in π -electron radicals the isotropic proton hyperfine splitting for proton α , a_α , is proportional to the diagonal element of a π -electron spin density matrix²⁹

$$a_\alpha = Q\rho_{\alpha\alpha}^\pi$$

Which means in aromatic radicals, the extent to which the C-H σ electrons are polarized is directly proportional to the net unpaired electron population, or " π -electron spin density" on the carbon atom.⁸ For the isotropic hyperfine coupling on aromatic nitrogen atom, similar relation applies

$$a_N = Q^N \rho_\pi$$

Where the effective value of Q^N varies depends on different structural environment. The effective Q^N can be calculated from the table below.

	Room Temperature				Liquid N_2 (77 K)			
	A (MHz)	$2B'$ (MHz)	$2B_{atm}$ (MHz)	$2B'/2B_{atm}$	A (MHz)	$2B'$ (MHz)	$2B_{atm}$ (MHz)	$2B'/2B_{atm}$
^{14}N in $NH_2^+SO_3^-$	+51	+52	+96	0.54	+55	+67	+96	0.71
^{14}N in $NHSO_3^-$	+38	+60	+96	0.62	+38	+70	+96	0.73
^{14}N in $N(SO_3^-)_2$	+37	+70	+96	0.73	+37	+70	+96	0.73

Table. Isotropic (A) and anisotropic coupling parallel to 2pN orbital ($2B'$) at room temperature and liquid nitrogen temperature. With corresponding calculated 2p spin population.³⁰

For example, at room temperature, the Q^N values at for $NH_2^+SO_3^-$, $NHSO_3^-$, and $N(SO_3^-)_2$ are calculated to be 99.44 MHz, 61.29 MHz, and 50.68 MHz. At liquid nitrogen temperature, the Q^N values are 77.46 MHz, 52.05 MHz, and 50.68 MHz. When compared with the nitrogen atoms of N1-deprotonated cytosine cation radical, the structural environment of N1 resemble that of the nitrogen atom in $NH_2^+SO_3^-$, while N3 the nitrogen atom in $N(SO_3^-)_2$ and N4 the nitrogen atom in $NH_2^+SO_3^-$. Thus, it might be reasonable to adopt different effective Q^N values to predict the isotropic hyperfine couplings at nitrogen atoms using McConnell's relation. The Q^N values for $NH_2^+SO_3^-$ and $NHSO_3^-$ is highly dependent on temperature between room temperature and

liquid nitrogen temperature. The Q^N value of $N(SO_3^-)_2$ appears to be the same at both temperatures. However, since EPR/ENDOR experimental analyses are based on radical species stabilized at 10 K²⁷ and detailed $Q^N - temperature$ relations are not available, I decide not to use these Q^N values to predict the isotropic hyperfine couplings at N atoms basing on the spin densities in their π -orbitals.

Cm	Principle values	Isotropic value	Dipolar value	Computational isotropic	Computational dipolar
C5-H	-62.4 -42.2 -19.6	-41.4	-21.0 -0.8 22.8	-30.7	-19.7 -0.4 20.1
C4-NH1	-23.6 -16.1 -3.2	-14.3	-9.3 -1.8 11.1	-1.1	-1.3 -0.8 2.1
C4-NH2	-19.2 -16.6 -3.3	-13.0	-6.2 -3.6 9.8	-0.9	-1.9 -1.5 3.4

Table 2. Comparison of N1 deprotonated cytosine cation HFCC values between the experimental values from cytosine monohydrate single crystal and the calculated values from gas phase DFT calculations by Wetmore *et al.*, at PWP86/6-311G(2d,p) level of theory.²⁰

2.2.2. Native Guanine Cation Radical

In the crystalline structure of Guanine Hydrochloride Monohydrate,³¹ the guanine base ring is protonated at N7 and forms two type of H-bonds pairing, N7-H \cdots O6 and N2-H \cdots N3, with its two neighboring guanines. Besides, complex H-bonding network is formed among guanine cations, water and chlorine anions. The guanine molecule has a slightly non-planar structure with the dihedral angle between its imidazole and pyrimidine ring determined as about 1.7 $^\circ$.³² The N2 amino group departs slightly from the general base plane in such a direction that it forms a stronger hydrogen bond with adjacent N3 site. Upon oxidation, the N-7 protonated guanine cation deprotonates at N7 and results in a native guanine cation. This will be equivalent to the guanine cation in irradiated DNA structure. Experimental results from Close and coworkers³³ characterize this N7 deprotonated native guanine cation with unpaired spin density as $\rho(C8)=0.18$, $\rho(N2)=0.17$, and $\rho(N3)=0.28$. Wetmore *et al.*¹⁶ report native guanine cation calculations where the guanine molecule remains a planar conformation upon optimization in gas phase, with spin densities $\rho(C8)=28$, $\rho(N2)=0.1$, $\rho(N3)=0.21$, $\rho(C5)=0.29$ and $\rho(C4)=0.17$. The

calculated $\rho(N2)$ and $\rho(N3)$ are in fair agreement with experimental values, but the other spin densities are not. Table 3 shows the detailed comparison of the native guanine cation HFCCs between experimental values in Guanine Hydrochloride Monohydrate single crystal structure and the calculated values in gas phase by Wetmore et al, at PWP86/ 6-311G(2d,p) level of theory. The considerable difference in hyperfine couplings between theoretical and experimental results leads Wetmore *et al.* to further demonstrate calculations on four other dehydrogenated guanine cation radicals, which do not seem to provide any better models for the guanine cation.

	Principle value	Isotropic value	Dipolar values	Computational Isotropic	Computational Dipolar
N1				-2.2	
N3		16.8		6.9	
N7				-1.3	
N9				-4.1	
N2		10.0		3.4	
N2-H1		12.1		-8.2	
N2-H2		12.1		-7.1	
C8-H	-21.0 -14.0 -8.4	-14.5	-6.5 0.5 6.0	-22.7	-6.5 -1.6 8.1
N9-H				0.6	

Table 3. The comparison of the native guanine cation HFCCs between experimental values in Guanine Hydrochloride Monohydrate single crystal structure and the calculated values in gas phase by Wetmore et al, at PWP86/ 6-311G(2d,p) level of theory.²⁰

2.2.3. N3-deprotonated 5'-dCMP Cation Radical

In the crystal structure of Deoxycytidine 5'-Phosphate Monohydrate (5'dCMP), the cytosine nucleotide prefers a zwitterion structure where the migration of a proton from the phosphate oxygen results in the protonation at N3 site. In this crystal structure, there is no base stacking and all hydrogen atoms participate in Hydrogen bonding.³⁴ From the experiment conducted by Close and coworkers,³⁵ the oxidation of the cytosine base produces a N3-deprotonated cation which exhibits major hyperfine couplings from C5- H_α , C1'- H_β and significant nitrogen hyperfine couplings. It is characterized by unpaired spin densities $\rho(C5)=0.60$, $\rho(N4)=0.17$ and $\rho(N1)=0.30$. Wetmore et al.¹⁷ have performed gas phase calculations on a 1-methyl cytosine cation, which appears to be equivalent in structure to the N3 deprotonated cation observed experimentally in 5'-dCMP, with the deoxyribose and phosphate

group substituted by a methyl group. They report spin densities $\rho(\text{C5})=0.33$, $\rho(\text{N3})=0.24$ and $\rho(\text{O2})=0.45$, which are not very close to the experimental values. Table 4 gives the detailed comparison of HFCC values between the experimental values of the N3 deprotonated 5'-dGMP cation in 5'-dGMP Monohydrate single crystal and the calculated value of 1-Methyl cytosine cation in gas phase by Wetmore *et al.*, at PWP86/6-311G(2d,p) level of theory. As shown in Table 4, the computed isotropic hyperfine of the primary site of the unpaired spin, C5- H_α , is too small, though the computed dipole couplings are in good agreement with the experimental values. The theoretical calculations nicely reproduce the large N1-C1'- H_β hyperfine coupling, which indicates the significant spin density on N1. The theoretical calculations do not, however, reproduce the small C4-NH $_\alpha$ couplings determined experimentally. Overall, the agreement between the theoretical and experimental results is rated as fair in Table 1.

sites	Principle values	Isotropic values	Dipolar Values	Computational Isotropic	Computational Dipolar
C5-H	-62.6 -42.9 -18.0	-41.2	-21.4 -1.7 23.1	-32.9	20.4 -1.4 21.8
N1-C1'-H	46.8 39.5 39.5	41.9	-2.4 -2.4 4.8	40.6	-3.4 0.7 4.1
C4-NH1	-18.6 -16.4 -2.3	-12.4	-6.2 -4.0 10.2	-0.9	-1.3 -1.0 2.3
C4-NH2	-24.5 -16.8 -2.3	-14.5	-10.0 2.3 12.3	0.1	-1.9 -1.8 3.7

Table 4. Comparison of HFCC values between the experimental values of the N3 deprotonated 5'-dCMP cation in 5'-dCMP Monohydrate single crystal and the calculated value of 1-Methyl cytosine cation in gas phase by Wetmore *et al.*, at PWP86/6-311G(2d,p) level of theory.²⁰

2.2.4. N7-H, O6-H Protonated 5'-GMP Anion

The nucleotide of Guanine 5'-Monophosphate (5'-GMP) single crystal structure³⁶ demonstrates a zwitterion property with the N7 site of the guanine base being protonated. Three water molecules form a hydration bridge between the protonated N7 site and a phosphate group oxygen through Hydrogen bonding. A very complex H-bonding network is formed among 5'-GMP molecules and water molecules. It is worth mentioning that the protonation site of the guanine base is directly H-bonded with a H₂O instead of an anionic phosphate oxygen atom as is

usually observed in nucleotide zwitterions. Experimentally, the N7-H, O6-H protonated GMP anion is characterized by $\rho(\text{C8})=0.28$, $\rho(\text{N1})=0.15$ and $\rho(\text{N7})=0.11$. Wetmore et al.¹⁶ conducted gas phase calculations on N7-H, O6-H protonated 5'-GMP anion by substituting the ribose and phosphate group with a hydrogen atom. The full relaxed optimization results in the H which is attached to O6 bending out of the guanine plane with the N1-C6-O6-H torsion angle greater than 70°. It also results in extremely large O6-H coupling, which is very small in the experiment. Constraints on O6-H are made to remain a planar structure. It is calculated that the planar radical lies only 1.7 kcal/mol above in energy higher than the non-planar radical, which indicates that the orientation of O6-H is highly subjective to the influence of the electrostatic environment in the crystal structure. Table 5 shows the detailed HFCC comparison among the experimentally determined N7-H, O6-H protonated 5'-GMP anion values within the 5'-GMP single crystal structure, and the calculated values of the planar and non-planar N7-H, O6-H protonated guanine anion in gas phase, by Wetmore et al. at PWP86/ 6-311G(2d,p) level of theory. The spin densities agreement level with experimental values for the planar structure is improved from its non-planar counterpart, which is indicated by the planar structure's small O6-H isotropic coupling and good agreements of N1-H and N7-H isotropic couplings. However, the planar structure's isotropic and anisotropic hyperfine couplings that relate to the main spin density site, C8, is still very different from experimental results. The overall HFCC agreement for the planar structure is rated as fair in Table 1.

Due to a mistake of lacking diffuse functions in basis set in all the geometry optimizations for the N7-H, O6-H protonated 5'-GMP anion radical system, the calculated HFCC results are expected to be inaccurate and will not be presented in the following text. But a detailed description of the optimized anion radical geometries without using diffuse functions will be described in the appendix. All the calculated single point data will be included in the supplementary materials.

sites	Principle values	Isotropic values	Dipolar Values	Computational Isotropic (Planar)	Computational Isotropic (Non-planar)	Computational Dipolar
N1				1.2	5.4	
N3				2.1	2.7	
N1-H	-17.6 -12.0 -1.2	-10.3	-7.3 -1.7 9.0	-8.6	-0.6	-7.5 -2.8 10.3
N2-H1				0.0	-0.5	

N2-H2				-0.1	-0.1	
N7-H	-13.9 -12.1 -2.0	-9.3	-4.6 -2.8 7.4	-8.0	-5.9	-4.9 -3.3 8.2
C8-H	-30.1 -21.2 -9.3	-20.2	-9.9 -1.0 10.9	-35.3	-32.6	-19.6 1.7 17.9
N9-H				2.5	2.5	
O6-H	5.5 1.4 -3.4	1.2	4.3 0.2 -4.5	4.7	60.5	-5.9 -3.5 9.4

Table 5. HFCC comparison among the experimentally determined N7-H, O6-H protonated 5'-GMP anion values within the 5'-GMP single crystal structure, and the calculated values of the planar and non-planar N7-H, O6-H protonated guanine anion in gas phase, by Wetmore et al. at PWP86/ 6-311G(2d,p) level of theory.²⁰

Chapter 3 Methods

All the calculations in this present work are performed with the Gaussian 09 program³⁷. An overview of the equation used for evaluating the different components of the diagonalized hyperfine interaction tensor within the density functional theory (DFT) framework, and their performance, have been presented by Malkin et al.³⁸ and by Barone.³⁹

The initial geometry parameters for geometry optimization are adopted directly from crystal structures determined by X-ray diffraction techniques.^{31, 32, 36, 40, 41} Two-layer ONIOM method is applied for geometry optimizations. The radicals of interest, i.e., the deprotonated cation or the protonated anion, are set as model system and are fully relaxed. Atoms, including the deprotonated proton from the cation radical, in the surrounding environment as parts of the real cluster system are fixed in their Cartesian coordinates. Frequency calculations are conducted to ensure the structures of the model systems were local minima on potential energy surfaces. Here, one probably will question the legitimacy of partitioning the deprotonated site and protonated site into two ONIOM layers and freezing the deprotonated hydrogen in the cation radical system. The reason for doing this is because we cannot simulate effective proton shuttling paths⁴² within our simulation due to limited system sizes. An effective shuttling requires three components, a proton donor (the cation radical), a path to transfer proton (the chain reaction path), and a final proton acceptor (the anion radical). In our simulation jobs, we put either a single cation or anion radical in each job. The direct proton acceptor near a cation radical or the direct proton donor near an anion radical will be rendered as unstable cation or anion due to the lack of effective shuttling mechanisms; and the expected protonation procedure is prone to be reversed. The above mentioned constraints are added in order to reproduce experimental conditions.

Subsequently, single point calculations are carried out on models of different levels of completeness that are extracted from the optimization jobs, from single radicals in gas phase, to partially including the H-bonding environment, to finally including the complete H-bonding environment. These single point calculations are conducted with M05/6-2X, B3LYP (or B3PW91) functionals. Upon all the optimization calculations, direct inversion in the iterative subspace (GDIIS)⁴³ has been implemented when relatively flat regions of the potential energy surface are encountered. The detailed calculation procedures are as follows:

Single cytosine and guanine radicals are small compared with 5'-dCMP and 5'-GMP radicals. Thus, more complete environmental effects for the model radical are included for geometry optimizations of the N1 deprotonated cytosine cation and the native guanine cation. For the N1 deprotonated cytosine cation within cytosine monohydrate single crystal, the nearest 7 cytosine base molecules and all the nearby water molecules around the radical, are included in its geometry optimization job at ONIOM(uB3LYP/aug-cc-pvtz:uB3LYP/3-21+g*) level of theory. The native guanine cation radical is optimized within two different scales of system within the Guanine Hydrochloride Monohydrate single crystal environment. Here we refer these two optimizations as Gm-Opt-1 and Gm-Opt-2. The Gm-Opt-1 optimization includes the N7-deprotonated guanine cation radical, its eight nearest chloride ions, and the O-6 protonated guanine cation; this system is optimized on ONIOM(B3LYP/6-31+g(d):hf/6-31+g(d)) level of theory. The Gm-Opt-2 optimization includes another 5 nearest guanine bases based on the Gm-Opt-1 system, and it is optimized on ONIOM(B3LYP/6-31+g(d):B3LYP/3-21g) level of theory.

Similarly, two optimizations with different system scale are carried out for the N3 deprotonated 5'-dCMP cation radical within the 5'-dGMP Monohydrate single crystal environment. Here we refer these two optimizations as 5'-dCMP-Opt-1 and 5'-dCMP-Opt-2. The 5'-dCMP-Opt-1 optimization includes the N3-deprotonated radical, the corresponding OIII protonated cation, and waters and another three 5'dCMP molecules that covers all H-bonding environmental effects of the model radical. The 5'-dCMP-Opt-2 optimization further includes another eight 5'dCMP molecules to give a more complete electrostatic environment. Both the 5'-dCMP-Opt-1 and the 5'-dCMP-Opt-2 systems are optimized on ONIOM(uB3LYP/6-31+g(d):uB3LYP/3-21g) level of theory.

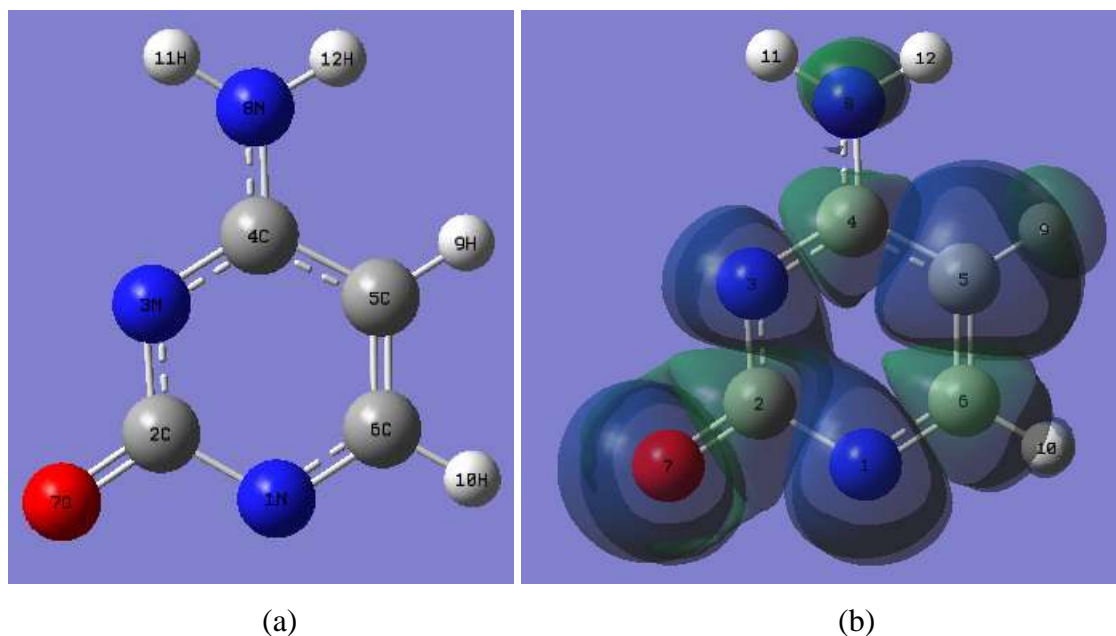
For the calculations on the N7-H, O6-H protonated 5'-GMP anion radical within the 5'-GMP single crystal structure, whose uniqueness resides on its large Hydrogen bonding networks within the crystalline structure, both 3-layer and 2-layer ONIOM optimizations are carried out at systems with various sizes. The aim of these optimizations is to find an effective yet less computationally demanding way to treat systems with such a large scale of Hydrogen bonding interactions. These optimizations are on ONIOM(uB3LYP/6-31g(d):uB3LYP/3-21g) or ONIOM(uB3LYP/6-31g(d):uB3LYP/3-21g:PM6) levels of theory, where the PM6 semi-empirical method is developed to improve its performance on H-bonds.⁴⁴ London dispersion

energy plays a key role in determining the biomolecular as well as crystal system. While, in the present case, London dispersion may not be as significant among the Van der Waals forces as the interactions involving molecular dipoles or ionic charges, it should be important for such a long range interaction to decide H-bonding structures, especially when all surrounding molecules, which forms Hydrogen bonds with the model radical, are frozen. However, calculations by Cerny and coworkers⁴⁵ have shown that current hybrid DFT methods fail to describe the dispersion energy. As a result, they fail to describe base stacking or the interaction of amino acids in the crystal geometry. M052x do not model the asymptotic dipolar nature of dispersive interactions explicitly. As a result, although M05/62x functionals demonstrate significant improvements over traditional density functionals in describing the medium-range part of non-covalent interactions,⁴⁶ their incapability to describe non-covalent interactions at lone range (>6 Å) limit its use in describing dispersive interactions, which is inherently long range electron correlation effect.⁴⁷ So, in our future work in examining environmental effects on accurate HFCC calculations, we might choose the long range corrected functionals for the real system or the inter-median system, and M06-2X for the model system. However, it is interesting to notice that, as demonstrated by Polo et al.⁴⁸, the traditional DFT's exchange self-interaction error did mimic long range (non-dynamic) pair correlation effects.

Chapter 4 Results and Discussions

4.1. N1-deprotonated Cytosine Cation Radical in Cytosine Monohydrate Single Crystal

In the cytosine monohydrate single crystal structure, the N1-H and N3 sites of a cytosine molecule form H-bonds with nearby cytosine bases at N3 and N1-H sites respectively, within one parallel cytosine ribbon. The C2-O forms three bonds in an approximately tetrahedral form with two water molecules (above and below the ribbon) and an amino group (within the ribbon). This strong H-bonding effect of the carboxyl group may account for its C-O bond length, which is 0.04 Å greater than the average value of 1.22 Å found in other pyrimidines.²⁶ One of the two H atoms on the N4 site (amino group) is H-bonded to a neighboring C6-O, and the other H atom is H-bonded to an H₂O molecule within the ribbon crystalline structure. In the cytosine monohydrate single crystal, there are 0.03-0.04 Angstrom deviations of C5, N1 and O2 from its ring plane for each cytosine base molecule. The amino nitrogen and carbonyl oxygen atoms are displaced below and above the plane. Geometry optimization of the N1 deprotonated cytosine cation radical demonstrates that the bond lengths of the radical remain almost unchanged after optimization. The major bond angle change within the radical's ring comes from C2-N1-C6, which decreases by 4.42°, while angle N3-C2-N1 increasing by 3.44°. The non-planar feature of the cytosine ring remains after the optimization. In particular, the H atom on C5 deviates above the plane at a dihedral angle of 172.7 degrees (with respect to N3 and N1). This small deviation from the single occupied molecular orbital (SOMO) nodal plane will result in small delocalization contributions to the spin density at C5-H, which further contributes to its HFCC value.



Figurer. 3 (a)Isolated N1-deprotonated cytosine cation radical, (b) The spin density of N1-deprotonated cytosine cation radical calculated at M062x/6-311+g(d,p) level of theory (isoval=0.0004)

Cm	N1	C2	O2	N3	C4	N4	C5	C6
Experiment	0.30						0.57	
Wetmore	0.29		0.35				0.49	
ub3lyp/6-311+g(d,p)	0.35	-0.14	0.47	0.13	-0.11	0.00	0.49	-0.18
m052x/6-311+g(d,p)	0.40	-0.20	0.50	0.15	-0.11	-0.01	0.50	-0.21
m062x/6-311+g(d,p)	0.37	-0.18	0.51	0.15	-0.12	-0.01	0.50	-0.19
m052x/aug-cc-pvtz	0.37	-0.12	0.46	0.14	-0.06	0.00	0.30	-0.11
m062x/aug-cc-pvtz	0.39	-0.14	0.47	0.16	-0.17	-0.01	0.58	-0.28
ub3lyp/epr-II	0.33	-0.12	0.47	0.12	-0.07	-0.01	0.44	-0.15
ub3lyp/epr-III	0.33	-0.10	0.45	0.12	-0.07	0.00	0.44	-0.15
m052x/epr-II	0.38	-0.18	0.50	0.14	-0.10	-0.01	0.50	-0.21
m052x/epr-III	0.36	-0.14	0.48	0.13	-0.11	-0.01	0.47	-0.18
m062x/epr-II	0.35	-0.16	0.50	0.14	-0.10	-0.01	0.48	-0.18
m062x/epr-III	0.39	-0.19	0.50	0.14	-0.10	-0.02	0.47	-0.20

Table 6. The Mulliken spin populations on the isolated N1-deprotonated cytosine cation radical.

Cm	C5-H		N4-H1		N4-H2		N1		N3		N4		C6-H	
	isotropic	dipolar	isotropic	dipolar	isotropic	dipolar	isotropic	dipolar	isotropic	dipolar	isotropic	dipolar	isotropic	dipolar
Experiment		-21.00		-9.30		-6.20								
	-41.40	-0.80	-14.30	-1.80	-13.00	-3.60								
		22.80		11.10		9.80								
Wetmore		-19.70		-1.30		-1.90								
	-30.70	-0.40	-1.10	-0.80	-0.90	-1.50								
		20.10		2.10		3.40								
ub3lyp/6-311+g(d,p)		-17.53		-1.19		-1.83								
	-27.47	-0.97	-0.61	-0.72	0.11	-1.65	8.89	-14.64	2.61	-5.23	-0.28	0.17	7.23	-3.70
		18.49		1.91		3.49		29.55		10.59		0.44		4.46
m052x/6-311+g(d,p)		-18.34		-1.11		-2.38		-15.68		-5.83		-1.50		-3.74
	-31.38	-1.12	0.27	-0.97	0.97	-1.74	10.41	-15.39	4.27	-5.70	-0.59	0.59	10.90	-2.16
		19.46		2.08		4.12		31.07		11.53		0.91		5.90
m062x/6-311+g(d,p)		-17.26		4.69		-2.40		-14.00		-5.66		-1.61		-3.39
	-31.78	-2.00	0.36	-1.02	1.13	-1.66	15.69	-13.68	7.14	-5.45	-0.81	0.66	7.47	-1.30
		19.26		2.19		4.05		27.68		11.10		0.96		4.69
m052x/aug-cc-pvtz		-18.91		-1.13		-2.11		-15.93		-5.60		-1.00		-4.03
	-33.15	0.01	-0.34	-0.77	0.60	-1.91	20.34	-15.55	6.62	-5.41	-0.34	0.33	11.10	-1.87
		18.90		1.90		4.01		31.49		11.01		0.67		5.90
m062x/aug-cc-pvtz		-17.78		-1.07		-2.14		-14.15		-5.42		-1.17		-3.54
	-32.38	-1.61	-0.19	-0.91	0.83	-1.84	25.43	-13.80	9.09	-5.17	-0.52	0.42	6.65	-1.06
		19.39		1.99		3.97		27.95		10.59		0.74		4.60
ub3lyp/epr-II		-17.50		-1.15		-1.86		-14.55		-5.29		-0.74		-3.69
	-29.15	-1.00	-0.54	-0.79	0.19	-1.73	10.89	-14.29	3.34	-5.17	-0.48	0.24	7.72	-0.78
		18.50		1.94		3.59		28.83		10.46		0.50		4.46
ub3lyp/epr-III		-17.60		-1.17		-1.91		-15.47		-5.43		-0.50		-3.89
	-29.10	0.04	-0.86	-0.72	-0.04	-1.56	11.32	-15.09	3.36	-5.26	-0.32	0.12	7.68	-0.48
		17.55		1.88		3.47		30.56		10.69		0.39		4.38
m052x/epr-II		-18.51		-1.13		-2.49		-15.17		-5.54		-1.49		-3.78
	-25.09	-1.11	0.06	-0.99	0.55	-1.71	13.75	-14.89	5.22	-5.40	-0.83	0.58	9.06	-2.17
		19.62		2.12		4.20		30.06		10.94		0.91		5.95
m052x/epr-III		-18.59		-1.11		-2.16		-16.22		-5.74		-1.14		-3.86
	-27.89	-0.36	-0.38	-0.83	0.26	-1.86	17.13	-15.87	5.48	-5.56	-0.39	0.40	9.66	-1.87
		18.95		1.94		4.02		32.09		11.31		0.74		5.73
m062x/epr-II		-17.44		-1.22		-2.49		-13.62		-5.43		-1.60		-3.49
	-34.07	-1.88	0.30	-1.00	1.15	-1.65	18.57	-13.36	7.95	-5.22	-1.00	0.64	7.90	-1.24
		19.32		2.21		4.13		26.97		10.65		0.96		4.73
m062x/epr-III		-17.71		-1.09		-2.22		-14.39		-5.56		-1.33		-3.43
	-33.15	-1.70	-0.08	-0.97	0.87	-1.77	21.71	-14.05	8.11	-5.32	-0.68	0.51	6.87	-1.13
		19.41		2.05		3.99		28.44		10.88		0.82		4.56

Table 7. The calculated HFCC of the isolated N1-deprotonated cytosine cation radical.

Figure. 3 shows the spin density of the optimized N1-deprotonated cytosine cation radical. Table 6 and Table 7 show B3LYP and M05/6-2X single point calculation results on the spin densities and HFCC with three levels of basis sets, namely, the split valence basis set 6-311+g(d,p), EPR-II/III basis sets, which are optimized for the computation of hyperfine coupling constants by DFT methods (particularly B3LYP), and augmented triple-zeta correlation consistent basis sets aug-cc-pvtz. All the chosen method/basis sets combinations give similar spin density distributions that are very different from the experimental pattern. No obvious advantages of M05/6-2X functionals and aug-cc-pvtz basis set are shown for both spin density and hyperfine couplings results. All single point calculations give acceptable spin densities at the main spin density sites C5 and N1, however, small spin densities at C2 and C6 are also present, which are not detected from experiment. No experimental data from isotope O(17) are provided

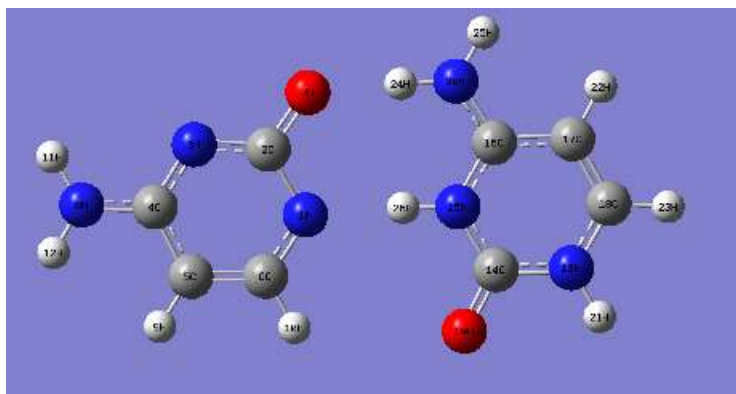
to compare the calculated spin density at O2. Most of the calculated isotropic hyperfine couplings on C5-H are about 10 MHz too weak compared with the experimental value of -41.5 MHz, though the calculated anisotropic hyperfine couplings are close to experimental values. The best calculated isotropic HFCCs at C5-H are given by M06-2X/EPR-II/III and M05-2X/aug-cc-pvtz, which are about 7 MHz weaker than -41.5 MHz. Besides, all calculations give negligible isotropic hyperfine couplings at the amino group hydrogen atoms. Non-negligible amount of hyperfine couplings are calculated at C6-H, whereas the experiment does not detect noticeable values at this site. Thus, we can come to the conclusion that, all the tested jobs' performance on the isotropic hyperfine coupling can be rated as poor for isolated N1-deprotonated cytosine cation radical.

Let's consider a larger scale of system size that includes environmental effects for the single point calculation. As shown in Figure. 4, the N3-protonated cytosine cation, which accepts the proton deprotonated from the radical's N1 site, is included that forms N3-H...N1 and N4-H...O6 H-bonds with the radical. The σ -orbital components shown in the spin density distribution at the radical's N1 and O2 sites, along their H-bonding direction, indicate the polarization contribution to the spin density due to the H-bonding effect. From Figure. 4 (b), we can see that all the single point calculations demonstrate localized spin density distribution at the cytosine radical. In Table 8, the spin density at C5 is in excellent agreement with the experimental value for all the M05/6-2X calculations as well as the B3LYP/6-311+g(d,p) calculation. The inclusion of N1...H-N3 does not improve the small overestimation of spin density at the N1 site, while, the density at O2 is suppressed due to the O...H-N4 hydrogen bonding by about 30% from 0.48 to about 0.34.

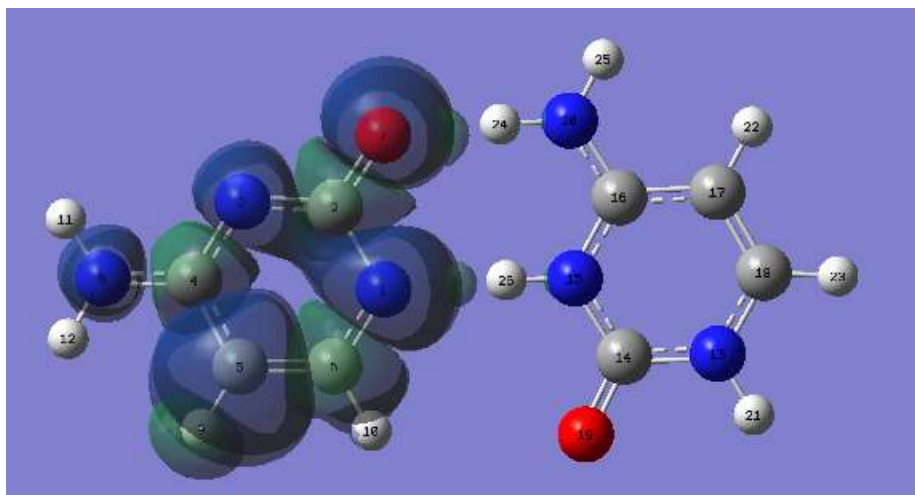
As can be seen in Table 9, the advantage of M06-2X functional over the B3LYP and M05-2X functionals shows up where M06-2X gives excellent isotropic and anisotropic hyperfine couplings at the C5-H site. Take the B3LYP/6-311+g(d,p) and the M06-2X/6-311+g(d,p) in Table 8 and Table 9 for example, both these two jobs calculated similar spin densities at the radical's C5 site at values 0.57 and 0.58 in respect. However, the B3LYP/6-311+g(d,p) calculated the iHFCC value at C5-H as -32.50 MHz, which is much lower than the corresponding M06-2X value, -40.54 MHz. This can be explained as follows: B3LYP hybridizes 20% Hartree-Fock exchange components in its exchange-correlation functional, while it is 54%

for M06-2X functional. Higher percentage of the exact exchange functional allow M06-2X functional to give better description, in this case, a description of stronger exchange interaction between the spin density at C5 and the parallel electron in C5-H bond. As a result, M06-2X functional calculated a stronger polarization contribution to the spin density at H atom at C5 than B3LYP functional, based on the similar spin densities at C5 site, and thus results in the difference in calculated iHFCCs at C5-H. However, as mentioned in the introduction section, cautions should be made for this analysis when using the spin population data instead of using the real spin density at the nuclei. Besides, we should not over credit the excellent agreement of M06-2X calculated HFCCs at the C5-H site with the experimental value, considering the incompleteness of environmental effects and poor its performance at amino group, as shown in Table 9.

Though small improvements are achieved at the calculated N4-H1 and N4-H2 isotropic HFCC, they are still generally underestimated by about 10 MHz by all tested jobs. Due to the significant change in spin densities at O2 through including one of its three H-bonds, let us consider further include the other two water molecules near O2 for a more complete H-bonding environment, as shown in Figure. 5.



(a)



(b)

Figure. 4 (a) the N1-deprotonated cytosine cation radical H-bonds with the N3-protonated cytosine cation, (b) The spin density of this bi-molecule system calculated at M062x/6-311+g(d,p) level of theory (isoval=0.0004)

Cm	N1	C2	N3	C4	C5	C6	O2	N4
Experiment	0.30				0.57			
Wetmore	0.29				0.49		0.35	
ub3lyp/6-311+g(d,p)	0.37	-0.10	0.08	-0.09	0.57	-0.17	0.35	0.04
ub3lyp/epr-II	0.34	-0.08	0.07	-0.06	0.51	-0.13	0.34	0.04
ub3lyp/epr-III	0.34	-0.06	0.07	-0.05	0.50	-0.13	0.33	0.04
um052x/6-311+g(d,p)	0.39	-0.12	0.08	-0.07	0.58	-0.19	0.33	0.03
um052x/epr-II	0.37	-0.10	0.07	-0.08	0.59	-0.18	0.32	0.04
um052x/epr-III	0.35	-0.10	0.07	-0.08	0.50	-0.09	0.31	0.05
um062x/6-311+g(d,p)	0.38	-0.12	0.08	-0.09	0.58	-0.17	0.36	0.03
um062x/epr-II	0.36	-0.10	0.08	-0.08	0.58	-0.17	0.34	0.03
um062x/epr-III	0.39	-0.15	0.06	-0.08	0.56	-0.17	0.35	0.03

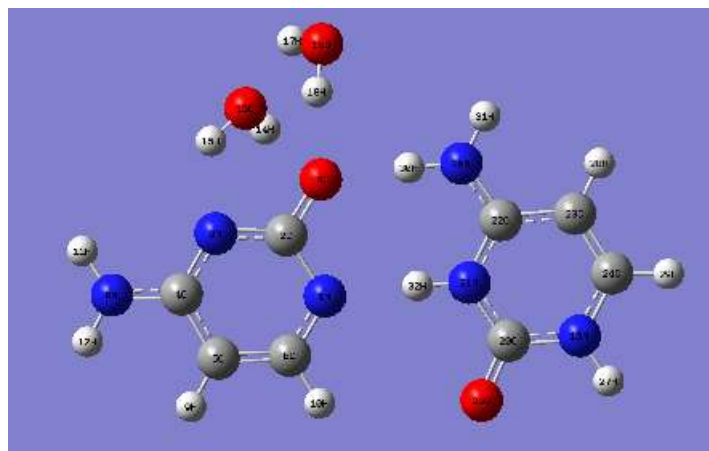
Table 8. The calculated Mulliken spin populations on the N1-deprotonated cytosine cation radical when it is H-bonded to the N3-protonated cytosine cation.

Cm	C5-H		N4-H1		N4-H2		N1		N3		N4		C6-H	
	isotropic	dipolar	isotropic	dipolar	isotropic	dipolar	isotropic	dipolar	isotropic	dipolar	isotropic	dipolar	isotropic	dipolar
Experiment		-21.00		-9.30		-6.20								
	-41.40	-0.80	-14.30	-1.80	-13.00	-3.60								
		22.80		11.10		9.80								
Wetmore		-19.70		-1.30		-1.90								
	-30.70	-0.40	-1.10	-0.80	-0.90	-1.50								
		20.10		2.10		3.40								
ub3lyp/6-311+g(d,p)		-20.08		-2.23		-2.55		-14.84		-2.97		-1.90		-3.97
	-32.50	-1.89	-3.86	-1.60	-2.74	-0.59	9.76	-14.81	1.23	-2.87	1.27	-1.56	6.03	-0.26
		21.97		3.83		3.15		29.65		5.84		3.46		4.24
ub3lyp/epr-II		-20.03		-2.13		-2.51		-14.57		-2.91		-1.79		-3.97
	-34.53	-1.94	-3.91	-1.57	-2.74	-0.60	11.93	-14.50	1.62	-2.82	1.37	-1.44	6.50	-0.27
		21.97		3.70		3.12		29.06		5.72		3.23		4.24
ub3lyp/epr-III		-20.12		-2.42		-2.55		-15.43		-2.95		-2.08		-4.10
	-34.39	-0.81	-4.26	-1.48	-2.98	-0.58	12.34	-15.34	1.55	-2.83	1.55	-1.72	6.42	-0.12
		20.93		3.90		3.13		30.77		5.78		3.80		4.22
um052x/6-311+g(d,p)		-21.71		-2.15		-2.73		-15.44		-2.86		-1.76		-4.12
	-39.81	-2.31	-4.13	-1.67	-2.99	-0.59	11.91	-15.02	1.90	-2.81	2.51	-1.36	9.40	-1.55
		24.03		3.82		3.32		30.46		5.67		3.12		5.66
um052x/epr-II		-21.93		-2.14		-2.71		-14.85		-2.67		-1.70		-4.15
	-33.57	-2.41	-3.72	-1.64	-2.73	-0.62	15.02	-14.53	2.27	-2.62	2.60	-1.29	8.15	-1.56
		24.34		3.78		3.33		29.38		5.29		2.98		5.71
um052x/epr-III		-21.82		-2.56		-2.83		-15.91		-2.67		-2.12		-4.15
	-36.96	-1.60	-4.44	-1.63	-3.29	-0.50	17.66	-15.48	2.17	-2.58	2.60	-1.72	8.45	-1.39
		23.42		4.19		3.32		31.40		5.25		3.84		5.54
um062x/6-311+g(d,p)		-20.99		-1.67		-2.56		-14.14		-3.07		-1.28		-3.87
	-40.54	-3.05	-3.28	-1.51	-1.97	-0.81	17.72	-13.63	3.90	-2.88	2.16	-0.91	5.82	-1.12
		24.04		3.18		3.37		27.77		5.95		2.19		4.99
um062x/epr-II		-21.16		-1.67		-2.56		-13.69		-2.90		-1.26		-3.96
	-43.84	-3.04	-3.57	-1.49	-2.13	-0.85	20.38	-13.28	4.22	-2.75	2.24	-0.87	6.15	-1.06
		24.20		3.16		3.40		26.97		5.64		2.12		5.02
um062x/epr-III		-21.41		-2.02		-2.70		-14.49		-2.85		-1.61		-3.88
	-43.07	-2.82	-4.27	-1.54	-2.67	-0.62	22.55	-13.99	3.96	-2.65	2.45	-1.23	5.21	-0.99
		24.22		3.56		3.32		28.48		5.50		2.83		4.88

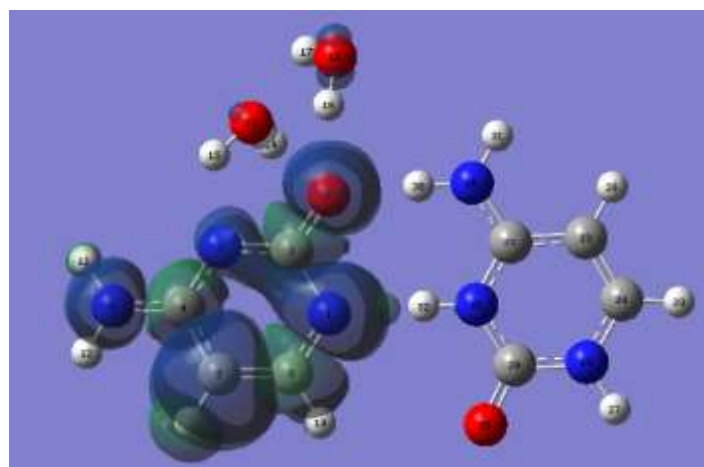
Table 9. The calculated HFCC on the N1-deprotonated cytosine cation radical when it is H-bonded to the N3-protonated cytosine cation.

As shown in Table 10, the introduction of another two O \cdots H-O Hydrogen bonds at the radical's O2 site further suppresses spin density at O2 by about 30% from about 0.34 to about 0.25 in all tested jobs. Meanwhile, small amount of spin densities delocalize to the two water molecules. This should be partially responsible for the delocalization error of DFT approximations from a mathematical viewpoint. But this might also accounts for a underlying mechanism which is similar to the Hydrogen bond cooperativity in water dimer,⁴⁹ where the water molecule that donating its H atom has electron density increased in its lone-pair region and has the electron density decreased at its oxygen atom which accepts the H atom. The decrease of the spin density at O2 leads to a decrease of its spin polarization contribution to the spin density at C2, as demonstrated from Table 10 and Table 11, as compared with Table 8 and Table 9. Meanwhile, in Figure. 5(b), the disappearance of σ component of O2 spin density in the direction towards N4-H1 reflects a counter balance effect upon the polarization contribution imposed by the tetrahedral H-bond conformation. Following the same idea, as shown in Figure. 6, we further

include an H₂O that forms an H-bond with N₄-H. Now, N₄ becomes a donor in the H-bond, and it gains spin densities as can be seen from Table 12, when comparing the calculated spin densities in Table 10. This stronger exchange interaction leads to an increase in the N₄'s polarization contribution to the spin densities at N₄-H₁ and N₄-H₂, and results in an increase in the calculated hyperfine coupling constants on these two H atoms, which are approaching to their experimental values. C₅ gains a little extra spin densities as calculated for the systems in Figure. 5 and Figure. 6, which corresponds to the increases in C₅-H hyperfine couplings, especially by M05/6-2X method. By comparing the M05-2X and M06-2X functionals from these two tables, it is obvious that, though they give similar spin densities and anisotropic hyperfine couplings at C₅-H and N₁ sites, M06-2X tends to give greater hyperfine couplings than does M05-2X functional. It is noticeable, in Table 11 and Table 13, that by combining with M05-2X functional, EPR-II basis set keeps underestimating the C-5 isotropic hyperfine couplings by about 5 MHz comparing with M05-2X's combinations with 6-311+g(d,p) and EPR-III basis sets, though similar spin densities and anisotropic hyperfine couplings are achieved all these three combinations. This reflects that the M05-2X functional might be less tolerant with small basis sets in iHFCC calculations when compared with B3LYP and M06-2X functionals. However, in both systems in Figure. 5 and Figure. 6, the issue with overestimated N₁ spin density remains unresolved by adding additional water molecules. With the attempt of tackling this unexpected big spin density issue, we further complete the H-bonding environment for the N₃-protonated cytosine, i.e., by adding two H₂O to its O₂ site, in hoping that this could influence the calculated interactions between the radical and the protonated base. However, no obvious difference in calculated spin densities and HFCCs is observed when we compare the data listed in Table 14 and Table 15 with those listed in Table 12 and Table 13. Up to this point, all of our single point calculations demonstrate localized spin density distribution properties on the radical.



(a)



(b)

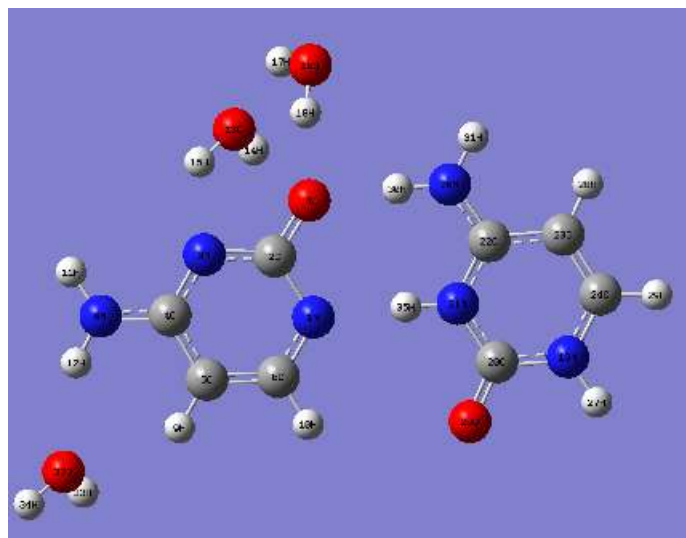
Figure. 5 (a) the N1-deprotonated cytosine cation radical H-bonding to the N3-protonated cytosine cation and two water molecules at C2-O site (b) The spin density of) the N1-deprotonated cytosine cation radical H-bonding to the N3-protonated cytosine cation and two water molecules at C2-O site, calculated at M062x/6-311+g(d,p) level of theory (isoval=0.0004)

Cm	N1	C2	N3	C4	C5	C6	O2	N4
Experiment	0.30				0.57			
Wetmore	0.29				0.49		0.35	
ub3lyp/6-311+g(d,p)	0.38	-0.08	0.04	-0.08	0.58	-0.17	0.26	0.09
ub3lyp/epr-II	0.35	-0.06	0.03	-0.05	0.52	-0.13	0.26	0.08
ub3lyp/epr-III	0.34	-0.04	0.03	-0.03	0.51	-0.13	0.25	0.08
um052x/6-311+g(d,p)	0.40	-0.08	0.03	-0.05	0.60	-0.18	0.24	0.09
um052x/epr-II	0.38	-0.06	0.02	-0.07	0.61	-0.18	0.23	0.09
um052x/epr-III	0.36	-0.08	0.03	-0.05	0.51	-0.08	0.22	0.09
um062x/6-311+g(d,p)	0.38	-0.09	0.03	-0.07	0.61	-0.17	0.26	0.08
um062x/epr-II	0.36	-0.07	0.03	-0.07	0.61	-0.17	0.25	0.08
um062x/epr-III	0.40	-0.12	0.02	-0.05	0.59	-0.17	0.25	0.09

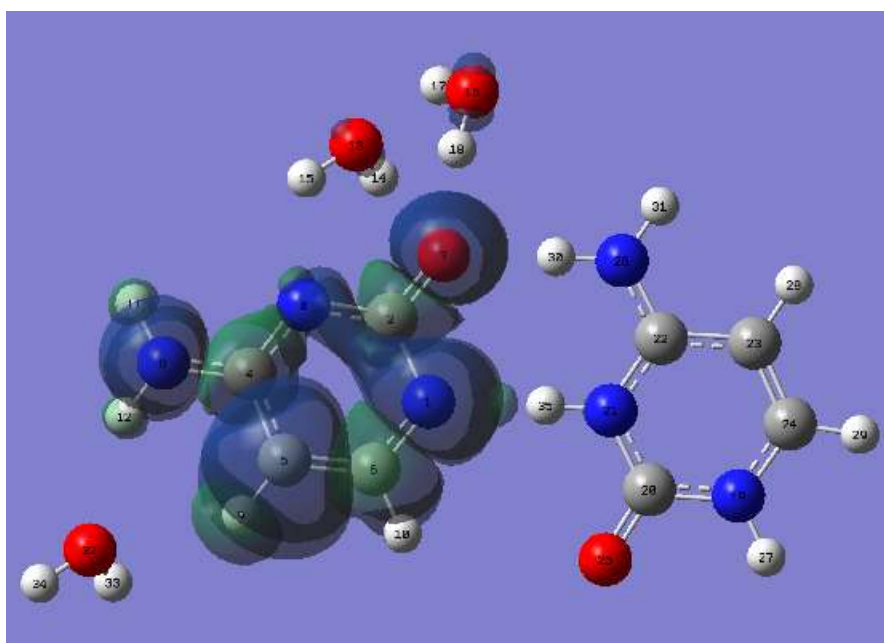
Table 10. The Mulliken spin populations on the N1-deprotonated cytosine cation radical when it is H-bonded to the N3-protonated cytosine cation and two water molecules at C2-O site.

Cm	C5-H		N4-H1		N4-H2		N1		N3		N4		C6-H	
	isotropic	dipolar	isotropic	dipolar	isotropic	dipolar	isotropic	dipolar	isotropic	dipolar	isotropic	dipolar	isotropic	dipolar
Experiment		-21.00		-9.30		-6.20								
	-41.40	-0.80	-14.30	-1.80	-13.00	-3.60								
		22.80		11.10		9.80								
Wetmore		-19.70		-1.30		-1.90								
	-30.70	-0.40	-1.10	-0.80	-0.90	-1.50								
		20.10		2.10		3.40								
ub3lyp/6-311+g(d,p)		-20.57		-5.03		-3.22		-15.30		-1.20		-4.21		-4.07
	-33.74	-2.22	-7.40	-2.10	-6.04	-2.08	10.10	-15.23	0.09	-1.07	3.06	-3.83	5.95	-0.33
		22.79		7.13		5.30		30.54		2.27		8.04		4.40
ub3lyp/epr-II		-20.29		-4.80		-3.13		-14.80		-1.17		-3.92		-4.02
	-35.46	-2.25	-7.40	-2.04	-5.99	-1.92	12.18	-14.77	0.21	-1.06	3.41	-3.56	6.33	-0.32
		22.54		6.84		5.05		29.57		2.23		7.48		4.34
ub3lyp/epr-III		-20.61		-5.06		-3.08		-15.84		-1.27		-4.29		-4.20
	-35.68	-1.12	-7.64	-1.84	-6.09	-2.03	12.72	-15.80	0.22	-1.12	3.54	-3.91	6.32	-0.19
		21.73		6.90		5.11		31.64		2.39		8.20		4.39
um052x/6-311+g(d,p)		-22.47		-5.27		-3.59		-15.78		-0.92		-4.27		-4.26
	-42.04	-2.79	-8.82	-2.35	-7.40	-1.77	11.95	-15.33	0.19	-0.82	5.92	-3.84	9.18	-1.59
		25.26		7.62		5.36		31.10		1.74		8.11		5.85
um052x/epr-II		-22.65		-5.17		-3.52		-15.15		-0.84		-4.02		-4.29
	-35.66	-2.90	-7.71	-2.28	-6.31	-1.68	15.10	-14.83	0.26	-0.77	6.23	-3.58	8.05	-1.60
		25.55		7.45		5.21		29.98		1.61		7.60		5.89
um052x/epr-III		-22.45		-5.35		-3.51		-16.12		-0.91		-4.41		-4.27
	-39.06	-2.04	-8.22	-2.14	-6.69	-1.76	17.81	-15.68	0.23	-0.80	5.44	-3.98	8.26	-1.41
		24.49		7.50		5.27		31.80		1.72		8.39		5.68
um062x/6-311+g(d,p)		-22.15		-4.78		-3.46		-14.48		-1.02		-3.80		-4.05
	-43.54	-3.50	-7.79	-2.22	-6.20	-1.48	17.94	-13.94	0.93	-0.83	6.20	-3.38	5.44	-1.32
		25.65		7.00		4.94		28.42		1.85		7.18		5.37
um062x/epr-II		-22.26		-4.68		-3.41		-14.02		-0.96		-3.61		-4.13
	-47.01	-3.52	-8.16	-2.17	-6.48	-1.41	20.60	-13.58	0.97	-0.80	6.46	-3.19	5.71	-1.26
		25.78		6.86		4.82		27.60		1.77		6.80		5.39
um062x/epr-III		-22.38		-4.89		-3.48		-14.72		-1.00		-3.92		-4.05
	-46.08	-3.24	-8.57	-2.10	-6.78	-1.48	22.84	-14.20	0.90	-0.80	6.06	-3.51	4.68	-1.19
		25.63		7.00		4.96		28.92		1.80		7.43		5.23

Table 11. The calculated HFCC on the N1-deprotonated cytosine cation radical when it is H-bonded to the N3-protonated cytosine cation and two water molecules at C2-O site.



(a)



(b)

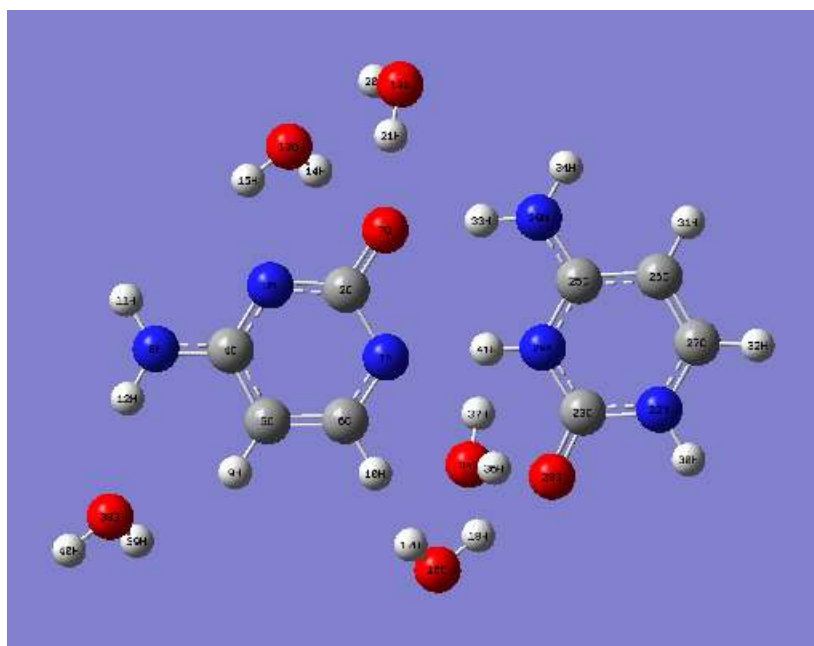
Figure. 6 (a) the N1-deprotonated cytosine cation radical H-bonding with the N3-protonated cytosine cation, two water molecules at its C2-O site, and one water molecule at its N4-H1 site (b) The spin density of the system in Figure. 6 (a) as calculated at M062x/6-311+g(d,p) level of theory (isoval=0.0004)

Cm	N1	C2	N3	C4	C5	C6	O2	N4
Experiment	0.30				0.57			
Wetmore	0.29				0.49		0.35	
ub3lyp/6-311+g(d,p)	0.39	-0.07	0.02	-0.08	0.63	-0.21	0.23	0.12
ub3lyp/epr-II	0.36	-0.05	0.01	-0.05	0.53	-0.13	0.23	0.11
ub3lyp/epr-III	0.35	-0.04	0.02	-0.03	0.52	-0.13	0.22	0.11
um052x/6-311+g(d,p)	0.40	-0.07	0.01	-0.04	0.56	-0.14	0.21	0.12
um052x/epr-II	0.38	-0.06	0.01	-0.06	0.61	-0.17	0.21	0.12
um052x/epr-III	0.37	-0.07	0.01	-0.05	0.51	-0.08	0.19	0.12
um062x/6-311+g(d,p)	0.38	-0.08	0.01	-0.07	0.62	-0.17	0.23	0.11
um062x/epr-II	0.36	-0.06	0.01	-0.07	0.62	-0.17	0.22	0.11
um062x/epr-III	0.41	-0.12	0.00	-0.05	0.60	-0.17	0.23	0.11

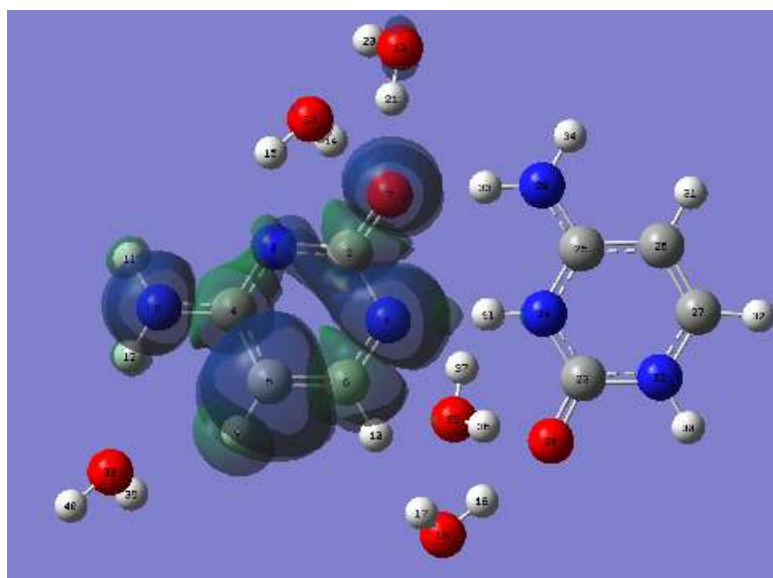
Table 12. The Mulliken spin populations on the N1-deprotonated cytosine cation radical when it is H-bonded to the N3-protonated cytosine cation, two water molecules at its C2-O site, and one water molecule at its N4-H1 site.

Cm	C5-H		N4-H1		N4-H2		N1		N3		N4		C6-H	
	isotropic	dipolar	isotropic	dipolar	isotropic	dipolar	isotropic	dipolar	isotropic	dipolar	isotropic	dipolar	isotropic	dipolar
Experiment		-21.00		-9.30		-6.20								
	-41.40	-0.80	-14.30	-1.80	-13.00	-3.60								
		22.80		11.10		9.80								
Wetmore		-19.70		-1.30		-1.90								
	-30.70	-0.40	-1.10	-0.80	-0.90	-1.50								
		20.10		2.10		3.40								
ub3lyp/6-311+g(d,p)		-20.54		-6.70		-3.72								
	-34.45	-2.29	-9.45	-2.38	-7.92	-3.28	10.41	-15.57	-0.34	-0.68	4.05	-5.55	5.74	-0.31
		22.83		9.08		7.00		31.24		1.06		10.71		4.45
ub3lyp/epr-II		-20.37		-6.58		-3.65		-15.25		-0.63		-5.31		-4.12
	-36.38	-2.35	-9.66	-2.35	-8.02	-3.20	12.64	-15.20	-0.36	-0.35	4.67	-4.93	6.13	-0.30
		22.72		8.93		6.85		30.45		0.98		10.25		4.42
ub3lyp/epr-III		-20.56		-6.63		-3.53		-16.15		-0.73		-5.57		-4.26
	-36.30	-1.19	-9.57	-2.03	-7.83	-3.11	13.05	-16.13	-0.31	-0.44	4.64	-5.19	6.09	-0.17
		21.76		8.66		6.64		32.28		1.17		10.76		4.43
um052x/6-311+g(d,p)		-22.28		-6.81		-4.00		-15.89		-0.45		-5.46		-4.30
	-42.73	-2.89	-11.01	-2.67	-9.81	-2.98	12.13	-15.43	-0.40	-0.12	7.50	-5.05	8.70	-1.52
		25.17		9.47		6.98		31.32		0.56		10.51		5.82
um052x/epr-II		-22.47		-6.78		-3.94		-15.26		-0.43		-5.21		-4.33
	-37.02	-3.02	-9.53	-2.60	-8.63	-2.94	15.32	-14.93	-0.49	-0.06	8.05	-4.79	7.49	-1.53
		25.49		9.38		6.88		30.19		0.49		9.99		5.86
um052x/epr-III		-22.28		-6.74		-3.84		-16.22		-0.46		-5.52		-4.30
	-40.16	-2.15	-9.82	-2.38	-8.74	-2.87	18.00	-15.77	-0.44	-0.14	6.85	-5.11	7.73	-1.36
		24.43		9.13		6.71		31.99		0.60		10.63		5.66
um062x/6-311+g(d,p)		-22.09		-6.38		-3.88		-14.64		-0.50		-5.02		-4.11
	-43.86	-3.59	-10.03	-2.55	-8.37	-2.67	18.20	-14.08	-0.13	-0.07	8.27	-4.61	5.17	-1.33
		25.67		8.93		6.54		28.72		0.57		9.63		5.43
um062x/epr-II		-22.20		-6.34		-3.84		-14.18		-0.48		-4.84		-4.20
	-47.79	-3.63	-10.73	-2.51	-8.85	-2.63	20.92	-13.72	-0.27	-0.03	8.76	-4.42	5.43	-1.26
		25.82		8.85		6.47		27.89		0.51		9.26		5.46
um062x/epr-III		-22.30		-6.36		-3.84		-14.86		-0.50		-5.05		-4.09
	-46.59	-3.32	-10.94	-2.38	-8.83	-2.59	23.11	-14.33	-0.21	-0.10	7.94	-4.65	4.51	-1.19
		25.61		8.74		6.42		29.19		0.60		9.70		5.29

Table 13. The calculated HFCC on the N1-deprotonated cytosine cation radical when it is H-bonded to the N3-protonated cytosine cation, two water molecules at its C2-O site, and one water molecule at its N4-H1 site.



(a)



(b)

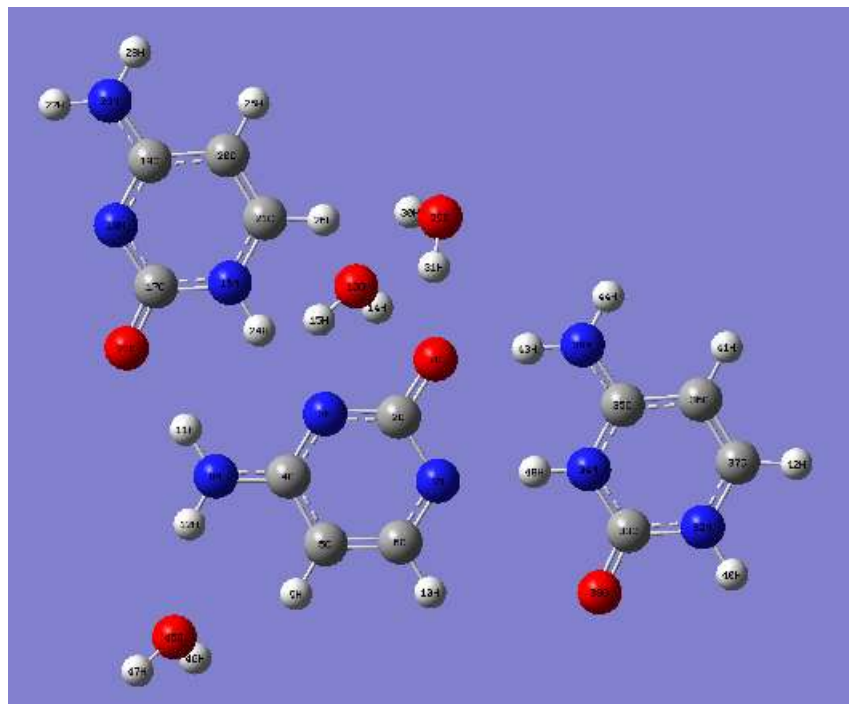
Figure. 7 (a) Two water molecules H-bonding to the protonated cytosine are included in attempt to resolve the big spin density issue at the radical's N1 site. (b) The spin density of the system in Figure. 7 (a) as calculated at M062x/EPR-III level of theory (isoval=0.0004)

Cm		N1	C2	N3	C4	C5	C6	O2	N4	Cyto2 N3	Cyto2 N3-H
Experiment		0.30				0.57					
Wetmore		0.29				0.49		0.35			
ub3lyp/6-311+g(d,p)		0.38	-0.06	0.01	-0.08	0.64	-0.20	0.21	0.14	0.00	-0.01
ub3lyp/epr-II		0.34	-0.04	0.01	-0.05	0.54	-0.12	0.21	0.13	0.00	-0.01
ub3lyp/epr-III		0.33	-0.03	0.01	-0.03	0.53	-0.12	0.20	0.12	0.00	0.00
um052x/6-311+g(d,p)		0.37	-0.06	0.00	-0.03	0.57	-0.13	0.19	0.13	0.00	-0.01
um052x/epr-II		0.36	-0.05	0.00	-0.06	0.62	-0.16	0.19	0.13	0.00	-0.01
um052x/epr-III		0.36	-0.06	0.01	-0.05	0.51	-0.07	0.18	0.12	0.00	0.00
um062x/6-311+g(d,p)		0.36	-0.06	0.00	-0.06	0.62	-0.15	0.21	0.12	0.00	-0.01
um062x/epr-II		0.35	-0.05	0.00	-0.06	0.63	-0.16	0.20	0.12	0.00	-0.01
um062x/epr-III		0.40	-0.11	-0.01	-0.05	0.61	-0.17	0.21	0.12	0.01	0.00

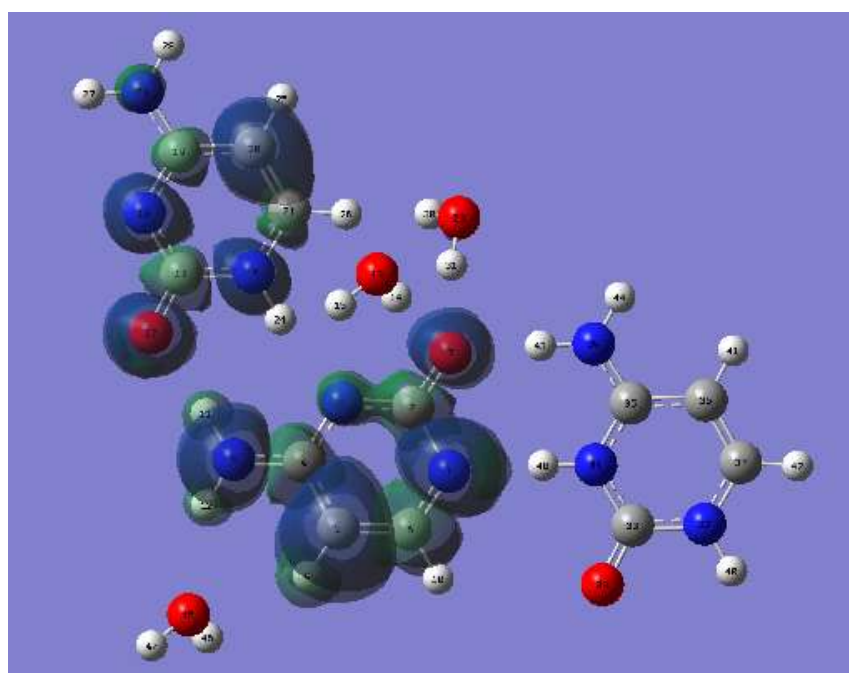
Table 14. The calculated Mulliken spin populations on the N1-deprotonated cytosine cation radical of the system shown in Figure. 7. The last two columns list the calculated spin densities at the N3 and N3-H sites of the protonated cytosine base.

Cm	C5-H		N4-H1		N4-H2		N1		N3		N4		C6-H		Cyto2 N3		Cyto2 N3-H	
	isotropic	dipolar	isotropic	dipolar	isotropic	dipolar	isotropic	dipolar	isotropic	dipolar	isotropic	dipolar	isotropic	dipolar	isotropic	dipolar	isotropic	dipolar
Experiment		-21.00		-9.30		-6.20												
	-41.40	-0.80	-14.30	-1.80	-13.00	-3.60												
		22.80		11.10		9.80												
Wetmore		-19.70		-1.30		-1.90												
	-30.70	-0.40	-1.10	-0.80	-0.90	-1.50												
		20.10		2.10		3.40												
ub3lyp/6-311+g(d,p)		-20.79		-7.47		-4.19			-15.27		-0.58		-6.16		-4.10			
	-35.01	-2.46	-10.40	-2.53	-8.81	-3.62	10.26	-15.10	-0.47	-0.18	4.50	-5.76	5.17	-0.40	-1.05	0.05		
		23.24		10.00		7.81		30.37		0.75		11.92		4.50				
ub3lyp/epr-II		-20.66		-7.38		-4.13		-14.85		-0.55		-5.92		-4.09				
	-37.05	-2.54	-10.68	-2.50	-8.97	-3.55	12.46	-14.74	-0.52	-0.16	5.22	-5.53	5.54	-0.39	-1.12	-0.19		
		23.20		9.88		7.68		29.59		0.70		11.46		4.48				
ub3lyp/epr-III		-20.80		-7.35		-4.01		-15.73		-0.60		-6.15		-4.19				
	-36.83	-1.35	-10.47	-2.14	-8.67	-3.36	12.84	-15.67	-0.47	-0.24	5.14	-5.76	5.55	-0.29	-1.10	-0.11		
		22.14		9.49		7.37		31.40		0.84		11.91		4.48				
um052x/6-311+g(d,p)		-22.54		-7.48		-4.22		-15.11		-0.49		-5.99		-4.33				
	-43.46	-3.10	-12.00	-2.82	-10.78	-3.48	11.78	-14.62	-0.55	0.05	8.18	-5.56	7.76	-1.50	-1.09	0.57		
		25.65		10.30		7.70		29.73		0.44		11.55		5.83				
um052x/epr-II		-22.74		-7.45		-4.16		-14.39		-0.52		-5.70		-4.37				
	-37.89	-3.26	-10.37	-2.75	-9.48	-3.42	14.72	-14.05	-0.65	0.09	8.79	-5.27	6.92	-1.52	-1.16	-0.05		
		26.00		10.20		7.58		28.45		0.43		10.97		5.88				
um052x/epr-III		-22.53		-7.33		-4.02		-15.43		-0.46		-5.99		-4.30				
	-40.94	-2.35	-10.58	-2.50	-9.49	-3.30	17.07	-14.97	-0.60	0.01	7.43	-5.57	7.16	-1.39	-1.13	0.03		
		24.87		9.83		7.32		30.40		0.45		11.56		5.69				
um062x/6-311+g(d,p)		-22.39		-7.14		-4.12		-14.05		-0.54		-5.60		-4.15				
	-44.65	-3.78	-11.08	-2.72	-9.38	-3.22	17.75	-13.47	-0.42	0.13	9.18	-5.17	4.44	-1.45	-1.18	0.44		
		26.17		9.86		7.34		27.52		0.42		10.77		5.60				
um062x/epr-II		-22.52		-7.09		-4.08		-13.52		-0.56		-5.39		-4.26				
	-48.74	-3.85	-11.82	-2.68	-9.93	-3.18	20.27	-13.04	-0.57	0.15	9.74	-4.96	4.85	-1.41	-1.25	0.13		
		26.38		9.77		7.25		26.56		0.41		10.35		5.67				
um062x/epr-III		-22.59		-7.03		-4.04		-14.25		-0.50		-5.58		-4.14				
	-47.43	-3.51	-11.93	-2.52	-9.80	-3.08	22.10	-13.70	-0.49	0.08	8.75	-5.16	3.99	-1.33	-1.21	0.10		
		26.09		9.55		7.12		27.96		0.42		10.73		5.46				

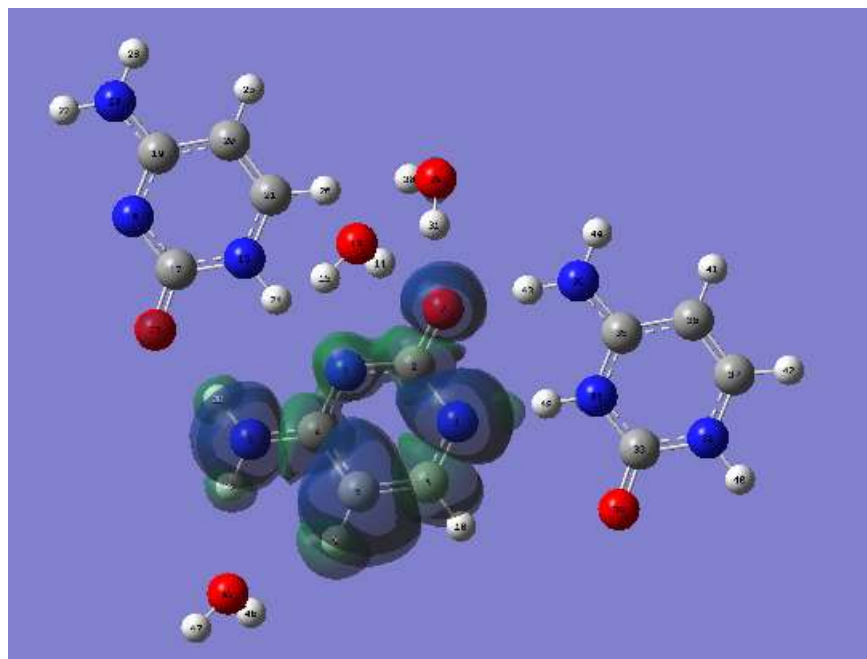
Table 15. The calculated HFCCs on the N1-deprotonated cytosine cation radical for the system in Figure. 7. The last two columns list the calculated HFCCs at the N3 and N3-H sites of the protonated cytosine base.



(a)



(b)



(c)

Figure. 8 (a) A native cytosine molecule is included into the single point calculation system based on the system shown in Figure. 6, now the N1-deprotonated cytosine cation radical is imbedded within the complete H-bonding environment as is presented in its single crystal structure

(b) The spin density of the system in Figure. 8 (a) as calculated at B3LYP/EPR-III level of theory (isoval=0.0004)

(c) The spin density of the system in Figure. 8 (a) as calculated at M062x/EPR-III level of theory (isoval=0.0004)

Cm		N1	C2	N3	C4	C5	C6	O2	N4
Experiment		0.30				0.57			
Wetmore		0.29				0.49		0.35	
ub3lyp/6-311+g(d,p)		0.29	-0.05	-0.01	-0.09	0.46	-0.14	0.08	0.21
ub3lyp/epr-II		0.26	-0.03	-0.01	-0.05	0.38	-0.09	0.08	0.19
ub3lyp/epr-III		0.26	-0.02	-0.01	-0.04	0.39	-0.09	0.08	0.19
um052x/6-311+g(d,p)		0.39	-0.07	-0.02	-0.06	0.53	-0.10	0.12	0.25
um052x/epr-II		0.37	-0.04	-0.02	-0.08	0.60	-0.16	0.12	0.25
um052x/epr-III		0.38	-0.07	-0.01	-0.04	0.48	-0.08	0.11	0.22
um062x/6-311+g(d,p)		0.39	-0.07	-0.03	-0.09	0.60	-0.14	0.13	0.25
um062x/epr-II		0.36	-0.04	-0.03	-0.08	0.61	-0.16	0.13	0.25
um062x/epr-III		0.42	-0.11	-0.03	-0.13	0.61	-0.13	0.13	0.25

(a)

Cyto 3		N1	C2	N3	C4	C5	C6	O2	N4
ub3lyp/6-311+g(d,p)		0.05	-0.05	0.07	-0.03	0.11	-0.01	0.16	-0.01
ub3lyp/epr-II		0.05	-0.04	0.07	-0.02	0.10	-0.01	0.16	-0.01
ub3lyp/epr-III		0.05	-0.03	0.06	-0.02	0.09	-0.01	0.15	-0.01
um052x/6-311+g(d,p)		0.00	0.00	0.00	0.00	0.00	0.00	0.00	0.00
um052x/epr-II		0.00	0.00	0.00	0.00	0.00	0.00	0.00	0.00
um052x/epr-III		0.01	0.00	0.00	0.00	0.00	0.00	0.00	0.00
um062x/6-311+g(d,p)		0.00	0.00	0.00	0.00	0.00	0.00	0.00	0.00
um062x/epr-II		0.00	0.00	0.00	0.00	0.00	0.00	0.00	0.00
um062x/epr-III		0.01	0.00	0.00	0.00	0.00	0.00	0.00	0.00

(b)

Table 16. (a) The calculated Mulliken spin populations on the N1-deprotonated cytosine cation radical of the system shown in Figure. 8 (a). (b) The calculated Mulliken spin populations on the native cytosine base molecule at the left up corner as shown in Figure. 8 (a). The delocalization error of B3LYP functional is obvious over that of M05/6-2X functionals.

Cm	C5-H		N4-H1		N4-H2		N1		N3		N4		C6-H		Cyto3 N1-H	Cyto3 C5-H
	isotropic	dipolar	isotropic	dipolar	isotropic	dipolar	isotropic	dipolar	isotropic	dipolar	isotropic	dipolar	isotropic	dipolar		
Experiment		-21.00		-9.30		-6.20										
	-41.40	-0.80	-14.30	-1.80	-13.00	-3.60										
		22.80		11.10		9.80										
Wetmore		-19.70		-1.30		-1.90										
	-30.70	-0.40	-1.10	-0.80	-0.90	-1.50										
		20.10		2.10		3.40										
ub3lyp/6-311+g(d,p)		-14.15		-11.97		-8.28		-11.57		-1.40		-9.06		-3.06		
	-24.68	-2.05	-13.45	-4.92	-13.16	-4.12	7.94	-11.39	-0.81	0.65	6.47	-8.80	3.99	-0.28	-3.55	-5.91
		16.20		16.88		12.40		22.96		0.75		17.86		3.34		
ub3lyp/epr-II		-13.98		-11.89		-8.15		-11.18		-1.39		-8.73		-3.04		
	-25.96	-2.08	-13.83	-4.82	-13.32	-4.04	9.57	-11.05	-0.97	0.65	7.51	-8.46	4.27	-0.27	-3.77	-6.42
		16.06		16.72		12.19		22.23		0.74		17.19		3.31		
ub3lyp/epr-III		-14.33		-11.84		-8.24		-12.04		-1.45		-9.21		-3.19		
	-26.22	-1.31	-13.69	-4.40	-13.16	-3.67	9.97	-11.94	-0.98	0.67	7.60	-8.96	4.27	-0.18	-3.64	-6.22
		15.64		16.23		11.91		23.98		0.78		18.17		3.37		
um052x/6-311+g(d,p)		-21.29		-13.68		-9.99		-15.89		-2.64		-11.15		-4.28		
	-42.28	-3.23	-21.45	-4.44	-20.67	-5.63	12.45	-15.39	-1.52	1.22	14.66	-10.75	8.08	-1.54	-0.01	-0.04
		24.52		18.12		15.62		31.28		1.43		21.89		5.81		
um052x/epr-II		-21.43		-13.67		-9.95		-15.21		-2.60		-10.66		-4.30		
	-36.97	-3.35	-18.80	-4.29	-18.31	-5.49	15.53	-14.86	-1.79	1.19	16.05	-10.24	6.95	-1.55	-0.01	-0.03
		24.78		17.96		15.45		30.07		1.41		20.90		5.85		
um052x/epr-III		-21.33		-13.20		-9.53		-16.24		-2.60		-11.05		-4.28		
	-40.06	-2.53	-18.57	-3.81	-18.18	-5.14	18.22	-15.76	-1.76	1.19	14.21	-10.67	7.16	-1.38	0.00	-0.03
		23.86		17.01		14.67		32.00		1.40		21.72		5.66		
um062x/6-311+g(d,p)		-21.12		-13.70		-10.05		-14.80		-3.04		-10.93		-4.11		
	-43.30	-3.96	-19.79	-4.42	-18.81	-5.62	18.71	-14.19	-2.31	1.42	17.87	-10.52	4.64	-1.40	0.00	-0.06
		25.09		18.12		15.67		28.99		1.62		21.45		5.51		
um062x/epr-II		-21.19		-13.66		-10.00		-14.31		-2.99		-10.55		-4.19		
	-47.01	-4.00	-21.34	-4.32	-19.61	-5.53	21.32	-13.79	-2.63	1.38	19.15	-10.13	4.86	-1.34	-0.01	-0.06
		25.19		17.97		15.52		28.10		1.61		20.68		5.53		
um062x/epr-III		-21.39		-13.24		-9.61		-15.04		-2.97		-10.75		-4.11		
	-45.77	-3.72	-20.93	-4.00	-18.80	-5.36	23.53	-14.47	-2.56	1.38	17.49	-10.36	3.95	-1.26	0.01	-0.04
		25.11		17.23		14.96		29.51		1.59		21.11		5.37		

Table 17. The calculated HFCCs on the N1-deprotonated cytosine cation radical for the system in Figure. 7. The last two columns list the calculated HFCCs at the N1-H and C5-H sites of the native cytosine base molecule, which are listed here to demonstrate the delocalization effects of B3LYP functional.

In order to examine the complete effects of H-bonding environment on the spin density and hyperfine coupling calculations, all the neighboring molecules that form H-bonds with the central cytosine radical are included in the single point calculation system, as shown in Figure. 8 (a). Compared with the system in Figure. 6, a third cytosine (native) is included, which has its O2 and N1-H H-bonded with the radical's N4-H and N3 sites. It is noticeable from Figure. 8 (b) that, when calculated using B3LYP functional, the third cytosine molecule is artificially assigned with a considerable amount of unpaired spin density at its O2 and C5 sites, which is a delocalization of the spin density distribution that is not observed experimentally. Meanwhile, as shown in Figure. 8 (b), M06-2X functional calculates localized spin density, which only resides at the cytosine radical. It is widely recognized that, when adding or removing an electron from a system, approximate DFT functionals produce an overly disperse distribution for the added electron or hole. This might relate to that B3LYP's exchange energy contribution contains 72% of the gradient corrections of the Becke88 exchange functional. And also a relatively low level

(20%) of non-local Hartree-Fock exchange in B3LYP compared with M052x's 56% and M062x's 54%.⁵⁰ The inclusion of spin kinetic energy density into exchange and correlation functionals in M05/6-2X should be partially responsible for their more localized prediction on the unpaired spin density distributions. Bally et al.⁵¹ carried out a case study on the radical ions of H-H⁺, where the charge and spin should be separated, and He-He⁺, where the charge and spin should be localized. Their study demonstrates that Becke's exchange functionals fail to energetically predict the correct dissociative behavior of the radical ions. Lundberg et al.⁵² attribute this error to the self-interaction error (SIE) in DFT approximations which tends to artificially stabilize radical's delocalized states by predicting lower energy levels. The incorporation of Hartree-Fock exchange components in hybrid DFT methods helps to correct SIE. By examining the energy difference between delocalized and localized state of complexes without distance dependence,⁵² Lundberg et al. also present the SIE's dependence on the system size, basis sets and the asymmetry among fragments on B3LYP level of theory. The system size dependence of SIE can be seen from the calculated systems in Figure. 9 and Figure. 10, which have less delocalized spin properties than the calculated system in Figure. 8.

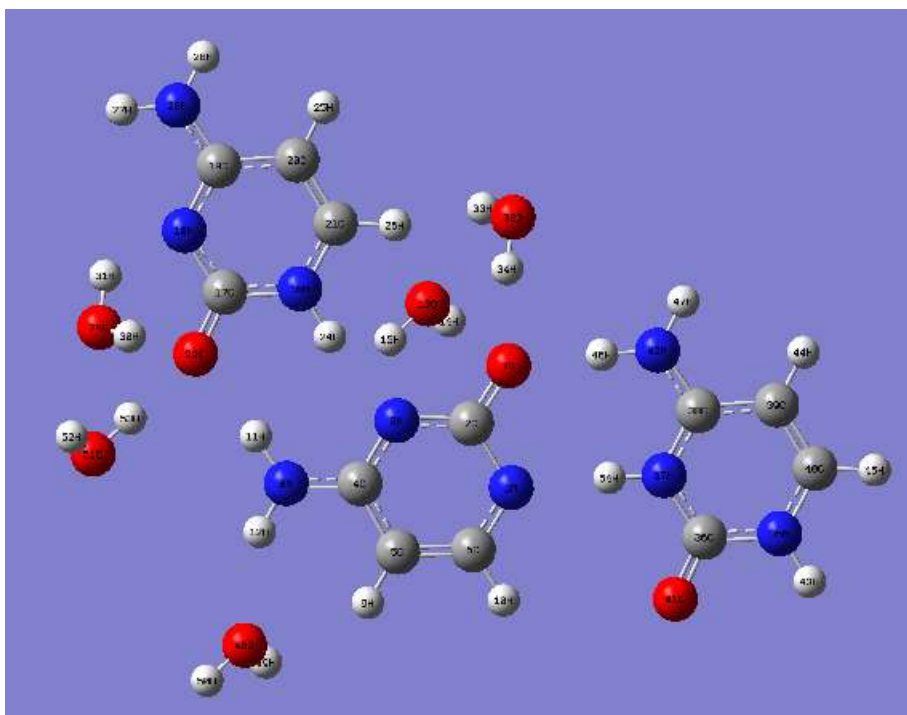
Now, let us add another two water molecules H-bonding to the O2 of both the second and the third cytosine, in order to see if these indirect H-bonding effects will improve the spin density performances on the radical's N1 and N4 sites. This system is shown in Figure. 10. Though this model improves B3LYP method to get more localized spin density distribution due to the size dependence of SIE, for M05/6-2X, no systematic improvements are achieved as shown in Table 18 and Table 19.

As expected in the system of Figure. 8, the radical's N4 site gains extra spin densities by denoting its second H atom, N4-H2, to the H-bond formed with the native cytosine base. However, as shown in Table 17, the M05/6-2X calculated hyperfine couplings at N4-H1 and N4-H2 are now overestimated by about 30% than the experimental values. Delicate error cancellations allow B3LYP to give good HFCC predictions on the amino site, but it should not be over credited due to B3LYP now only predicts a little more than half of the experimental iHFCC value at C5-H. The less accuracy of B3LYP functional in HFCC calculations makes it hard to distinguish the contributions from error cancellations and from environmental effects. So,

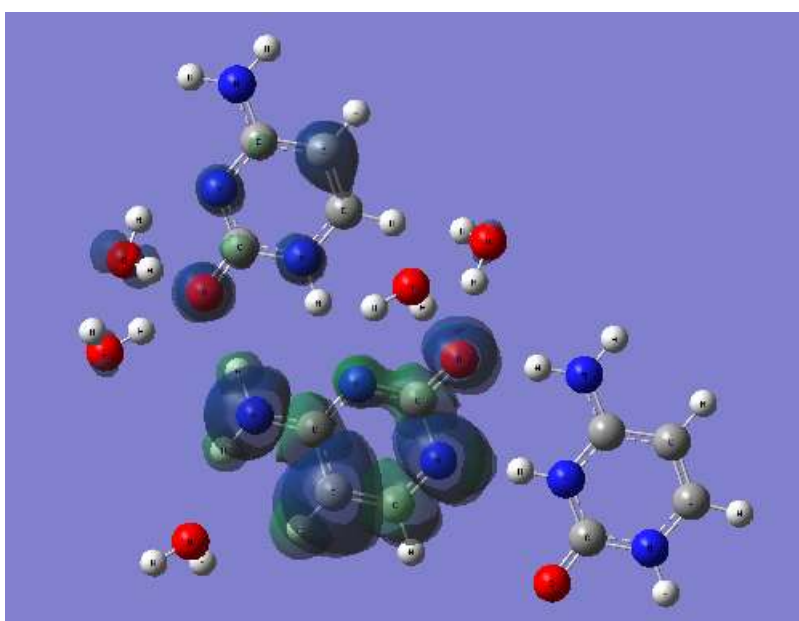
the mathematically more advanced M05/6-2X functionals are used as the main tool for examine the H-bonding effects in HFCC calculations.

It is obvious from the M05/6-2X results from Table 17 that an extra amount of spin densities is assigned to N4 when compared with the experimental value (0.17). Meanwhile, the overestimation of the HFCC at the N1 site remains unresolved. From a view of environmental effects, three possible reasons can explain these two remaining discrepancies, after the radical has been embedded in its complete H-bonding environment in Figure. 8. Firstly, electrostatically, it might be the environmental completeness on BOTH sides of an H-bond that affect its properties. For example, in the real crystalline structure, all water molecules experience the same electrostatic environment; but, obviously, this is not satisfied in these current single point models. As a result, though the H-bonds are qualitatively present, but they are not quantitatively precise. Secondly, from a geometric perspective, the optimization with the surrounding molecules' coordinates frozen is artificial, and conceals the deformations of the surrounding molecules, which will feedback to the bond length and orientation of the H-bonds they form with the central radical. Thirdly, the dynamic motion of the deprotonated proton vibrating between the deprotonated N1 and the protonated N3 sites should also play a vital role in its H-bonding properties, resulting in a much stronger H-bonding effect. This averaging effect of this dynamic motion is not simulated in all the jobs in this work. The absent of temperature effects under the Born-Oppenheimer approximation, such as the vibration averaging motions,²⁴ also plays an important role in the current jobs. In addition, as indicated by Improta et al.,¹⁰ the accurate prediction of hyperfine couplings at heavy atoms (such as the Nitrogen atoms) in π radicals can be difficult due to the delicate balance between the spin polarizations of valence and core orbitals. But never the less, it comes to the two conclusions from the calculations on the cytosine cation radical: 1) the inclusion of H-bonding environment improves the DFT calculations on hyperfine coupling constants. 2) M05/6-2X functionals give more accurate hyperfine coupling predictions over the B3LYP functional.

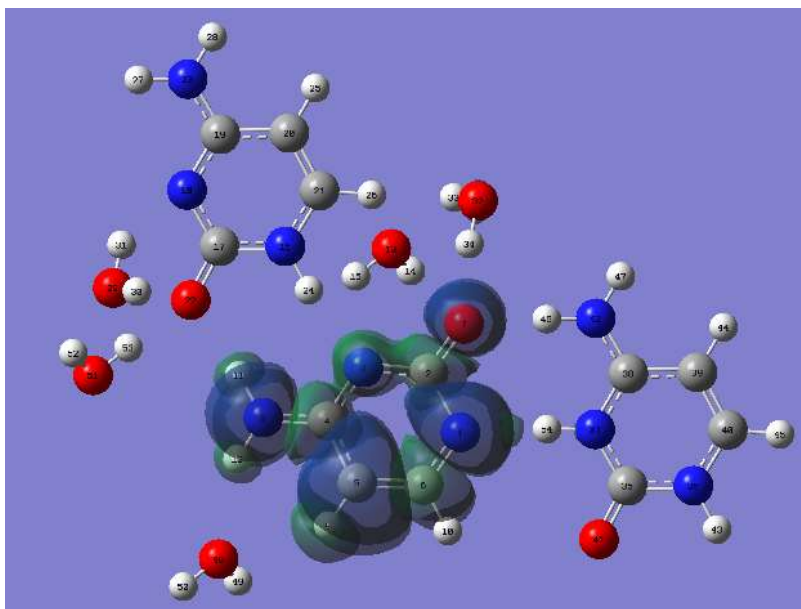
These two conclusions is further generalized in the following two sections of the HFCC calculations on the native guanine cation radical and the N3 deprotonated 5'-dGMP cation radical.



(a)



(b)

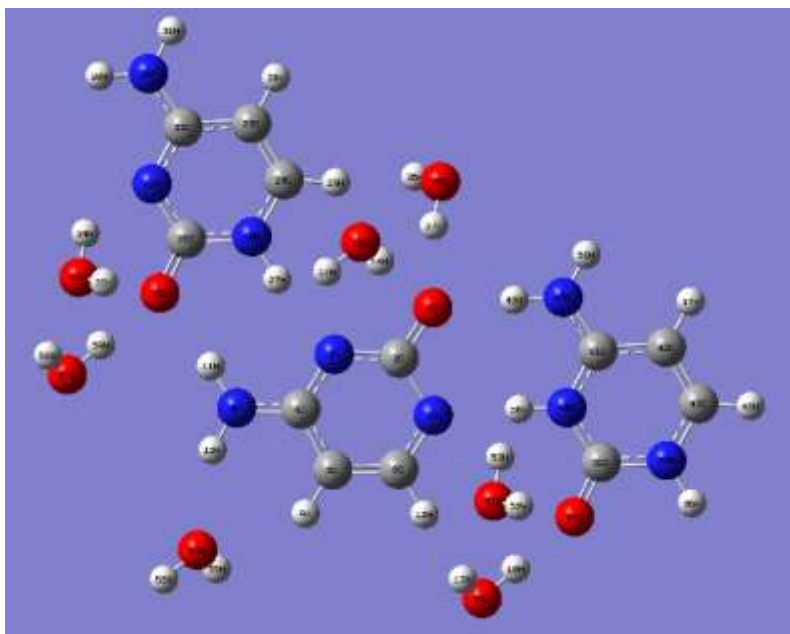


(c)

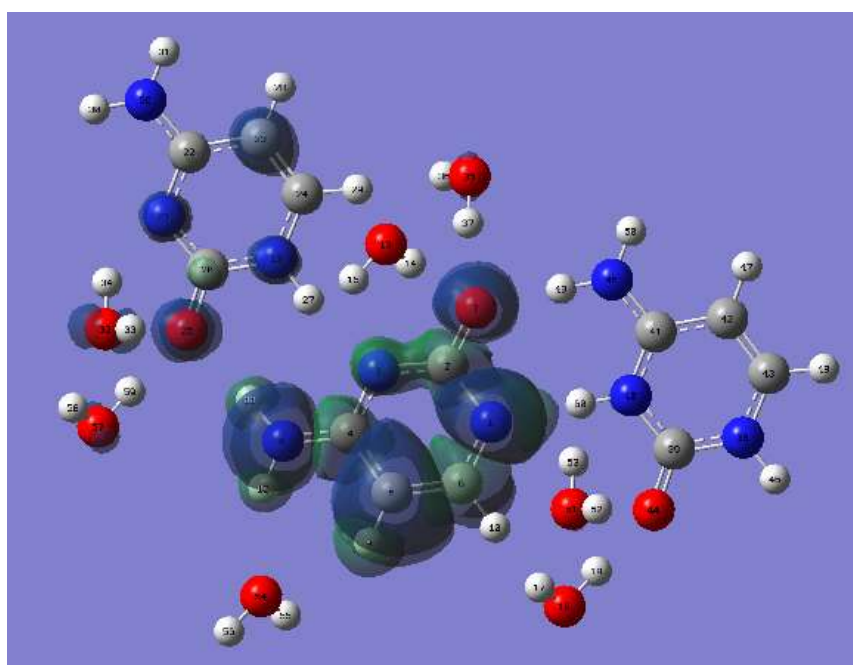
Figure. 9 (a) Two water molecules that forms H-bonds with the native cytosine base's O2 site are included based on the system in Figure. 8, in attempt to improve the description of the H-bonds between the native cytosine's O2 site with the radical's N4-H2 site.

(b) The spin density of the system in Figure. 9 (a) as calculated at B3LYP/EPR-III level of theory (isoval=0.0004)

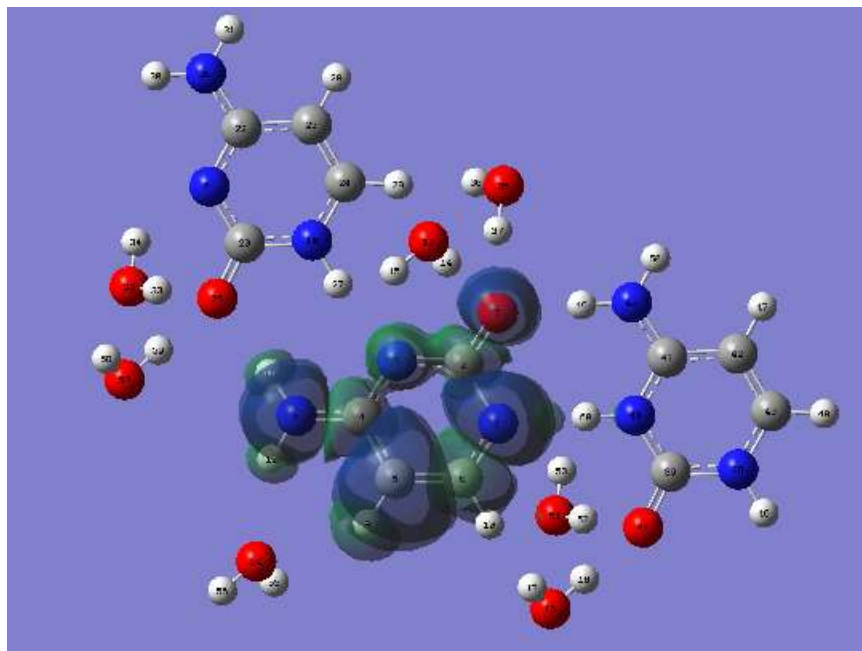
(c) The spin density of the system in Figure. 9 (a) as calculated at M062x/EPR-III level of theory (isoval=0.0004)



(a)



(b)



(c)

Figure. 10 (a) All the three cytosine base molecules' O2 sites are H-bonded with two water molecules. This system is to examine the indirect H-bonding effects on HFCC calculations.

(b) The spin density of the system in Figure. 10 (a) as calculated at B3LYP/EPR-III level of theory (isoval=0.0004)

(c) The spin density of the system in Figure. 10 (a) as calculated at M062x/EPR-III level of theory (isoval=0.0004)

Cm	N1	C2	N3	C4	C5	C6	O2	N4
Experiment	0.30				0.57			
Wetmore	0.29				0.49		0.35	
ub3lyp/6-311+g(d,p)	0.35608	-0.0518	-0.0123	-0.1188	0.59786	-0.1687	0.10475	0.27433
ub3lyp/epr-II	0.31449	-0.0326	-0.0144	-0.0574	0.48613	-0.1028	0.10138	0.25102
ub3lyp/epr-III	0.31612	-0.0212	-0.0143	-0.0556	0.4922	-0.0975	0.10451	0.2508
um052x/6-311+g(d,p)	0.36218	-0.053	-0.0232	-0.0533	0.52481	-0.08	0.10688	0.26007
um052x/epr-II	0.34839	-0.0345	-0.0242	-0.0839	0.60955	-0.144	0.10441	0.26352
um052x/epr-III	0.36496	-0.0603	-0.0213	-0.027	0.46566	-0.0639	0.09591	0.22785
um062x/6-311+g(d,p)	0.36514	-0.0589	-0.0347	-0.0834	0.5888	-0.1105	0.11452	0.26063
um062x/epr-II	0.34194	-0.0359	-0.0258	-0.0844	0.61955	-0.1435	0.11217	0.25904
um062x/epr-III	0.41521	-0.115	-0.0494	-0.1034	0.60594	-0.1275	0.11245	0.26073

Table 18. (a) The calculated Mulliken spin populations on the N1-deprotonated cytosine cation radical of the system shown in Figure. 10 (a).

Cm	C5-H		N4-H1		N4-H2		N1		N3		N4		C6-H	
	isotropic	dipolar	isotropic	dipolar	isotropic	dipolar	isotropic	dipolar	isotropic	dipolar	isotropic	dipolar	isotropic	dipolar
Experiment		-21.00		-9.30		-6.20								
	-41.40	-0.80	-14.30	-1.80	-13.00	-3.60								
		22.80		11.10		9.80								
Wetmore		-19.70		-1.30		-1.90								
	-30.70	-0.40	-1.10	-0.80	-0.90	-1.50								
		20.10		2.10		3.40								
ub3lyp/6-311+g(d,p)		-18.33		-14.37		-11.14			-14.39		-1.98		-11.95	-3.81
	-32.23	-2.72	-17.97	-4.37	-17.44	-5.07	9.87	-14.14	-1.01	0.90	8.76	-11.65	4.52	-0.49
		21.05		18.73		16.21		28.53		1.08		23.60	4.30	
ub3lyp/epr-II		-17.80		-13.92		-10.70			-13.61		-1.90		-11.24	-3.71
	-33.32	-2.74	-17.98	-4.20	-17.31	-4.87	11.66	-13.42	-1.19	0.87	9.95	-10.94	4.74	-0.49
		20.54		18.12		15.57		27.02		1.04		22.19	4.20	
ub3lyp/epr-III		-18.56		-14.20		-10.97			-15.01		-2.04		-12.06	-3.94
	-34.25	-1.76	-18.13	-3.70	-17.33	-4.48	12.45	-14.87	-1.25	0.93	10.20	-11.76	4.91	-0.39
		20.32		17.90		15.45		29.87		1.11		23.82	4.33	
um052x/6-311+g(d,p)		-21.48		-14.26		-10.41			-14.91		-2.65		-11.58	-4.28
	-43.13	-3.48	-22.43	-4.50	-21.57	-5.82	11.93	-14.39	-1.52	1.21	15.16	-11.17	6.94	-1.59
		24.96		18.76		16.23		29.30		1.44		22.74	5.87	
um052x/epr-II		-21.64		-14.22		-10.33			-14.15		-2.60		-11.04	-4.31
	-38.12	-3.63	-19.61	-4.35	-19.28	-5.66	14.71	-13.78	-1.79	1.18	16.56	-10.61	6.14	-1.62
		25.27		18.57		15.99		27.93		1.42		21.65	5.94	
um052x/epr-III		-21.53		-13.66		-9.82			-15.25		-2.59		-11.38	-4.25
	-41.10	-2.77	-19.28	-3.83	-18.97	-5.29	17.05	-14.77	-1.76	1.18	14.61	-10.99	6.39	-1.48
		24.30		17.49		15.11		30.03		1.41		22.37	5.73	
um062x/6-311+g(d,p)		-21.35		-14.27		-10.45			-14.04		-3.00		-11.35	-4.15
	-43.98	-4.18	-20.74	-4.45	-19.55	-5.80	18.04	-13.42	-2.28	1.39	18.46	-10.91	3.79	-1.57
		25.53		18.72		16.25		27.45		1.61		22.26	5.72	
um062x/epr-II		-21.45		-14.20		-10.37			-13.47		-2.94		-10.93	-4.24
	-47.82	-4.25	-22.36	-4.35	-20.39	-5.68	20.42	-12.94	-2.59	1.35	19.72	-10.49	4.09811	-1.56
		25.69		18.55		16.05		26.41		1.59		21.42	5.80	
um062x/epr-III		-21.60		-13.70		-9.89			-14.26		-2.92		-11.09	-4.15
	-46.50	-3.93	-21.81	-4.00	-19.42	-5.50	22.26	-13.68	-2.51	1.35	17.95	-10.67	3.32	-1.45
		25.53		17.71		15.39		27.94		1.57		21.76	5.59	

Table 19. The calculated HFCCs on the N1-deprotonated cytosine cation radical for the system in Figure. 10 (a).

4.2. Native Guanine Cation Radical in Guanine Hydrochloride Monohydrate Single Crystal

In Guanine Hydrochloride Monohydrate single crystal structure, both the pyrimidine and imidazole sides of a N7-protonated guanine molecule are surrounded by 4 chloride ions, each side with two Cl⁻ in the guanine plane and one below and above the plane. These chloride ions incorporate strong Van der Waals contacts with the N7 protonated guanine molecule. For each guanine molecule, its N1 site forms an H-bond with a nearby water molecule. The amino group is H-bonded from its two H atoms to both a chloride ion and a neighboring guanine's N3 site. The C6-O and N7-H sites are H-bonded to a nearby guanine's N7-H and C6-O sites respectively. Only the guanine's N9-H site forms an H-bond with a Cl⁻. The Guanine base's H-bonds with a chloride ion is weaker than the normal ones, such as with an oxygen or nitrogen atom.

It is worth to mention that the completeness of environmental effects plays a vital role in the N7-deprotonated native guanine radical's optimization. Theoretical optimization on the systems without including symmetric Cl⁻ ions distribution often results in a non-planar structure the guanine radical. For example, in Figure. 11, the optimization job on ONIOM(m052x/aug-cc-pvtz:uB3LYP/3-21+g*) level of theory, which includes only one Cl⁻ on the guanine radical's pyrimidine ring side above its plane, leads to an amino hydrogen being attracted toward the Cl⁻ and departing from the plane about 55° dihedral angle with respect to N1. Even in the condition where stacking effects are not presented, by including all the eight nearest Cl⁻s around and its O6 protonated neighbor, the guanine radical's optimization results in a planar structure within its ribbon plane. In all the optimization jobs, the radical's deprotonating proton is assigned by freezing it at the opposite protonation site, O2, due to the lack of proton shuttling path in the simulation models. Optimizations without fixing this proton result in a reversion of the deprotonating process. As mentioned in the Method section, the native guanine cation radical optimized within two different scales of environmental completeness and their calculated HFCC properties will be presented in this section. They are called Gm-Opt-1 and Gm-Opt-2.

Now, let us first look at the spin density distribution and hyperfine coupling properties for the Gm-Opt-1 jobs.

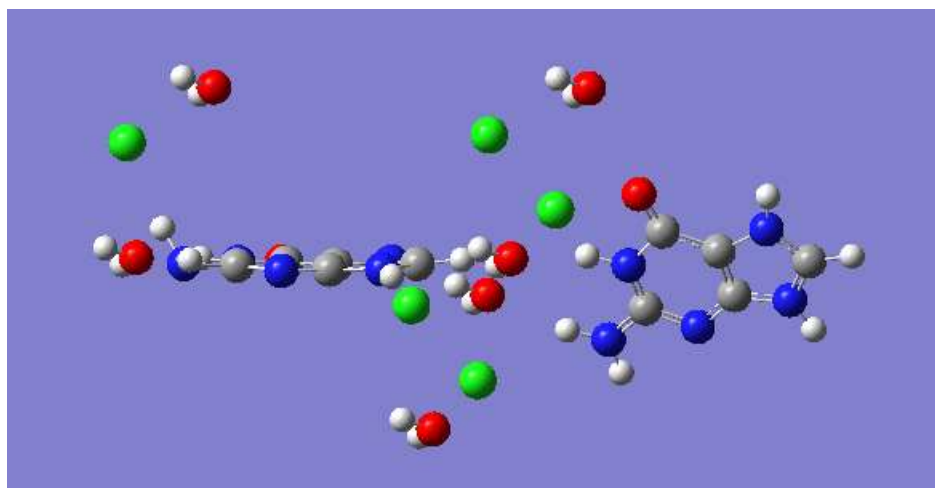
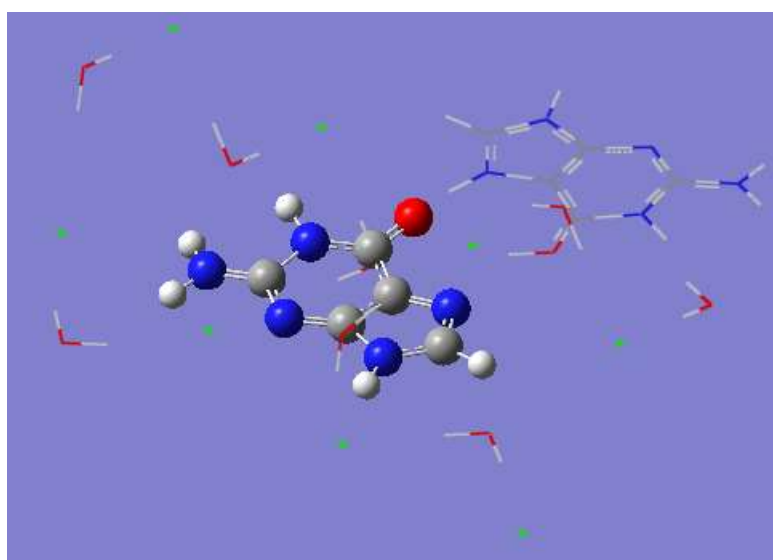
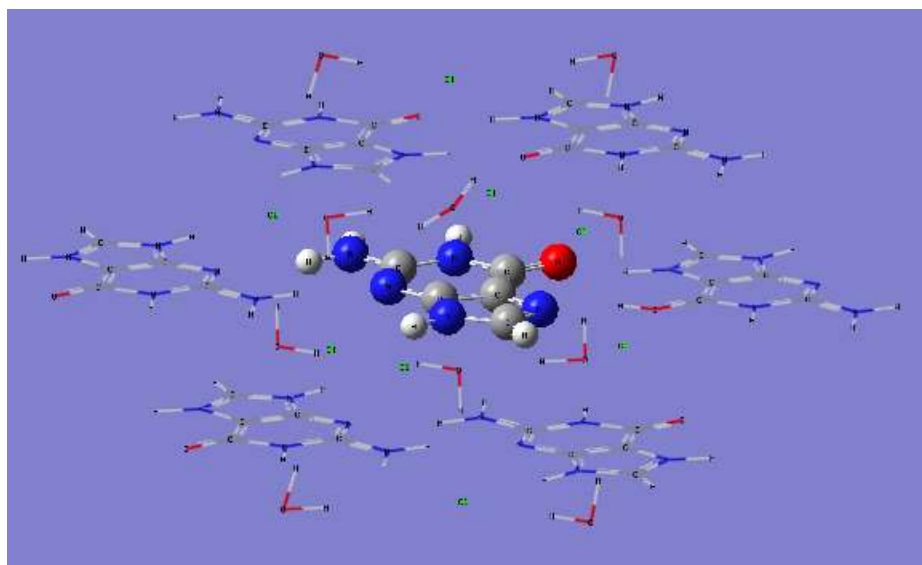


Figure. 11 The optimization on a system without including symmetric Cl⁻ ions distribution results in a non-planar structure the guanine radical (on the left).



(a)

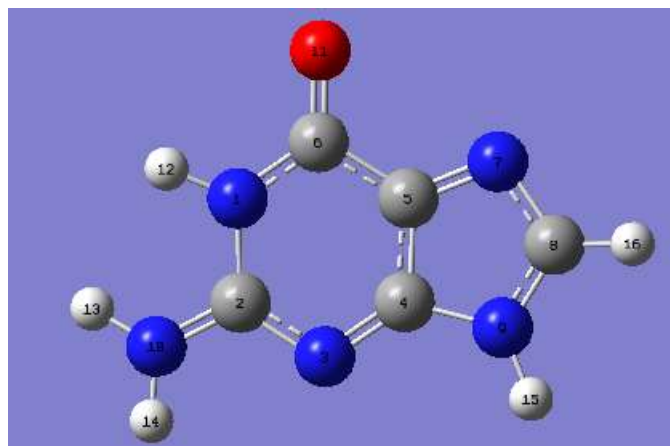


(b)

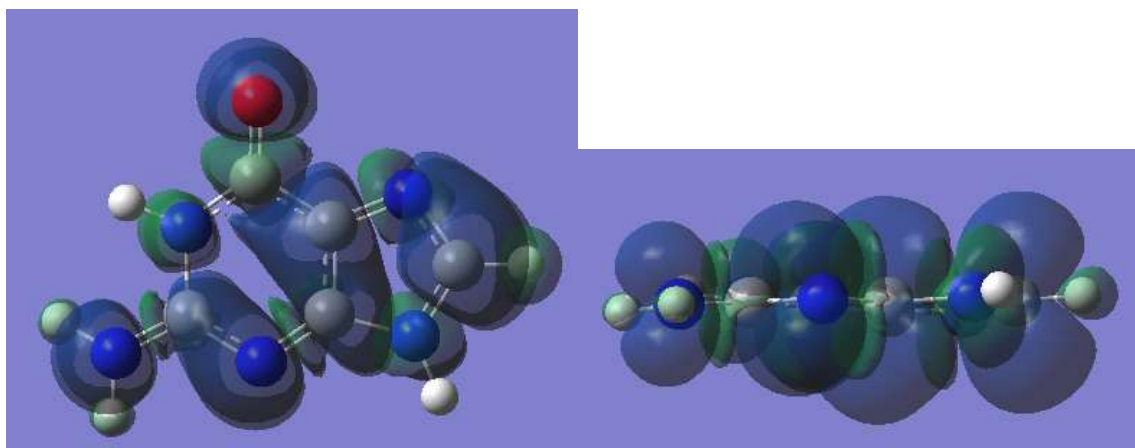
Figure. 12 The two different scale optimizations of the native guanine cation radical, within the Guanine Hydrochloride Monohydrate single crystal environment, referred as Gm-Opt-1 and Gm-Opt-2. (a) The Gm-Opt-1 optimization includes the N7-deprotonated guanine cation radical, its eight nearest chloride ions, and the O-6 protonated guanine cation; this system is optimized on ONIOM(B3LYP/6-31+g(d):HF/6-31+g(d)) level of theory. (b) The Gm-Opt-2 optimization includes another 5 nearest guanine bases based on the Gm-Opt-1 system, and it is optimized on ONIOM(B3LYP/6-31+g(d):B3LYP/3-21g) level of theory.

4.2.1. HFCCs for Gm-Opt-1 Optimized Geometry

Following the route of the cytosine jobs, the single guanine native radical is first isolated from its Gm-Opt-1 optimization, as shown in Figure. 13. The calculated data listed in Table 20 and Table 20 poorly match the experimental results, with systematic underestimations of the spin densities at N2 and N3 sites, and overestimations of spin densities at C5 site. As a result, the iHFCCs at C5-H site are overestimated by at least 50% in all the tested jobs. M06-2X functional shows advantages in predicting iHFCCs at the amino sites and N3 site by giving closer results to the experimental values, but the HFCCs calculated on these sites are generally underestimated. As a conclusion, the tested DFT calculations on the isolated model can be rated as poor.



(a)



(b)

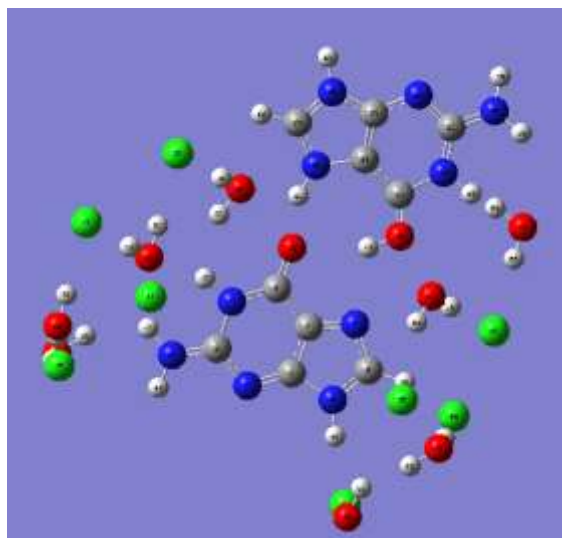
Figure. 13 (a) The isolated N7-deprotonated native guanine cation radical from Gm-Opt-1 optimization. (b) The calculated spin density distribution at M05-2X/6-311+g(d,p) level of theory. (isoval=0.0004)

G:HCl:H2O	N1	C2	N3	C4	C5	C6	N7	C8	N9	N2	O6
Experiment			0.28					0.18		0.17	
Wetmore			0.21	0.17	0.29			0.28		0.10	
ub3lyp/6-311+g(d,p)	-0.01	0.04	0.21	0.12	0.20	-0.06	0.02	0.30	-0.06	0.10	0.18
m052x/6-311+g(d,p)	-0.02	0.04	0.18	0.13	0.24	-0.06	-0.01	0.33	-0.07	0.10	0.17
m062x/6-311+g(d,p)	-0.01	0.04	0.19	0.12	0.22	-0.07	0.00	0.31	-0.07	0.10	0.17
ub3lyp/epr-II	-0.01	0.04	0.19	0.12	0.23	-0.06	0.01	0.29	-0.04	0.10	0.17
m052x/epr-II	-0.02	0.04	0.18	0.12	0.26	-0.07	0.00	0.32	-0.06	0.10	0.16
m062x/epr-II	-0.02	0.04	0.18	0.12	0.24	-0.08	0.00	0.31	-0.05	0.10	0.17

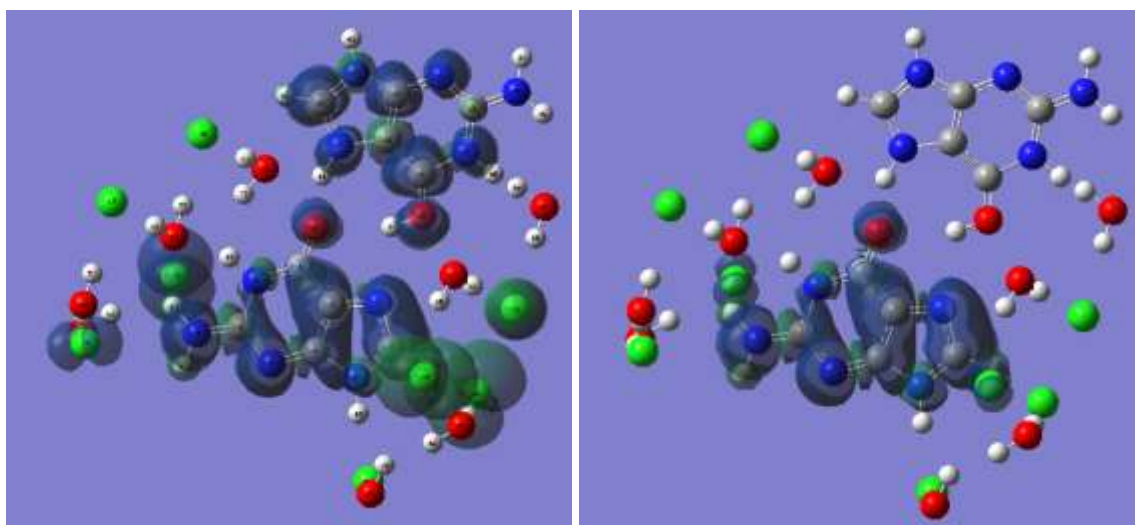
Table 20. The calculated Mulliken spin populations on the N7-deprotonated native guanine cation radical of the isolated system shown in Figure. 13 (a).

G:HCl:H2O	N1	N3	N7	N9	N2	N2-H1	N2-H2	C8-H		N9-H
	isotropic	isotropic	isotropic	isotropic	isotropic	isotropic	isotropic	isotropic	dipolar	isotropic
Experiment									-6.50	
		16.80			10.00	12.10	12.10	-14.50	0.50	
									6.00	
Wetmore									-6.50	
	-2.20	6.90	-1.30	-4.10	3.40	-8.20	-7.10	-22.70	-1.60	0.60
									8.10	
ub3lyp/6-311+g(d,p)									-12.75	
	-2.02	6.10	-0.73	-5.08	2.96	-7.95	-7.06	-23.48	-1.99	0.97
									14.74	
m052x/6-311+g(d,p)									-13.34	
	-3.05	6.40	-3.02	-8.14	5.73	-8.96	-8.40	-26.85	-2.32	2.19
									15.66	
m062x/6-311+g(d,p)									-12.50	
	-3.36	11.09	-2.12	-7.89	6.89	-9.19	-8.22	-21.66	-2.70	0.34
									15.20	
ub3lyp/epr-II									-12.79	
	-2.23	7.65	-0.55	-5.32	3.59	-8.15	-7.23	-25.12	-1.99	0.94
									14.78	
m052x/epr-II									-13.51	
	-3.25	7.80	-2.81	-8.46	6.20	-7.56	-7.28	-24.84	-2.34	1.69
									15.85	
m062x/epr-II									-12.61	
	-3.59	12.38	-2.07	-8.46	7.26	-9.55	-8.56	-23.15	-2.60	0.38
									15.21	

Table 21. The calculated hyperfine coupling constants on the N7-deprotonated native guanine cation radical of the isolated system shown in Figure. 13 (a).



(a)



(b)

(c)

Figure. 14 (a) The N7-deprotonated native guanine cation radical imbedded into the whole Gm-Opt-1 optimization system. (b) The calculated spin density distribution at B3LYP/6-311+g(d,p) level of theory (isoval=0.0004). (c) The calculated spin density distribution at M05-2X/6-311+g(d,p) level of theory (isoval=0.0004).

G:HCl:H2O	N1	C2	N3	C4	C5	C6	N7	C8	N9	N2	O6
Experiment			0.28					0.18		0.17	
Wetmore			0.21	0.17	0.29			0.28		0.10	
ub3lyp/6-311+g(d,p)	0.00	-0.03	0.19	0.04	0.13	0.03	0.10	0.18	-0.03	0.20	0.03
m052x/6-311+g(d,p)	-0.01	-0.01	0.19	0.04	0.20	0.05	0.11	0.21	-0.05	0.21	0.04
m062x/6-311+g(d,p)	-0.01	-0.01	0.20	0.02	0.17	0.05	0.14	0.17	-0.04	0.22	0.04

(a)

Guanine-2	N1	C2	N3	C4	C5	C6	N7	C8	N9	N2	O6
	0.01	0.00	0.03	0.09	-0.05	0.22	0.04	0.10	-0.03	0.00	0.06
	0.00	0.00	0.00	0.00	0.00	0.00	0.00	0.00	0.00	0.00	0.00
	0.00	0.00	0.00	0.00	0.00	0.00	0.00	0.00	0.00	0.00	0.00

(b)

Cl-1	Cl-2	Cl-3	Cl-4	Cl-5	Cl-6	Cl-7	Cl-8
13	15	17	18	33	35	36	49
0.13	0.02	0.00	0.00	-0.04	-0.20	0.00	-0.19
0.01	0.00	0.00	0.00	0.00	0.01	0.00	0.00
0.01	0.00	0.00	0.00	0.00	0.02	0.00	0.00

(c)

Table 22. (a) The calculated Mulliken spin populations on the N7-deprotonated native guanine cation radical of the system shown in Figure. 14 (a). (b) The calculated Mulliken spin populations on the O6-protonated guanine base molecule within the same system. (c) The calculated Mulliken spin populations on the eight chloride ions

G:HCl:H2O	N1	N3	N7	N9	N2	N2-H1	N2-H2	C8-H		N9-H
	isotropic	isotropic	isotropic	isotropic	isotropic	isotropic	isotropic	isotropic	dipolar	isotropic
Experiment		16.80			10.00	12.10	12.10	-14.50	-6.50	
									0.50	
									6.00	
Wetmore									-6.50	
	-2.20	6.90	-1.30	-4.10	3.40	-8.20	-7.10	-22.70	-1.60	0.60
									8.10	
ub3lyp/6-311+g(d,p)									-6.53	
	-0.60	9.24	4.00	-1.90	10.12	-14.34	-14.95	-14.43	-3.07	-0.03
									9.60	
m052x/6-311+g(d,p)									-8.86	
	-1.23	6.72	1.67	-4.84	12.55	-18.30	-18.01	-17.83	-2.48	1.21
									11.34	
m062x/6-311+g(d,p)									-8.11	
	-1.50	11.29	4.58	-4.51	-4.51	-17.47	-17.50	-14.83	-2.66	-0.33
									10.77	

(a)

Cl-1		Cl-2		Cl-3		Cl-4		Cl-5		Cl-6		Cl-7		Cl-8	
isotropic	dipolar	isotropic	dipolar	isotropic	dipolar	isotropic	dipolar	isotropic	dipolar	isotropic	dipolar	isotropic	dipolar	isotropic	dipolar
13		15		17		18		33		35		36		49	
	-21.03		-3.59		-0.07		-0.15		-14.73		-63.96		-0.09		-59.66
5.63	-20.92	0.93	-3.56	0.00	-0.03	-0.03	0.02	-1.87	7.24	-6.31	30.98	-0.07	-0.03	-6.04	29.46
	41.96		7.15		0.11		0.13		7.49		32.98		0.11		30.19
	-2.50		-0.55		-0.02		-0.11		-0.12		-2.30		-0.03		-0.59
-0.11	-2.43	-0.13	-0.50	0.00	-0.02	0.04	-0.05	-0.09	0.05	0.08	-2.19	-0.01	-0.02	0.01	-0.59
	4.93		1.05		0.04		0.15		0.07		4.50		0.05		1.18
	-2.77		-0.57		-0.02		-0.05		-0.08		-2.59		-0.03		-0.65
1.09	-2.67	0.00	-0.53	0.00	-0.02	-0.06	-0.02	-0.12	-0.01	1.51	-2.36	-0.01	-0.03	0.34	-0.64
	5.44		1.10		0.04		0.07		0.08		4.95		0.06		1.29

(b)

Table 23. (a) The calculated HFCCs on the N7-deprotonated native guanine cation radical of the system shown in Figure. 14 (a). (b) The calculated HFCCs on the eight chloride ions within the same system.

Now, single point calculations on the whole Gm-Opt-1 system are carried out, as shown in Figure. 14. Because of the introduction of the crystalline environment, the calculated spin densities at C8 and N2 sites and the calculated HFCCs at C8-H site, as listed in Table 22 and Table 23, are generally improved. Physically, radical's O2 site becomes an H-bond acceptor and experiences a decrease in its unpaired spin density, while the radical's N1-H and N2-H sites becoming H-bond donors and experiencing an increase in their unpaired spin densities. Similar to situations observed in the cytosine radical calculations, B3LYP functional delocalizes substantial amount of unpaired spin density to the protonated guanine base as well as to chloride ions. The calculated agreement of the remaining spin densities of B3LYP on the radical then falls into the causality of getting the right answer from a wrong reason. Nevertheless, all three methods give good excellent densities at C8, B3LYP and M06-2X remarkably reproduced the iHFCC at C8-H, which is -14.5 MHz. Obviously, that the lack of H-bonding on the radical's N2 and N3 sites partially response for the underestimations at N3 and slight overestimations at N2. It is time to further complete the environmental effects.

4.2.2. HFCCs for Gm-Opt-2 Optimized Geometry

The Gm-Opt-2 optimization includes all the radical's H-bonds, stacking, electrostatic effects within the system. After the optimization starting from the crystalline structure, the radical's bond angle O6-C6-C5 decreases about 11.6° from 135.5° to 123.6° . The bond angle N1-C6-C5 increases by 4.8° and C2-N1-C6 and C6-C5-C4 both decrease about 3.5° . On another hand, the bond angle N7-C8-N8 increases about 3.2° . The main site of spin density, N3, only experiences a 0.5° decrease in bond angle C2-N3-C4. The amino group becomes more planar as the dihedral angle N2-C2-N1-N3 decreases from 172.5° to 176.0° , whereas, the dihedral angle O6-C6-N1-C6 increases from -179.96° to -176.55° . Generally, the Gm-Opt-2 optimized radical base is more planar than that in Gm-Opt-1 optimization. In the following single point calculations, four DFT functionals, B3LYP, B3PW91, M05-2X, M06-2X in combinations with three basis sets, 6-311+g(d,p), EPR-II and EPR-III are examined.

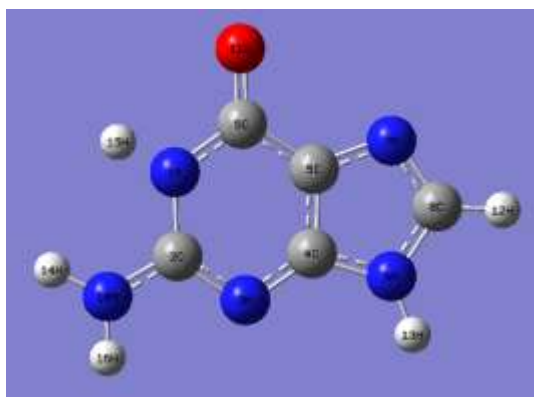


Figure. 15 The isolated N7-deprotonated native guanine cation radical extracted from Gm-Opt-2 optimization.

G:HCl:H2O	N1	C2	N3	C4	C5	C6	N7	C8	N9	N2	O6
Experiment			0.28					0.18		0.17	
Wetmore			0.21	0.17	0.29			0.28		0.10	
ub3lyp/6-311+g(d,p)	-0.01	0.01	0.23	0.08	0.27	-0.08	-0.02	0.27	-0.06	0.11	0.23
ub3pw91/6-311+g(d,p)	-0.01	0.01	0.23	0.08	0.28	-0.09	-0.03	0.28	-0.07	0.11	0.23
m052x/6-311+g(d,p)	-0.01	0.02	0.20	0.07	0.33	-0.09	-0.06	0.30	-0.07	0.10	0.23
m062x/6-311+g(d,p)	-0.01	0.02	0.21	0.07	0.31	-0.10	-0.04	0.29	-0.07	0.11	0.23
ub3lyp/epr-II	-0.01	0.01	0.21	0.07	0.29	-0.08	-0.02	0.26	-0.04	0.11	0.23
ub3pw91/epr-II	-0.01	0.01	0.20	0.07	0.30	-0.09	-0.03	0.27	-0.05	0.11	0.23
m052x/epr-II	-0.02	0.02	0.19	0.08	0.34	-0.11	-0.05	0.29	-0.06	0.10	0.23
m062x/epr-II	-0.01	0.02	0.20	0.07	0.33	-0.11	-0.04	0.28	-0.05	0.10	0.23
ub3lyp/epr-III	-0.01	0.02	0.21	0.09	0.27	-0.08	-0.01	0.25	-0.05	0.10	0.22
ub3pw91/epr-III	-0.01	0.02	0.21	0.09	0.28	-0.08	-0.02	0.27	-0.06	0.11	0.23
m052x/epr-III	-0.02	0.02	0.21	0.09	0.27	-0.08	-0.02	0.27	-0.04	0.10	0.22
m062x/epr-III	-0.02	0.01	0.25	0.04	0.30	-0.10	-0.01	0.25	-0.06	0.11	0.23

Table 24. The calculated Mulliken spin populations on the N7-deprotonated native guanine cation radical of the system shown in Figure. 15.

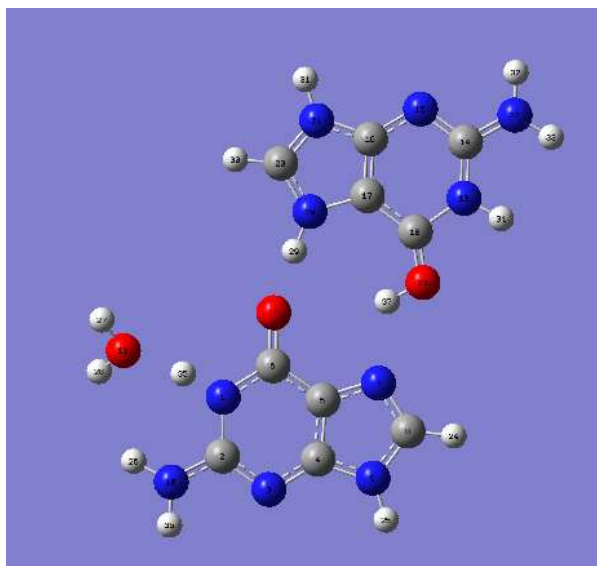
G:HCl:H2O	N1	N3	N7	N9	N2	N2-H1	N2-H2	C8-H		N9-H	
	isotropic	isotropic	isotropic	isotropic	isotropic	isotropic	isotropic	isotropic	dipolar	isotropic	
Experiment										-6.50	
		16.80			10.00	12.10	12.10	-14.50		0.50	
										6.00	
Wetmore										-6.50	
	-2.20	6.90	-1.30	-4.10	3.40	-8.20	-7.10	-22.70		-1.60	0.60
										8.10	
ub3lyp/6-311+g(d,p)										-11.47	
	-2.22	6.57	-2.04	-4.60	3.94	-8.07	-7.46	-21.19		-1.92	1.27
										13.39	
b3pw91/6-311+g(d,p)										-11.73	
	-2.09	4.87	-2.33	-4.75	3.21	-8.03	-7.39	-22.66		-1.85	1.41
										13.59	
m052x/6-311+g(d,p)										-12.27	
	-3.26	7.05	-4.45	-7.64	6.85	-8.79	-8.49	-24.82		-2.23	2.59
										14.49	
m062x/6-311+g(d,p)										-11.37	
	-3.55	12.24	-4.27	-7.65	8.02	-8.95	-8.26	-19.72		-2.59	1.02
										13.97	
ub3lyp/epr-II										-11.50	
	-2.45	8.20	-2.06	-4.89	4.60	-8.17	-7.62	-22.73		-1.91	1.25
										13.41	
b3pw91/epr-II										-11.77	
	-2.32	6.60	-2.35	-5.05	3.89	-8.04	-7.47	-24.28		-1.87	1.35
										13.63	
m052x/epr-II										-12.42	
	-3.47	8.40	-4.77	-8.00	7.29	-7.19	-7.33	-23.20		-2.23	2.01
										14.64	
m062x/epr-II										-11.47	
	-3.80	13.51	-4.57	-8.21	8.36	-9.26	-8.52	-21.25		-2.48	1.00
										13.94	
ub3lyp/epr-III										-11.42	
	-2.38	8.34	-1.70	-4.57	4.59	-8.06	-7.40	-22.50		-1.31	1.28
										12.73	
b3pw91/epr-III										-11.70	
	-2.28	7.11	-2.06	-4.80	4.05	-7.95	-7.27	-24.22		-1.17	1.41
										12.86	
m052x/epr-III										-12.17	
	-3.26	9.21	-4.60	-7.35	6.28	-7.46	-7.51	-23.97		-1.89	2.07
										14.06	
m062x/epr-III										-11.38	
	-3.66	14.24	-4.30	-7.68	7.73	-9.43	-8.53	-20.03		-2.34	0.91
										13.71	

Table 25. The calculated HFCCs on the N7-deprotonated native guanine cation radical of the system shown in Figure. 15.

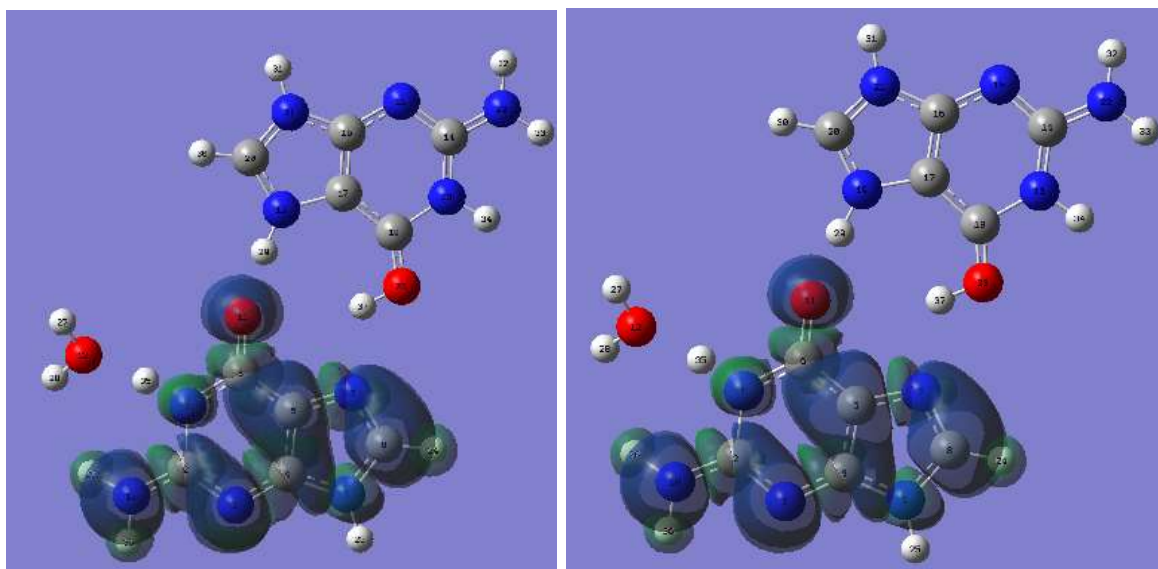
Firstly, the single optimized native guanine cation radical from Gm-Opt-2 is isolated into gas phase. It is interesting to mention that during this stage of work, I came to an idea that ONIOM method might need an extrapolation procedure when doing single point spin polulation

and HFCC calculations. In other words, currently, ONIOM's single point calculation on the model system give the same results as calculating the model system in gas phase.

As can be seen from Table 24 and Table 25, in gas phase calculation, all levels of examined theories give similar spin density distributions resembling to the results from Wetmore et al.¹⁶, except for smaller estimation of spin densities at C4. The calculations in this case tend to overestimate the spin density at C8 by about 50% whereas underestimate spin density at N2 by 40% and N3 by 25%. Correspondingly, the isotropic hyperfine coupling at C8-H is overestimated about -6 MHz on average than the experimental value of -14.5 MHz. At the N3, N2, N2-H1 and N2-H2 sites, the isotropic couplings are underestimated by the calculations. Though M06-2X functional gives slightly better isotropic coupling results than M05-2X and B3LYP, all the calculated anisotropic hyperfine couplings at C8-H are about twice larger than the experimental value.



(a)



(b)

(c)

Figure. 16 (a) The N7-deprotonated native guanine cation radical, which is extracted from Gm-Opt-2 optimization, is H-bonded with the O6-protonated guanine base and a water molecule at its N1-H site. (b) The calculated spin density distribution of the system shown in Figure. 16 (a) at B3LYP/6-311+g(d,p) level of theory (isoval=0.0004). (c) The calculated spin density distribution of the system shown in Figure. 16 (a) at M06-2X/6-311+g(d,p) level of theory (isoval=0.0004).

G:HCl:H2O	N1	C2	N3	C4	C5	C6	N7	C8	N9	N2	O6
Experiment			0.28					0.18		0.17	
Wetmore			0.21	0.17	0.29			0.28		0.10	
ub3lyp/6-311+g(d,p)	-0.02	-0.01	0.29	-0.04	0.29	0.00	0.03	0.20	-0.04	0.23	0.11
ub3pw91/6-311+g(d,p)	-0.02	-0.01	0.29	-0.05	0.30	0.00	0.02	0.21	-0.05	0.24	0.11
m052x/6-311+g(d,p)	-0.02	-0.01	0.27	-0.04	0.34	0.01	-0.02	0.23	-0.05	0.21	0.11
m062x/6-311+g(d,p)	-0.03	-0.01	0.28	-0.04	0.31	0.01	0.00	0.22	-0.04	0.23	0.11
ub3lyp/epr-II	-0.02	-0.01	0.26	0.01	0.28	-0.01	0.02	0.20	-0.02	0.22	0.11
ub3pw91/epr-II	-0.02	-0.01	0.26	0.00	0.30	-0.02	0.01	0.21	-0.03	0.22	0.11
m052x/epr-II	-0.02	-0.01	0.25	-0.01	0.35	-0.02	-0.01	0.22	-0.04	0.21	0.10
m062x/epr-II	-0.02	-0.01	0.26	-0.01	0.33	-0.02	0.00	0.21	-0.03	0.21	0.11
ub3lyp/epr-III	-0.02	0.00	0.25	0.01	0.27	-0.01	0.03	0.20	-0.03	0.21	0.10
ub3pw91/epr-III	-0.02	0.00	0.26	0.01	0.28	-0.01	0.02	0.21	-0.04	0.22	0.11
m052x/epr-III	-0.02	0.00	0.26	0.01	0.28	0.00	0.05	0.18	-0.05	0.20	0.10
m062x/epr-III	-0.01	-0.03	0.30	-0.03	0.29	-0.01	0.04	0.18	-0.05	0.22	0.11

Table 26. The calculated Mulliken spin populations on the N7-deprotonated native guanine cation radical within the system shown in Figure. 16 (a).

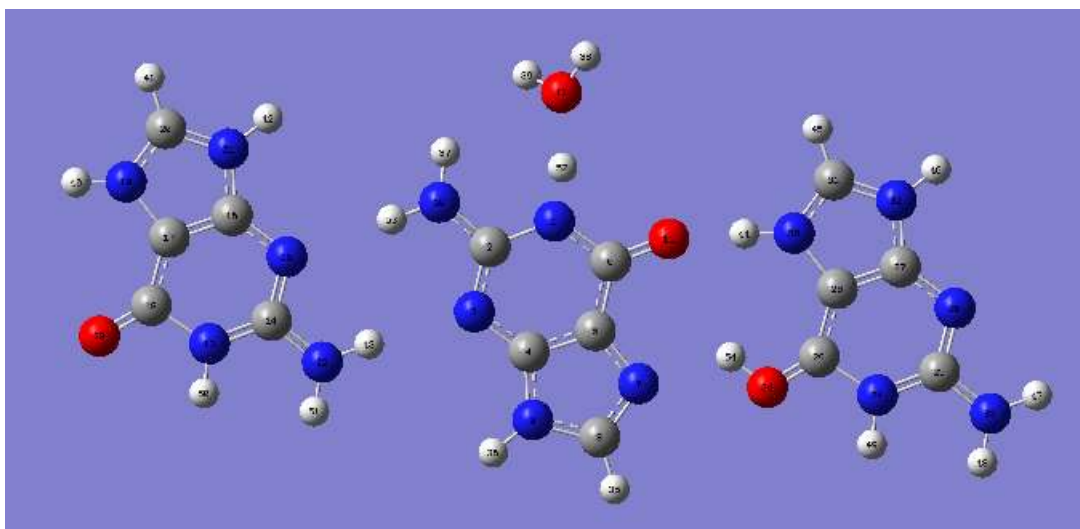
G:HCl:H2O	N1	N3	N7	N9	N2	N2-H1	N2-H2	C8-H		N9-H
	isotropic	isotropic	isotropic	isotropic	isotropic	isotropic	isotropic	isotropic	dipolar	isotropic
Experiment										-6.50
		16.80			10.00	12.10	12.10	-14.50		0.50
										6.00
Wetmore										-6.50
	-2.20	6.90	-1.30	-4.10	3.40	-8.20	-7.10	-22.70		-1.60
										0.60
										8.10
ub3lyp/6-311+g(d,p)										-9.07
	-1.77	8.10	-1.22	-3.07	8.68	-15.89	-15.27	-16.55		-1.91
										0.38
										10.98
ub3pw91/6-311+g(d,p)										-9.28
	-1.62	6.14	-1.79	-3.21	7.24	-15.95	-15.28	-17.67		-1.86
										0.53
										11.14
m052x/6-311+g(d,p)										-9.69
	-2.77	8.68	-3.18	-5.07	13.88	-17.60	-17.44	-19.41		-2.16
										1.48
										11.85
m062x/6-311+g(d,p)										-8.84
	-3.41	14.84	-2.05	-4.76	16.85	-17.36	-16.80	-14.99		-2.45
										-0.12
										11.29
ub3lyp/epr-II										-9.12
	-1.99	10.03	-1.00	-3.26	9.98	-16.13	-15.56	-17.86		-1.91
										0.31
										11.02
ub3pw91/epr-II										-9.33
	-1.84	8.20	-1.55	-3.41	8.61	-16.02	-15.41	-19.04		-1.87
										0.45
										11.20
m052x/epr-II										-9.85
	-2.95	10.57	-3.23	-5.36	14.72	-14.79	-15.23	-18.61		-2.15
										1.12
										12.00
m062x/epr-II										-8.95
	-3.63	16.56	-2.13	-5.19	17.47	-17.80	-17.52	-16.37		-2.36
										-0.16
										11.31
ub3lyp/epr-III										-9.11
	-1.91	10.16	-0.71	-3.08	9.91	-15.76	-15.08	-17.76		-1.45
										0.39
										10.56
ub3pw91/epr-III										-9.34
	-1.80	8.81	-1.26	-3.27	8.90	-15.70	-14.97	-19.10		-1.34
										0.55
										10.68
m052x/epr-III										-9.76
	-2.71	11.92	-2.91	-5.04	12.91	-15.06	-15.35	-19.36		-1.91
										1.22
										11.67
m062x/epr-III										-8.98
	-3.45	17.86	-1.78	-4.96	16.23	-17.67	-17.44	-15.69		-2.25
										-0.20
										11.23

Table 27. The calculated HFCCs on the N7-deprotonated native guanine cation radical within the system shown in Figure. 16 (a).

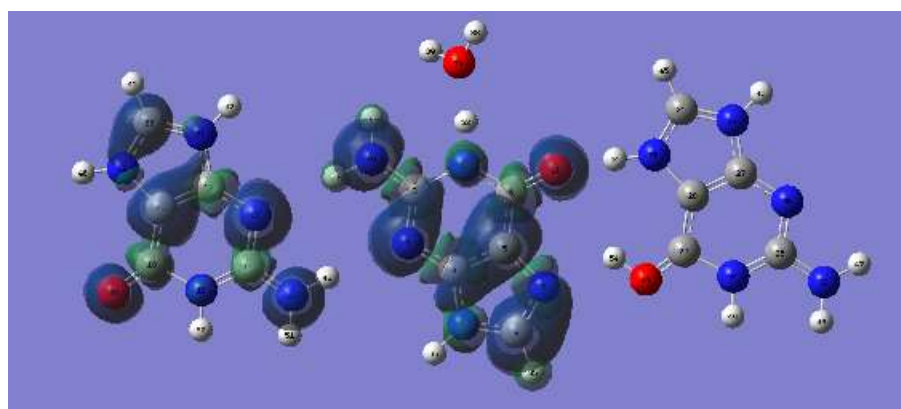
Now we include the nearby O6-protonated guanine and a water molecule which forms an H-bond with the radical's N1-H site into the single point calculation, as shown in Figure. 16 (a). The spin density distributions are localized at the radical in all the tested jobs. While the spin densities at N2 are about 17% overestimated on average at all tested levels of theories, the spin density at N3 and C8 are in good agreement with the experimental value. In the C8 column in Table 26, both B3LYP and B3PW91 functionals give the same spin populations, 0.20 and 0.21 in respect, at C8 atom for their combinations with 6-311+g(d,p), EPR-II and EPR-III. Meanwhile, M05/6-2X demonstrate gradual improvement at this site, from the C8 spin population values of 0.23 and 0.22 with 6-311+g(d,p) basis set, to 0.22 and 0.21 with EPR-II basis set, and finally 0.18 and 0.18 with EPR-III basis set, which is exactly the experimental value.

The inclusion of the N-H...O hydrogen bond at the radical's O6 suppresses the calculated spin population at O6 by half from the value of 0.23 in the gas phase system to the value of 0.11 in the system shown in Figure. 16. As can be seen in Table 27, the M06-2X functional gives excellent isotropic hyperfine couplings at N3 and C8-H, though the H-bond at N3 site has not yet included. Interesting patterns can be found between the functional/basis set combinations and their calculated iHFCC at the N3 and C8-H sites in Table 27. With the combination of each basis set, B3LYP and M05-2X functionals give very close iHFCC values at N3, while B3PW91 gives lower values and M06-2X gives higher values at N3. At C8-H sites, B3PW91 and M05-2X functionals always give higher iHFCC values than those given by B3LYP and M06-2X functionals when combining with each basis set.

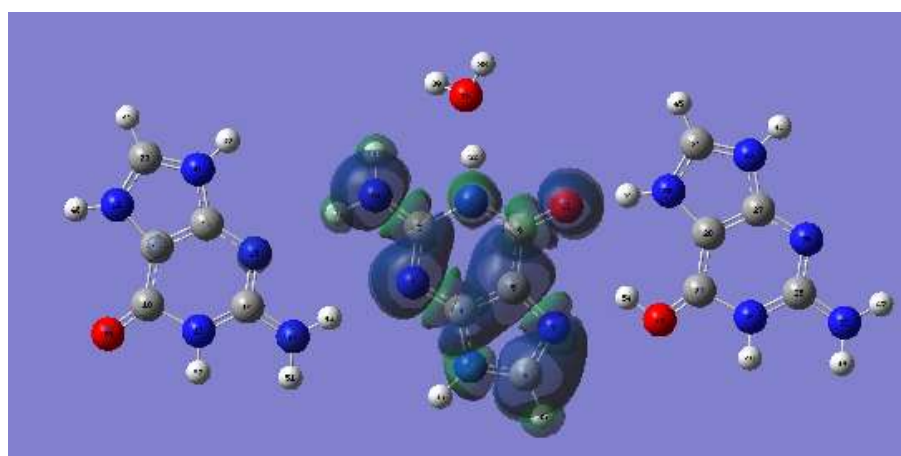
In Table 27, the isotropic hyperfine couplings at N2-H1 and N2-H2 sites, and the anisotropic coupling constants at C8-H site are universally overestimated in all the calculations. More complete environmental factors need to be covered, as will be shown in Figure. 17.



(a)



(b)



(c)

Figure. 17 (a) A third native guanine base, which forms N2-H2...N3 and N3...H2-N2 Hydrogen bonds with the radical, is further included based on the single point calculation system shown in Figure. 16. (b) The calculated spin density distribution of the system shown in Figure. 17 (a) at B3LYP/EPR-III level of theory (isoval=0.0004). (c) The calculated spin density distribution of the system shown in Figure. 17 (a) at M06-2X/EPR-III level of theory (isoval=0.0004).

G:HCl:H2O	N1	C2	N3	C4	C5	C6	N7	C8	N9	N2	O6
Experiment			0.28					0.18		0.17	
Wetmore			0.21	0.17	0.29			0.28		0.10	
ub3lyp/6-311+g(d,p)	-0.01	-0.01	0.18	0.01	0.19	0.00	0.01	0.16	-0.04	0.14	0.08
ub3pw91/6-311+g(d,p)	-0.01	-0.01	0.19	0.00	0.20	-0.01	0.01	0.17	-0.04	0.15	0.08
m052x/6-311+g(d,p)	-0.03	-0.01	0.24	0.00	0.33	0.01	-0.03	0.26	-0.06	0.19	0.11
m062x/6-311+g(d,p)	-0.03	-0.01	0.25	-0.01	0.31	0.00	-0.01	0.24	-0.05	0.20	0.11
ub3lyp/epr-II	-0.01	0.00	0.16	0.02	0.20	-0.02	0.01	0.16	-0.02	0.14	0.08
ub3pw91/epr-II	-0.01	-0.01	0.16	0.02	0.21	-0.02	0.00	0.16	-0.03	0.14	0.08
m052x/epr-II	-0.02	-0.01	0.23	0.02	0.35	-0.03	-0.02	0.24	-0.05	0.19	0.11
m062x/epr-II	-0.02	-0.01	0.24	0.01	0.33	-0.03	0.00	0.23	-0.04	0.19	0.11
ub3lyp/epr-III	-0.01	0.00	0.16	0.03	0.19	-0.01	0.02	0.15	-0.03	0.13	0.08
ub3pw91/epr-III	-0.01	0.00	0.16	0.03	0.20	-0.01	0.01	0.16	-0.04	0.14	0.08
m052x/epr-III	-0.01	-0.02	0.24	0.03	0.29	-0.01	0.04	0.20	-0.05	0.17	0.11
m062x/epr-III	-0.01	-0.05	0.30	-0.01	0.30	-0.02	0.04	0.20	-0.06	0.19	0.11

(a)

Guan 3	N1	C2	N3	C4	C5	C6	N7	C8	N9	N2	O6
Experiment											
Wetmore											
ub3lyp/6-311+g(d,p)	0.00	-0.02	0.14	-0.03	0.10	-0.03	0.00	0.03	-0.01	0.07	0.06
ub3pw91/6-311+g(d,p)	0.00	-0.02	0.15	-0.03	0.11	-0.03	-0.01	0.03	-0.01	0.07	0.06
m052x/6-311+g(d,p)	0.00	0.00	0.00	0.00	0.00	0.00	0.00	0.00	0.00	0.00	0.00
m062x/6-311+g(d,p)	0.00	0.00	0.01	0.00	0.01	0.00	0.00	0.00	0.00	0.01	0.00
ub3lyp/epr-II	0.00	-0.02	0.13	-0.02	0.10	-0.02	0.00	0.03	0.00	0.06	0.06
ub3pw91/epr-II	0.00	-0.02	0.13	-0.02	0.10	-0.02	-0.01	0.03	0.00	0.06	0.06
m052x/epr-II	0.00	0.00	0.00	0.00	0.00	0.00	0.00	0.00	0.00	0.00	0.00
m062x/epr-II	0.00	0.00	0.01	0.00	0.01	0.00	0.00	0.00	0.00	0.01	0.00
ub3lyp/epr-III	0.00	-0.01	0.13	-0.01	0.09	-0.02	0.00	0.03	-0.01	0.06	0.06
ub3pw91/epr-III	0.00	-0.02	0.13	-0.01	0.09	-0.02	0.00	0.03	-0.01	0.07	0.06
m052x/epr-III	0.00	0.00	0.00	0.00	0.00	0.00	0.00	0.00	0.00	-0.01	0.00
m062x/epr-III	0.00	0.00	0.01	0.00	0.00	0.00	0.00	0.00	0.00	-0.01	0.00

(b)

Table 28. (a) The calculated Mulliken spin populations on the N7-deprotonated native guanine cation radical within the system shown in Figure. 17 (a). (b) The calculated Mulliken spin

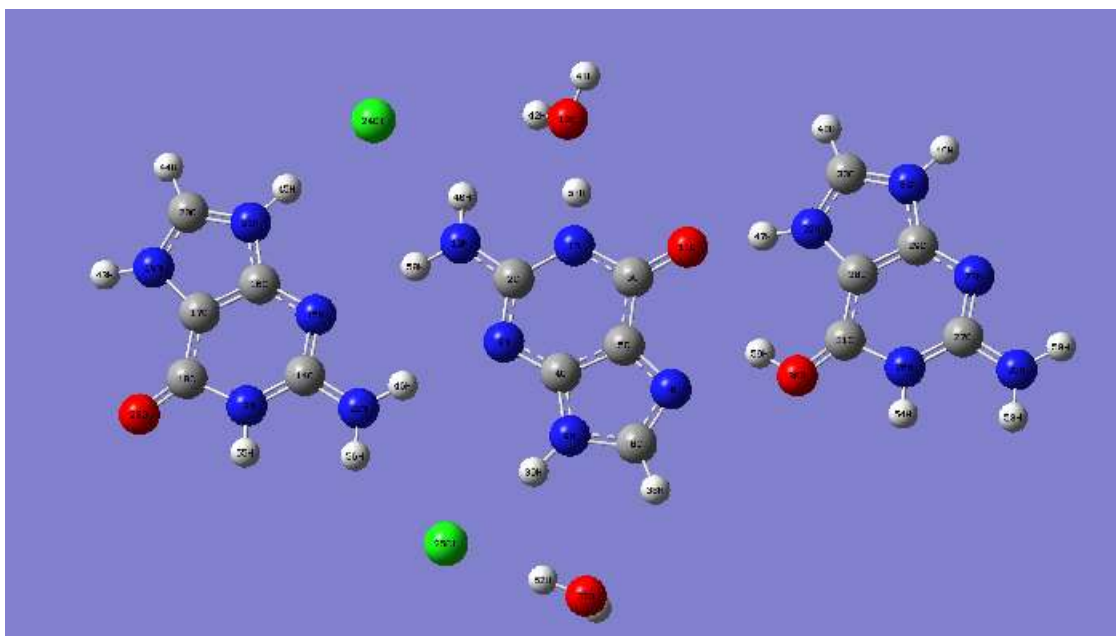
populations on the native guanine base molecule within the system shown on the left in Figure. 17 (a).

G:HCl:H2O	N1	N3	N7	N9	N2	N2-H1	N2-H2	C8-H		N9-H
	isotropic	isotropic	isotropic	isotropic	isotropic	isotropic	isotropic	isotropic	dipolar	isotropic
Experiment									-6.50	
		16.80			10.00	12.10	12.10	-14.50	0.50	
									6.00	
Wetmore									-6.50	
	-2.20	6.90	-1.30	-4.10	3.40	-8.20	-7.10	-22.70	-1.60	0.60
									8.10	
ub3lyp/6-311+g(d,p)									-7.00	
	-1.14	5.28	-1.05	-2.59	5.16	-9.61	-8.93	-12.79	-1.46	0.52
									8.46	
ub3pw91/6-311+g(d,p)									-7.18	
	-1.04	4.12	-1.42	-2.69	4.31	-9.62	-8.91	-13.64	-1.43	0.62
									8.60	
m052x/6-311+g(d,p)									-10.47	
	-2.63	8.63	-3.41	-6.07	12.60	-15.77	-15.65	-21.25	-2.28	2.07
									12.75	
m062x/6-311+g(d,p)									-9.45	
	-3.21	14.47	-2.34	-5.80	15.25	-15.55	-15.03	-16.19	-2.56	0.39
									12.01	
ub3lyp/epr-II									-7.05	
	-1.30	6.51	-0.92	-2.76	5.95	-9.75	-9.12	-13.83	-1.46	0.49
									8.51	
ub3pw91/epr-II									-7.23	
	-1.19	5.42	-1.28	-2.87	5.14	-9.66	-9.01	-14.73	-1.43	0.57
									8.66	
m052x/epr-II									-10.64	
	-2.80	10.23	-3.50	-6.40	13.38	-13.09	-13.51	-20.52	-2.29	1.62
									12.92	
m062x/epr-II									-9.59	
	-3.42	15.94	-2.46	-6.31	15.84	-15.89	-15.68	-17.70	-2.47	0.38
									12.06	
ub3lyp/epr-III									-7.04	
	-1.25	6.62	-0.69	-2.60	5.97	-9.62	-8.89	-13.75	-1.12	0.53
									8.16	
ub3pw91/epr-III									-7.24	
	-1.17	5.84	-1.06	-2.75	5.37	-9.57	-8.82	-14.78	-1.03	0.63
									8.28	
m052x/epr-III									-10.50	
	-2.60	11.16	-3.17	-5.96	11.74	-13.42	-13.56	-21.23	-2.03	1.71
									12.53	
m062x/epr-III									-9.62	
	-3.27	16.82	-2.09	-6.00	14.76	-15.87	-15.74	-16.98	-2.37	0.33
									11.99	

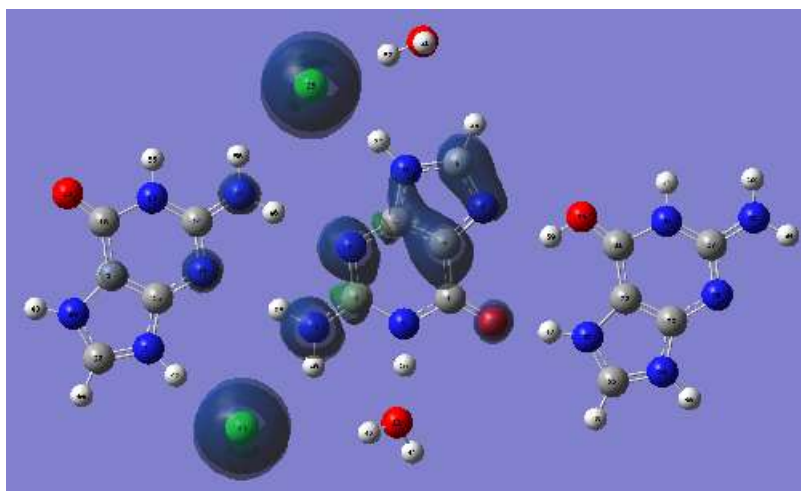
Table 29. The calculated HFCCs on the N7-deprotonated native guanine cation radical within the system shown in Figure. 17 (a).

In the system shown in Figure. 17 (a), a third guanine base is further included, which forms two $N3\cdots H2-N2$ H-bonds with the radical. Up to this point, the H-bonding environment for the radical is complete if the weak $N9-H\cdots Cl-$ and $N2-H1\cdots Cl-$ hydrogen bonds can be ignored. For B3LYP and B3PW91 functionals, their calculated unpaired spin densities delocalize to the third guanine base, though the protonated guanine still keeps clear from unpaired spin densities. As shown in Table 28 (b), regardless of the different basis sets used, B3LYP and B3PW91 give non-negligible spin densities at the third guanine's N3 and C8 sites, which, noticeably, are also the experimentally determined main sites of spin densities on the radical. As a consequence, as indicated in Table 28 (a), the calculated spin densities by B3LYP and B3PW91 at the radical's N3, C8 and N2 sites are all smaller than those values determined by the experiment, as well as than those localized values predicted by M05/6-2X functionals. For those sites where M05/6-2X give unsubstantially overestimated spin densities, such as the C8 and N2 sites in Table 28 (a), B3LYP and B3PW91 happen to give more closing spin densities to experimental values. Correspondingly, in Table 29, while M05/6-2X give overestimated hyperfine couplings (both isotropic and anisotropic) at C8-H, B3LYP and B3PW91 give excellent hyperfine couplings at this site.

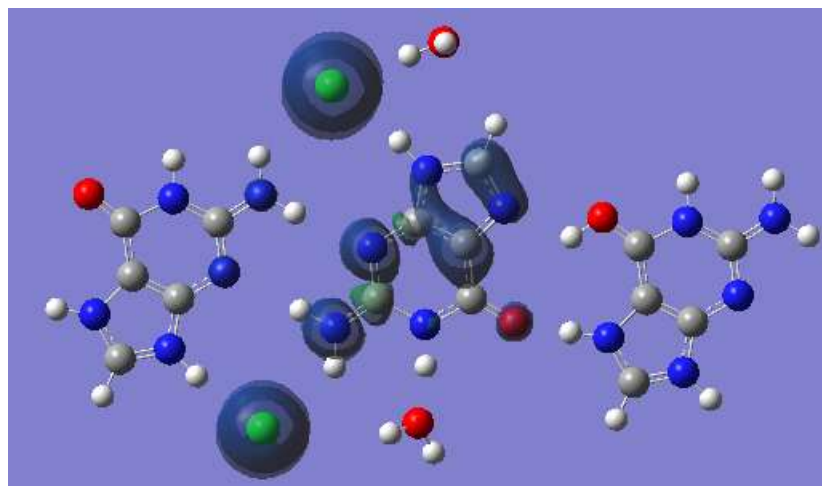
The inclusion of H-bonds to the radical's N3 and N2-H2 sites in the Figure. 17 system suppresses the N2 site's spin densities, and hence the hyperfine couplings at N2-H1 and N2-H2 sites, but it does not demonstrate obvious effects on the radical's N3 site as shown in Table 28 (a) and Table 29. Both these phenomena cannot be explained in terms of the H-bond donor and acceptor concept, which works fairly well in physically explaining cases in the N1-deprotonated cytosine cation radical calculations. At this point, we can conclude that, with the exclusion of the environmental factors introduced by the chloride ions, neither one of tested levels of DFT calculations can give satisfactory HFCC results that universally predict the experimental results. The situations should not be credited as accuracy where only one or two calculated HFCCs being matching the experimental values while the sites deviate from the experimental values. In the next step, chloride ions are included in the system, as shown in



(a)



(b)



(c)

Figure. 18 (a) The two chloride ions, which forms weak Cl \cdots H1-N2 and Cl \cdots H-N9 Hydrogen bonds with the radical with in the same ribbon plane, are included based on the single point calculation system shown in Figure. 17. (b) The calculated spin density distribution of the system shown in Figure. 18 (a) at B3LYP/6-311+g(d,p) level of theory (isoval=0.0004). (c) The calculated spin density distribution of the system shown in Figure. 18 (a) at M06-2X/6-311+g(d,p) level of theory (isoval=0.0004).

G:HCl:H2O	N1	C2	N3	C4	C5	C6	N7	C8	N9	N2	O6
Experiment			0.28					0.18		0.17	
Wetmore			0.21	0.17	0.29			0.28		0.10	
ub3lyp/6-311+g(d,p)	0.00	-0.02	0.09	-0.02	0.06	0.01	0.02	0.03	0.01	0.09	0.01
ub3pw91/6-311+g(d,p)	0.00	-0.02	0.09	-0.02	0.06	0.01	0.02	0.03	0.01	0.09	0.01
m052x/6-311+g(d,p)	0.00	-0.03	0.07	-0.02	0.05	0.01	0.01	0.02	0.01	0.08	0.01
m062x/6-311+g(d,p)	0.00	-0.03	0.07	-0.02	0.06	0.01	0.02	0.02	0.01	0.08	0.01

(a)

OW...H-N1	Cl...H1-N2	Cl...H-N9	OW...Cl
0.00	0.33	0.41	0.00
0.00	0.33	0.42	0.00
0.00	0.30	0.51	0.00
0.00	0.31	0.50	0.00

(b)

Table 30. (a) The calculated Mulliken spin populations on the N7-deprotonated native guanine cation radical within the system shown in Figure. 18 (a). (b) The calculated Mulliken spin populations on the two water molecules and two chloride ions in the system in Figure. 18 (a). The chloride ions are shown to bear the major delocalized spin densities in Figure. 18 (b) and (c).

G:HCl:H2O	N1	N3	N7	N9	N2	N2-H1	N2-H2	C8-H		N9-H	Cl(35)...H1-N2	Cl(35)...H-N9		
	isotropic	isotropic	isotropic	isotropic	isotropic	isotropic	isotropic	isotropic	dipolar	isotropic	isotropic	dipolar		
Experiment									-6.50					
		16.80			10.00	12.10	12.10	-14.50	0.50					
									6.00					
Wetmore									-6.50					
	-2.20	6.90	-1.30	-4.10	3.40	-8.20	-7.10	-22.70	-1.60	0.60				
									8.10					
ub3lyp/6-311+g(d,p)									-1.08		-50.07	-62.01		
	-0.15	2.37	0.02	-0.84	3.38	-5.77	-5.71	-3.03	-0.80	-0.18	3.08	-49.66	2.73	-61.68
									1.87			99.72		123.68
ub3pw91/6-311+g(d,p)									-1.10			-49.75		-61.73
	-0.13	1.83	-0.17	-0.87	2.81	-5.64	-5.57	-3.19	-0.78	-0.15	0.82	-49.36	-0.30	-61.36
									1.88			99.10		123.09
m052x/6-311+g(d,p)									-0.90			-49.00		-80.65
	-0.09	3.07	0.04	-0.84	5.54	-6.31	-6.38	-2.06	-0.35	-0.02	-18.90	-48.61	-32.41	-80.32
									1.24			97.61		160.96
m062x/6-311+g(d,p)									-0.93			-48.22		-76.89
	-0.19	4.76	0.48	-0.86	6.47	-6.12	-6.22	-1.92	-0.34	-0.11	-8.73	-48.21	-19.54	-76.67
									1.26			96.43		153.56

Table 31. (a) The calculated HFCCs on the N7-deprotonated native guanine cation radical within the system shown in Figure. 18 (a). The last four columns on the right listed the calculated HFCCs on the two chloride ions.

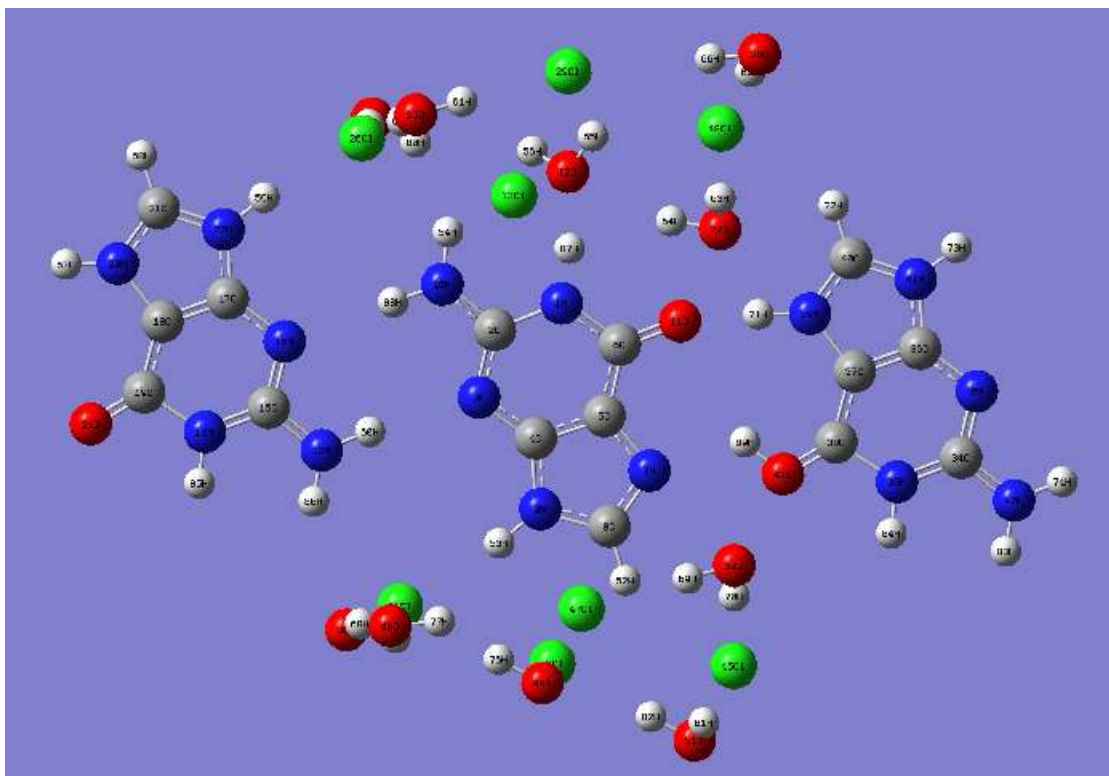
Dramatic failure happens when only the two chloride anions are added, which form weak Hydrogen bonds with the guanine radical' N2-H1 and N9-H sites. M05/6-2X functionals show even bigger delocalization errors than B3LYP and B3PW91. As shown in Table 30, the two chloride ions rob huge amount of spin densities from the radical. As a result, all hyperfine couplings at the radical are underestimated. It is worth noting that, though B3LYP, B3PW91, and M05/6-2X all predict big spin densities and anisotropic hyperfine couplings at the two chloride ions, B3LYP and B3PW91 give negligible isotropic hyperfine couplings at these two sites when compared with those given by M05/6-2X.

This delocalization error on chloride ions is partially cured, especially for M05-2X functional, by further including the other six chloride ions symmetrically located around the guanine radical, as shown in Figure. 19. B3PW91 gives broad spin density delocalization over the protonated guanine base, water molecules and chloride ions. But M05/6-2X now only predict

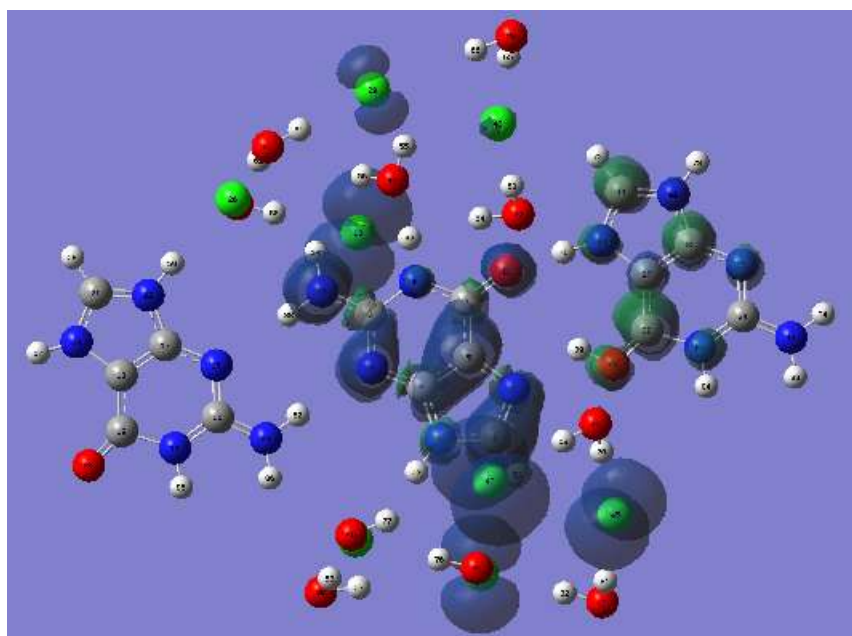
one chloride ions to be assigned with large spin densities. M05/6-2X's spin densities at the radical recovers, though still predicting underestimated values as shown in Table 32. However, M05-2X gives excellent hyperfine coupling predictions at the radical's C8-H site and amino group sites based on such underestimated spin density level. Let us compare the M05-2X's HFCC performance mentioned above in Table 33 with those listed in Table 29, where excellent spin densities are predicted but hyperfine couplings are overestimated in a system without the eight chloride ions. Also recall the McConnell relation mentioned in the introduction section, which empirically takes the spin density at the nucleus to be proportional to the populations of unpaired electrons in the neighboring π atomic orbital.¹¹ One should find the direct (delocalization) contribution of spin density at the protons due to the proton's out-of-plane coordinates in the optimized radical. This direct spin density contribution corresponds to the extra amount of spin densities at the protons in cases where the calculated iHCCs are agrees with experimental values, but the calculated Mulliken spin population at the neighboring atom is lower than those obtained from the McConnell relation.

From Table 30 to 33, it is noticeable that, though all M05/6-2X and B3LYP/PW91 functionals, at 6-311+g(d,p) level of basis set, predict large spin densities and large anisotropic hyperfine coupling constants at some chloride ions, B3LYP/PW91 functionals do not predict large isotropic hyperfine couplings at these sites, whereas M05/6-2X functionals do. Let us take the chloride ion which is labeled as Cl-6 in Table 32 and Table 33 for example, which is the chloride with the most significant spin densities in Figure 19. The side views from Figure. 19 (e) with isoval=0.00004 clearly demonstrates the d_{z^2} -orbital component of the unpaired spin density on the chloride ion.

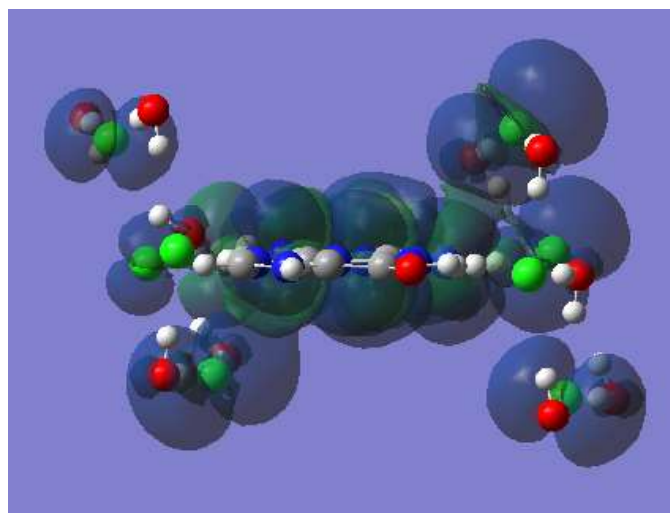
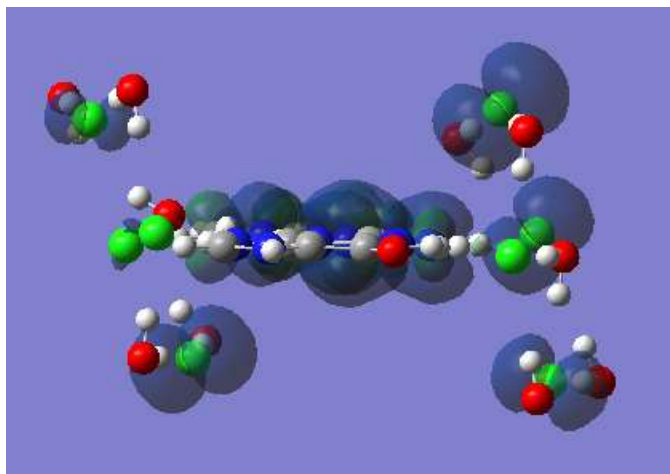
The unrealistic spin densities at chloride anion indicate wrong molecular orbital order assignments in SCF convergence process. The Alpha and Beta Kohn-Sham orbitals of the HOMO and LUMO are shown in Figure. 19 (f) and (g). Some promising procedures⁵³⁻⁵⁵ preventing such false MO assignments in initial guess stage are worth trying in order to fix this problem.



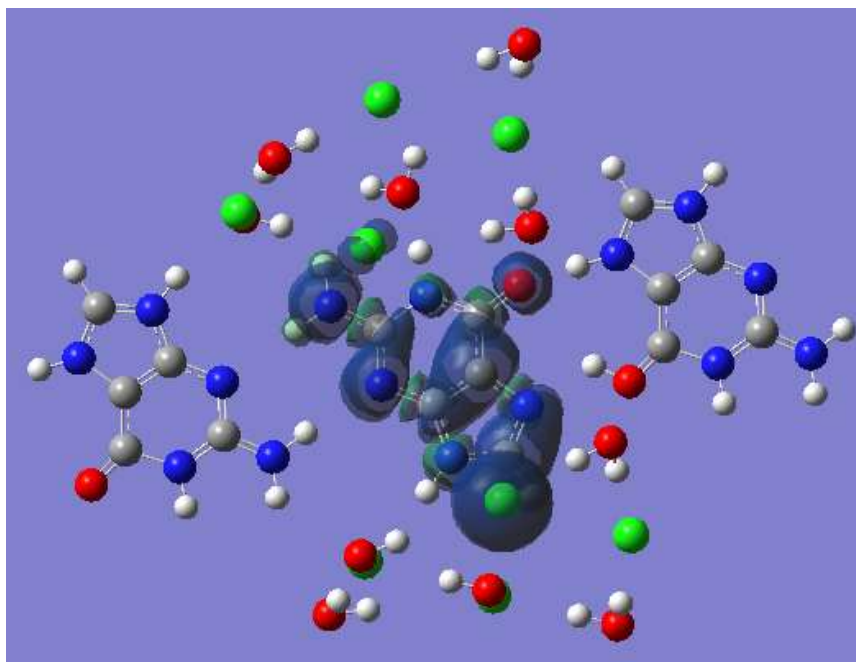
(a)



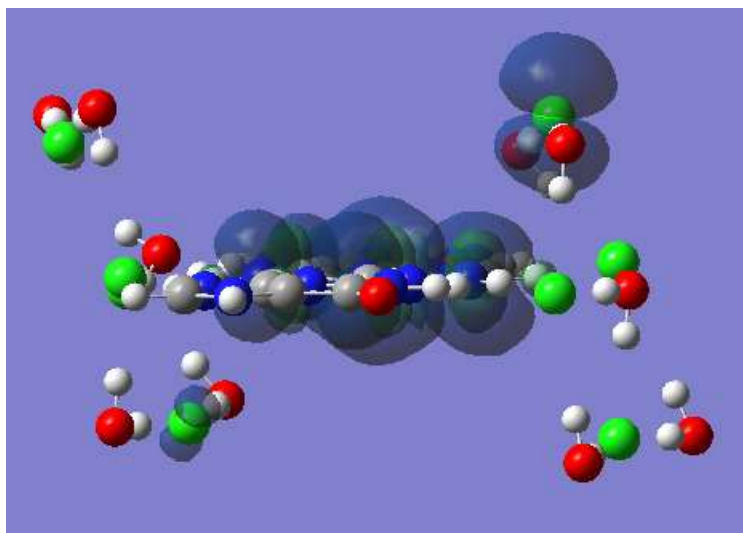
(b)

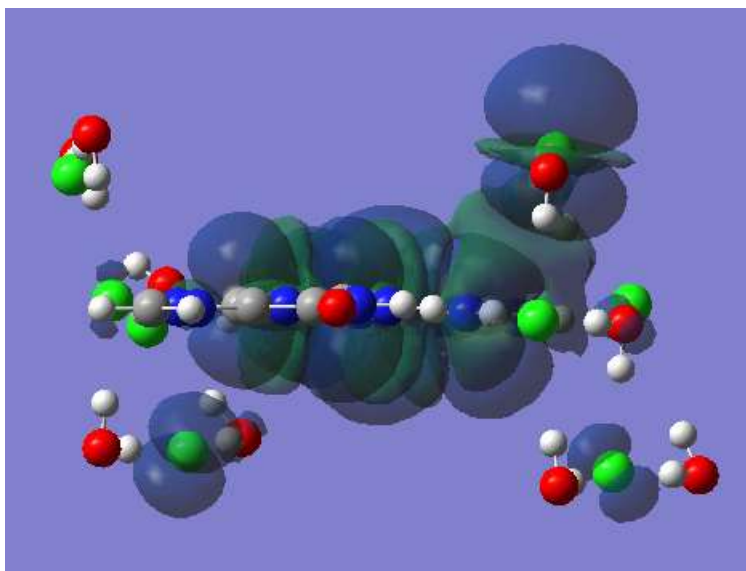


(c)

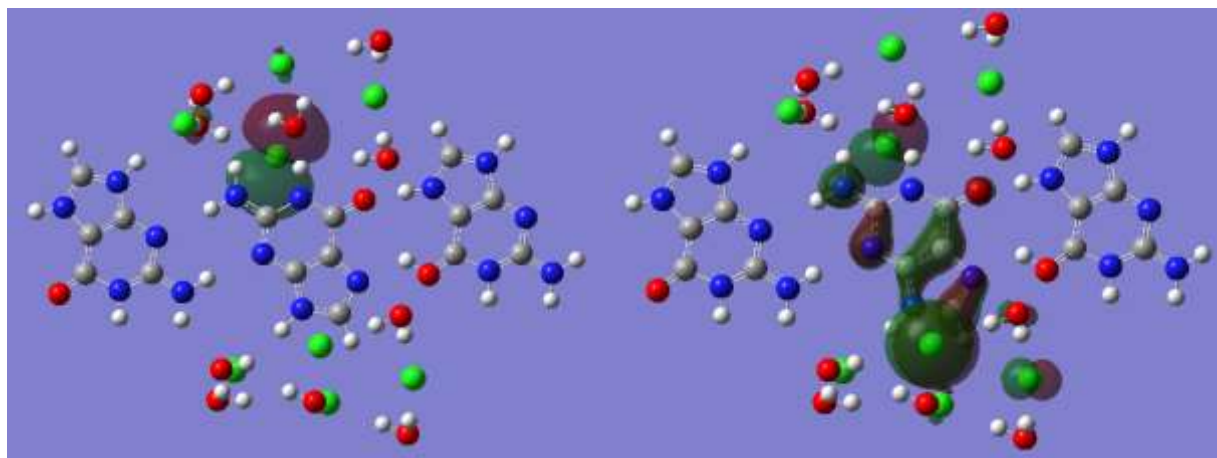


(d)

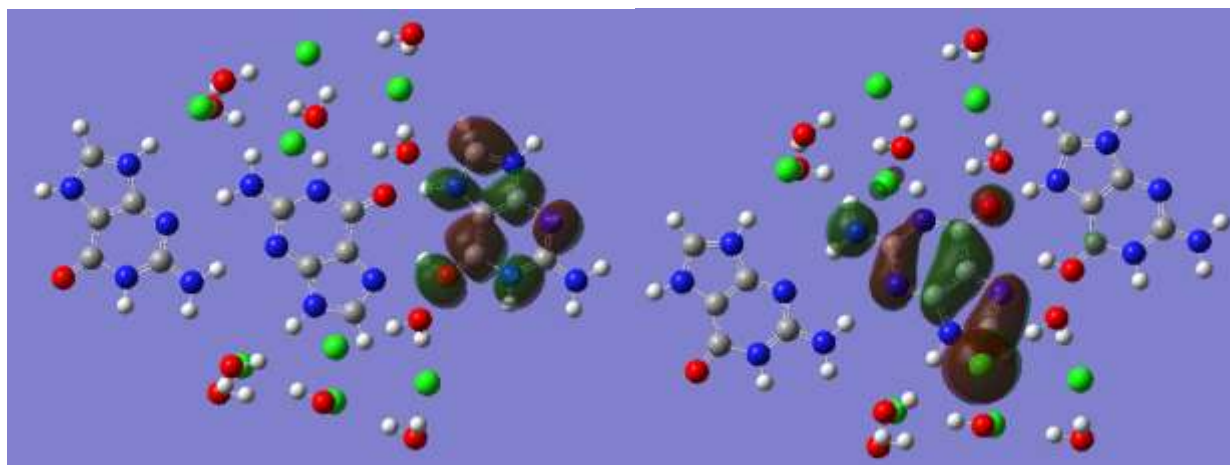




(e)



(f)



(g)

Figure. 19

(a) All the nearest eight chloride ions symmetrically located around the radical are included based on the single point calculation system shown in Figure. 17.

(b) The calculated spin density distribution of the system shown in Figure. 18 (a) at B3PW91/6-311+g(d,p) level of theory (isoval=0.0004).

(c) The side view (from left to right) of Figure. 19 (b) with isoval=0.0004 and isoval=0.00004.

(d) The calculated spin density distribution of the system shown in Figure. 18 (a) at M05-2X/6-311+g(d,p) level of theory (isoval=0.0004).

(e) The side view (from left to right) of Figure. 19 (d) with isoval=0.0004 and isoval=0.00004.

(f) The Alpha (left) and Beta (right) HOMO Kohn-Sham orbitals calculated at M05-2X/6-311+g(d,p) level of theory (isoval=0.02), this pattern matches the spin density pattern in Figure. 19 (d).

(g) The Alpha (left) and Beta (right) LUMO Kohn-Sham orbitals calculated at M05-2X/6-311+g(d,p) level of theory (isoval=0.02), this pattern matches the spin density pattern in Figure. 19 (d).

G:HCl:H2O	N1	C2	N3	C4	C5	C6	N7	C8	N9	N2	O6
Experiment			0.28					0.18		0.17	
Wetmore			0.21	0.17	0.29			0.28		0.10	
ub3pw91/6-311+g(d,j)	-0.01	0.00	0.09	-0.01	0.11	-0.01	0.02	0.10	-0.03	0.10	0.04
m052x/6-311+g(d,p)	-0.01	-0.01	0.13	0.04	0.26	-0.01	0.03	0.12	-0.04	0.14	0.06
m062x/6-311+g(d,p)	-0.01	0.00	0.12	0.03	0.23	0.00	0.05	0.06	-0.03	0.14	0.06

(a)

Cl-1	Cl-2	Cl-3	Cl-4	Cl-5	Cl-6	Cl-7	Cl-8
13	26	29	31	45	47	48	50
0.18	0.00	0.02	0.00	0.13	0.32	0.00	0.09
0.01	0.00	0.00	0.00	0.00	0.29	0.00	0.00
0.01	0.00	0.00	0.00	0.01	0.34	0.00	0.00

(b)

Guanine-2	N1	C2	N3	C4	C5	C6	N7	C8	N9	N2	O6
	33										43
	0.00	0.00	-0.01	-0.03	0.01	-0.06	-0.01	-0.03	0.01	0.00	-0.02
	0.00	0.00	0.00	0.00	0.00	0.00	0.00	0.00	0.00	0.00	0.00
	0.00	0.00	0.00	0.00	0.00	0.00	0.00	0.00	0.00	0.00	0.00

(c)

Guanine-3	N1	C2	N3	C4	C5	C6	N7	C8	N9	N2	O6
	14										24
	0.00	0.00	0.00	0.00	0.00	0.00	0.00	0.00	0.00	0.00	0.00
	0.00	0.00	0.00	0.00	0.00	0.00	0.00	0.00	0.00	0.00	0.00
	0.00	0.00	0.00	0.00	0.00	0.00	0.00	0.00	0.00	0.00	0.00

(d)

Table 32. (a) The calculated Mulliken spin populations on the N7-deprotonated native guanine cation radical within the system shown in Figure. 19 (a). (b) The calculated Mulliken spin populations on the eight chloride ions in the system in Figure. 19 (a). (c) The calculated Mulliken spin populations on the O6-protonated guanine base in the system in Figure. 19 (a).

(d) The calculated Mulliken spin populations on the native guanine molecule located on the left in Figure. 19 (a).

G:HCl:H2O	N1	N3	N7	N9	N2	N2-H1	N2-H2	C8-H		N9-H
	isotropic	isotropic	isotropic	isotropic	isotropic	isotropic	isotropic	isotropic	dipolar	isotropic
Experiment		16.80			10.00	12.10	12.10	-14.50		-6.50
										0.50
										6.00
Wetmore										-6.50
	-2.20	6.90	-1.30	-4.10	3.40	-8.20	-7.10	-22.70		-1.60
										0.60
										8.10
ub3pw91/6-311+g(d,p)										-4.62
	-0.48	2.01	-0.33	-1.65	2.73	-6.00	-6.38	-7.51		-0.50
										0.59
										5.12
m052x/6-311+g(d,p)										-7.15
	-1.44	7.85	0.88	-4.80	11.25	-11.89	-11.98	-13.53		-1.31
										2.02
										8.46
m062x/6-311+g(d,p)										-6.20
	-1.63	9.33	1.95	-4.45	11.53	-10.35	-10.49	-10.04		-1.40
										0.79
										7.60

Cl-2		Cl-3		Cl-4		Cl-5		Cl-6		Cl-7		Cl-8	
isotropic	dipolar	isotropic	dipolar	isotropic	dipolar	isotropic	dipolar	isotropic	dipolar	isotropic	dipolar	isotropic	dipolar
26		29		31		45		47		48		50	
	-0.10		-3.18		-0.05		-19.09		-47.70		-0.87		-13.06
-0.11	-0.09	0.17	-3.06	-0.03	-0.02	0.64	-18.80	0.08	-47.09	0.08	-0.72	0.60	-12.93
	0.18		6.24		0.06		37.89		94.79		1.59		25.98
	-0.17		-0.02		-0.08		-0.12		-46.52		-0.03		-0.40
-0.16	-0.08	0.00	-0.02	0.00	-0.03	-0.18	-0.06	14.72	-46.33	-0.02	-0.03	0.11	-0.39
	0.24		0.03		0.11		0.19		92.85		0.05		0.79
	-0.13		-0.02		-0.09		-0.27		-51.81		-0.04		-0.47
-0.17	-0.09	0.00	-0.02	-0.04	-0.04	0.05	-0.21	34.59	-51.62	-0.01	-0.03	0.41	-0.46
	0.23		0.03		0.13		0.48		103.43		0.07		0.92

Table 33. (a) The calculated HFCCs on the N7-deprotonated native guanine cation radical within the system shown in Figure. 19 (a). (b) The calculated HFCCs on the eight chloride ions in the system in Figure. 18 (a).

At the end of this section of calculations on the native guanine cation radical, we can come to the conclusions as follows,

1. Before the chloride ions are included into the system, the idea is generally followed that the inclusion of H-bonding effects gives better HFCC calculations than in gas phase condition, and M05/6-2X outperforms over B3LYP/PW91 functionals in suppressing the

delocalization errors in DFT approximation. However, the performed accuracy is less satisfactory when compared with the N1-deprotonated cytosine cation radical calculations.

2. After the inclusion of chloride ions into the single point calculations, M05/6-2X functionals begin to show obvious delocalization errors on the chloride ions. The symmetric allocation of the chloride ions partially cured the M05/6-2X's delocalization errors, but the error cannot be eliminated to a negligible level.
3. Further investigations in the functional approximation and in molecular orbital assignment procedures are suggested the future work.

In the next section of HFCC calculations on the N3-deprotonated 5'-dCMP cation radical, emphases are focused on the geometric parameter, including the H-bonds parameters' influences on the calculated spin densities and hyperfine coupling constants. In other words, the contributions of different external potentials in the energy functional expression on the calculated spin densities.

4.3. HFCC Calculations on N3-deprotonated 5'-dcmp Cation Radical In 5'-dgmp Monohydrate Single Crystal

In the single crystal structure of Deoxycytidine 5'-Phosphate Monohydrate determined by Viswamitra *et al.*,³⁴ one phosphate oxygen proton migrates to the N3 site of a neighboring 5'-dGMP molecule's cytosine base, which results in a zwitterion structure for each 5'-dCMP molecule. No base stacking is present in this crystal structure. The cytosine cation observed in the zwitterion structure is characterized with both bond length and bond angle differences from the cytosine bases observed in neutral cytosine derivatives. Specifically, the zwitterion's cytosine cation has its bond C2-O2 significantly shorter and C2-N3 is significantly longer than these values of a cytosine base from a neutral cytosine derivative. Its angle C(2)-N(3)-C(4) is 5° greater and N(1)-C(2)-N(3) and N(3)-C(4)-C(5) are about 4° to 5° smaller than the values observed in a neutral cytosine derivative. The 5'-dCMP zwitterion's pyrimidine ring is not

strictly planar in its single crystal structure where N3 and C2 deviate from the plane in opposite directions. This non-planar property can be attributed to its H-bonding environment. The oxygen on the cytosine base cation, as well as the C2 site, deviates from the base plane in a direction such that a stronger H-bond can be formed with a water molecule. The amino group involves in two H-bonds with the phosphate oxygen atoms from two different 5'-dCMP molecules. The protonated N3-H site forms H-bond with a phosphate oxygen atom which deprotonates and donates that proton. The 3'-hydroxyl group on the deoxyribose group forms H-bonds with a water molecule where the 3'-hydroxyl group is a donor, and with a hydroxyl group from another 5'-dCMP molecule's phosphate group where the 3'-hydroxyl group is an acceptor. The other two oxygen atoms in phosphate group each forms bifurcated hydrogen bonds. In general, as Viswamitra et al. mentioned, all the available hydrogen atoms participate in Hydrogen bonding.

4.3.1. H-bonds Parameters in Optimized Geometries

Two geometry optimizations at ONIOM(uB3LYP/6-31g:uB3LYP/3-21g) level of theory are conducted, where the initial geometry is assigned such as the cytosine oxidation radical deprotonates at N3 and the opposite phosphate oxygen atom protonates. The first optimization job, here we name it as 5'-dCMP-Opt-1, adopts fairly complete environment which includes eleven 5'-dCMP molecules surrounding the central radical, as shown in Figure. 20. The second optimization job, here we name it as 5'-dCMP-Opt-2, only includes a minimum set of four surrounding 5'-dCMP molecules and H-bonding water molecules, which, nevertheless covers all the direct H-bonding effects with the central radical, as shown in Figure. 21. In the radical of 5'-dCMP-Opt-1 optimized geometry, the bond angle C2-N3-C4 decreases by 3.6°, and angle N1-C2-N3 and N3-C4-C5 increases by 3.3° and 2.2°, which become closer to the parameters observed from the neutral cytosine derivatives. In 5'-dCMP-Opt-2 optimized geometry, these three angles changes by 4.1°, 4.2° and 2.2° in respect. The most significant differences between the optimized geometries from 5'-dCMP-Opt-1 and 5'-dCMP-Opt-2 come from the dihedral angles in the deoxyribose which could be attributed to 5'-dCMP-Opt-2' lack of environmental constraints around this sugar group.

In the crystalline H-bonds (here labeled as A-H...B) network, as shown in Table 34 (a), O3'-H...OW and O2...H-OW have the longest A-B distance of 2.98 Å and 2.95 Å respectively, while O3'...H-OII has the shortest A-B distance of only 2.61 Å. H-bond angles A-H-B are all

between 163 to 173 degrees except for the 149.6° of O2···H-OW, where the same water molecule also forms H-bonds OI···H-OW. The H-bonds in 5'-dCMP-Opt-1 optimized system as listed in Table 34 (b), O3'-H···OW is optimized to be 10.3° more linear, and N4-H2···OI is optimized to be 8.0° less linear (in contrast with the 7.2° and 5.9° degrees respectively in 5'-dCMP-Opt-1 optimization). The A-B distances are generally decreased in Table 34 (b) compared with those in Table 34 (a), where -0.16 Å and -0.12 Å of O2···H-OW and N4-H1···OIII are the two most obvious changes. In 5'-dCMP-Opt-2 optimized geometry as listed in Table 34 (c), the H-bonds pattern behaves fairly differently due to its lack of non-hydrogen-bonding constrains when compared with that of 5'-dCMP-Opt-1, which will reflect more purely H-bonding influences on the geometric optimization. The most obvious changes happen with its phosphate group, where the bond angle OIII···H1-N4 and OIII···H-N3 become 12.1° and 7.4° less linear. In both 5'-dCMP-Opt-1 and 5'-dCMP-Opt-2 optimized geometries, the P-O bond lengths are elongated about 0.12 Å for P-OI, P-OII and P-OIII, and are elongated about 0.16 Å for O5'-P, which results in changes in their H-bonds parameters. However, these P-O bond changes might be problematic since, as Foresman *et al.*⁵⁶ mentioned, both the tripe zeta basis set and multiple polarization functions are needed to produce a very accurate P-O bond structure at the B3LYP level of theory. The lack of diffuse functions in the adopted basis set in these two optimization jobs may also introduce problems in optimizing this anionic phosphate group.

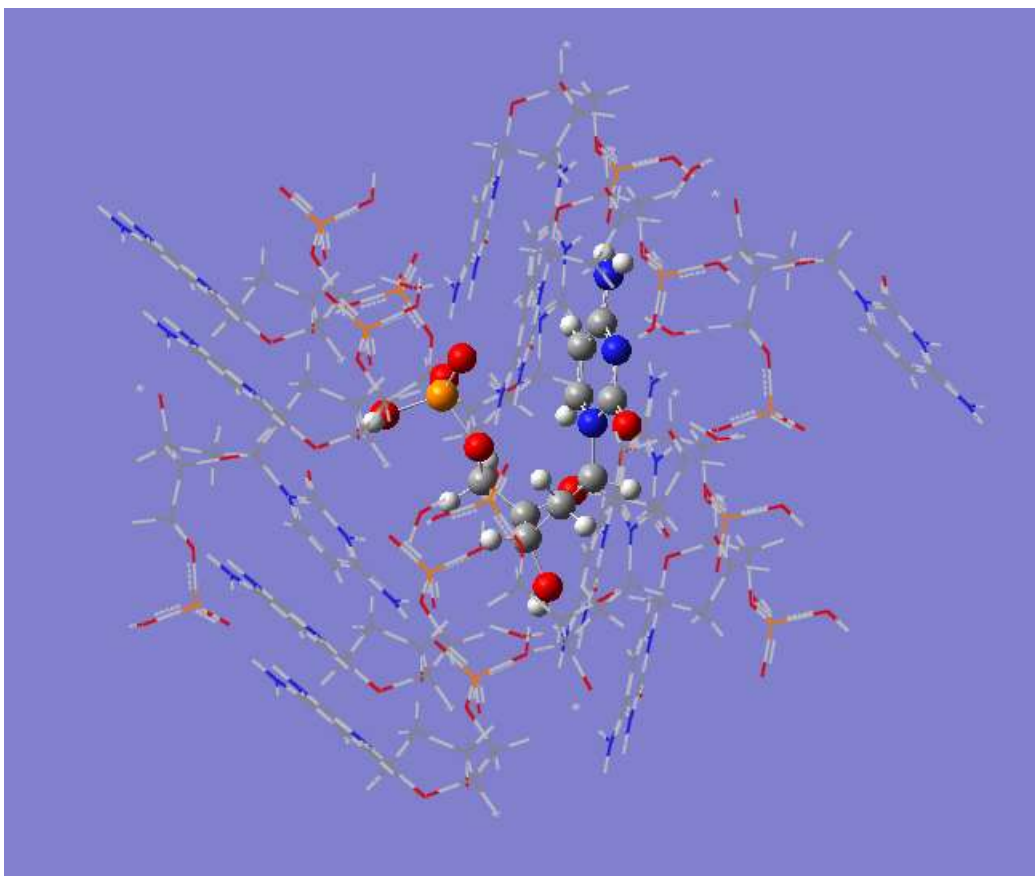


Figure. 20 The 5'-dCMP-Opt-1 optimization job, which adopts fairly complete environment that includes eleven 5'-dCMP molecules surrounding the central radical.

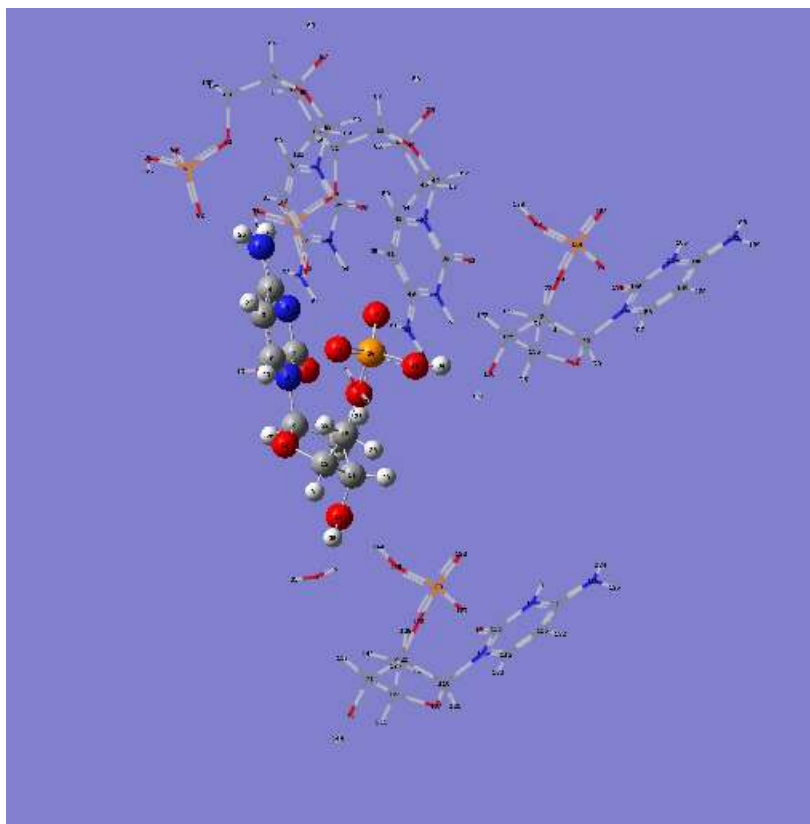


Figure. 21 The 5'-dCMP-Opt-2 optimization job, which only includes a minimum set of four surrounding 5'-dCMP molecules and H-bonding water molecules. It covers all the H-bonding effects with the central radical.

crystal	Bond length			Bond angle
A-H...B	A-H	A...B	H...B	A-H-B
O2...H-OW		2.94642	2.34206	149.6901
N3-H...OIII	0.99974	2.87379	1.88322	170.3924
N4-H2...OI	0.90668	2.69098	1.78906	172.787
N4-H1...OIII	1.04866	2.98034	1.9375	172.5024
O3'-H...OW	1.09782	2.69086	1.6196	163.6578
O3'...H-OII		2.60878	1.66086	167.388
OI...H2-N4		2.69098	1.78906	172.787
OI...H-OW		2.71177	1.81122	164.8653
OII-H...O3'	0.96268	2.60878	1.66086	167.388
OIII...H-N3		2.87379	1.88322	170.3924
OIII...H1-N4		2.98034	1.9375	172.5024

(a)

5'-dCMP-Opt-1 (Type 1)				5'-dCMP-Opt-1's difference from crystal paramters					
A-H...B	Bond length			Bond angle	A-H...B	Bond length			Bond angle
	A-H	A...B	H...B			A-H	A...B	H...B	
O2...H-OW		2.78477	1.90687	150.8326	O2...H-OW		-0.16165	-0.43519	1.14257
N3...H-OIII		2.68803	1.73081	174.5351	N3...H-OIII				
N4-H2...OI	1.01815	2.70418	1.70838	164.8189	N4-H2...OI	0.11147	0.0132	-0.08068	-7.96812
N4-H1...OIII	1.03525	2.85802	1.83675	168.2166	N4-H1...OIII	-0.01341	-0.12232	-0.10075	-4.28573
O3'-H...OW	1.00907	2.67358	1.66797	173.9915	O3'-H...OW	-0.08875	-0.01728	0.04837	10.33366
O3'...H-OII		2.58127	1.64117	164.3349	O3'...H-OII		-0.02751	-0.01969	-3.05317
OI...H2-N4		2.62331	1.71986	174.0206	OI...H2-N4		-0.06767	-0.0692	1.23364
OI...H-OW		2.62309	1.66945	171.6891	OI...H-OW		-0.08868	-0.14177	6.82382
OII-H...O3'	1.03959	2.51182	1.47747	172.4943	OII-H...O3'	0.07691	-0.09696	-0.18339	5.10628
OIII...H-N3		2.86651	1.88262	167.3712	OIII...H-N3		-0.00728	-0.0006	-3.02118
OIII...H1-N4		2.91614	1.87608	170.8247	OIII...H1-N4		-0.0642	-0.06142	-1.67771

(b)

5'-dCMP-Opt-2 (Type 2)				5'-dCMP-Opt-2's difference from crystal paramters					
A-H...B	Bond length			Bond angle	A-H...B	Bond length			Bond angle
	A-H	A...B	H...B			A-H	A...B	H...B	
O2...H-OW		2.9522	2.08907	148.4024	O2...H-OW		0.00578	-0.25299	-1.28765
N3...H-OIII		2.75261	1.80157	175.6665	N3...H-OIII				
N4-H2...OI	1.03422	2.67866	1.66118	166.8556	N4-H2...OI	0.12754	-0.01232	-0.12788	-5.93139
N4-H1...OIII	1.03798	2.8507	1.81995	171.5226	N4-H1...OIII	-0.01068	-0.12964	-0.11755	-0.97979
O3'-H...OW	0.99739	2.72179	1.73251	170.8266	O3'-H...OW	-0.10043	0.03093	0.11291	7.16882
O3'...H-OII		2.58397	1.62469	169.4546	O3'...H-OII		-0.02481	-0.03617	2.06661
OI...H2-N4		2.61289	1.72425	168.6048	OI...H2-N4		-0.07809	-0.06481	-4.18223
OI...H-OW		2.92049	1.96096	170.7584	OI...H-OW		0.20872	0.14974	5.89316
OII-H...O3'	1.00197	2.61851	1.63366	166.537	OII-H...O3'	0.03929	0.00973	-0.0272	-0.85101
OIII...H-N3		3.16598	2.20169	162.9595	OIII...H-N3		0.29219	0.31847	-7.43291
OIII...H1-N4		2.66645	1.65857	160.367	OIII...H1-N4		-0.31389	-0.27893	-12.13537

(c)

Difference of 5'-dCMP-Opt-2 from 5'-dCMP-Opt-1				
A-H...B	Bond length			Bond angle
	A-H	A...B	H...B	
O2...H-OW		0.16743	0.1822	-2.43022
N3...H-OIII		0.06458	0.07076	1.13144
N4-H2...OI	0.01607	-0.02552	-0.0472	2.03673
N4-H1...OIII	0.00273	-0.00732	-0.0168	3.30594
O3'-H...OW	-0.01168	0.04821	0.06454	-3.16484
O3'...H-OII		0.0027	-0.01648	5.11978
OI...H2-N4		-0.01042	0.00439	-5.41587
OI...H-OW		0.2974	0.29151	-0.93066
OII-H...O3'	-0.03762	0.10669	0.15619	-5.95729
OIII...H-N3		0.29947	0.31907	-4.41173
OIII...H1-N4		-0.24969	-0.21751	-10.45766

(d)

Table 34. (a) The H-bonds parameters of a normal 5'-dCMP molecule determined by Viswamitra *et al.*³⁴ (b) The H-bonds parameters of the optimized N3-deprotonated 5'-dCMP radical in 5'-dCMP-Opt-1 job, and their differences from those in the crystalline structure. (c) The H-bonds

parameters of the optimized N3-deprotonated 5'-dCMP radical in 5'-dCMP-Opt-2 job, and their differences from those in the crystalline structure. (d) The H-bond parameter differences of the 5'-dCMP-Opt-2 optimized system from the 5'-dCMP-Opt-1 optimized system.

4.3.2. Spin Density and HFCC Calculations

In the following single point calculations on different scales of systems extracted from the 5'-dCMP-Opt-1 and 5'-dCMP-Opt-2 optimized geometry, we focus on the influences of the geometric parameters on spin density and hyperfine coupling calculations.

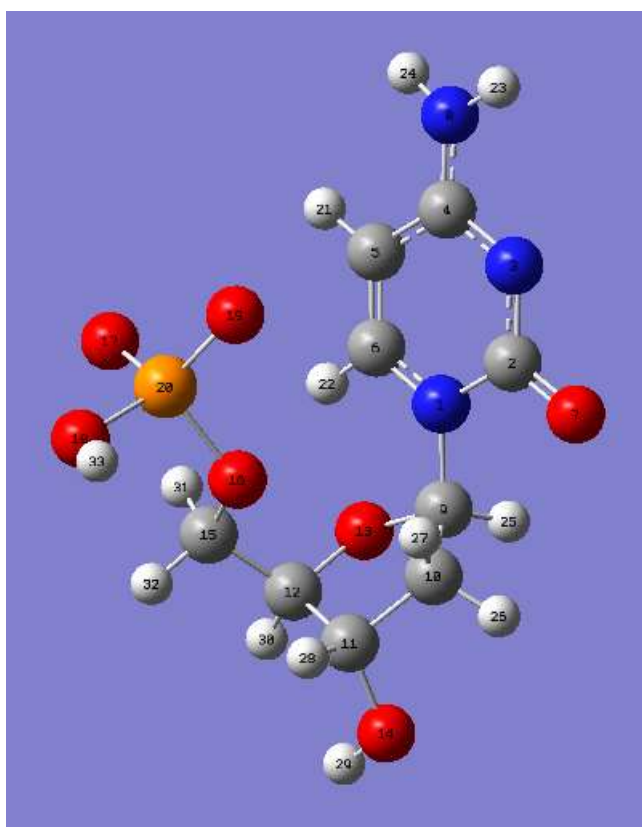


Figure. 22 The isolated N3-deprotonated 5'-dCMP cation radical.

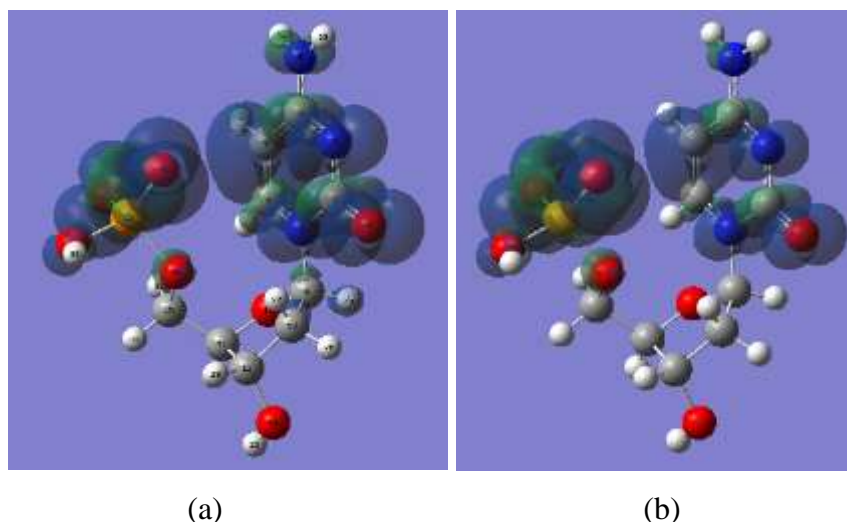


Figure. 23 The calculated spin density distribution of the isolated 5'-dCMP cation radical from 5'-dCMP-Opt-1 optimized geometry. (isoval=0.0004) (a) Calculated at B3LYP/6-311+g(d,p) level of theory. (b) Calculated at M06-2X/6-311+g(d,p) level of theory.

5'-dCMP	N1	C2	N3	C4	C5	C6	O2	N4	C1'	OI	OII	OIII	P
Experiment	0.3					0.6		0.17					
Wetmore			0.24		0.33		0.45						
ub3lyp/6-311+g(d,p)	0.08	-0.06	0.10	-0.05	0.18	-0.03	0.20	-0.01	-0.01	0.30	0.02	0.36	-0.08
um052x/6-311+g(d,p)	0.04	-0.03	0.03	-0.02	0.12	-0.03	0.08	0.00	0.00	0.38	0.02	0.59	-0.17
um062x/6-311+g(d,p)	0.04	-0.03	0.03	-0.03	0.11	-0.03	0.07	-0.01	0.00	0.43	0.02	0.58	-0.19

(a)

5'dCMP	N1		N3		N4		N4-H1		N4-H2		C5-H		N1-C1'-H		P	
	isotropic	dipolar	isotropic	dipolar	isotropic	dipolar	isotropic	dipolar	isotropic	dipolar	isotropic	dipolar	isotropic	dipolar	isotropic	dipolar
Experiment									-6.20	-10.00	-21.40		-2.40			
								-12.40	-4.00	-14.50	2.30	-41.20	-1.70	41.90	-2.40	
									10.20		12.30		23.10		4.80	
Wetmore								-1.30	-1.90		20.40		-3.40			
								-0.90	-1.00	0.10	-1.80	-32.90	-1.40	40.60	0.70	
									2.30		3.70		21.80		4.10	
ub3lyp/6-311+g(d,p)		3.21		-4.18		-1.35			1.87		1.56		-6.48		-1.22	-13.85
	3.21	-3.65	2.40	-4.15	-0.61	0.62	0.59	-0.42	0.62	-0.33	-9.35	0.24	8.29	-0.26	-121.68	5.87
		7.41		8.33		0.74			-1.45		-1.23		6.24		1.48	7.97
um052x/6-311+g(d,p)		-2.05		-1.41		-0.45			-0.91		-0.64		-3.84		-0.70	-25.91
	2.90	-1.97	1.10	-1.35	-0.28	0.17	0.26	-0.34	0.21	-0.21	-5.22	0.69	3.81	-0.24	-275.79	11.45
		4.01		2.76		0.28			1.25		0.85		3.15		0.94	14.46
um062x/6-311+g(d,p)		-1.77		-1.29		-0.52			-0.92		-0.67		-3.34		-0.67	-24.31
	2.92	-1.73	1.80	-1.23	-0.36	0.21	0.33	-0.31	0.28	-0.17	-5.04	0.70	3.56	-0.21	-236.67	10.72
		3.50		2.53		0.31			1.23		0.84		2.65		0.88	13.58

(b)

Table 35. The calculated Mulliken spin population (a) and the calculated HFCCs (b) on the isolated 5'-dCMP cation radical extracted from 5'-dCMP-Opt-1 optimized geometry.

Type2 Opt Model 1 SP

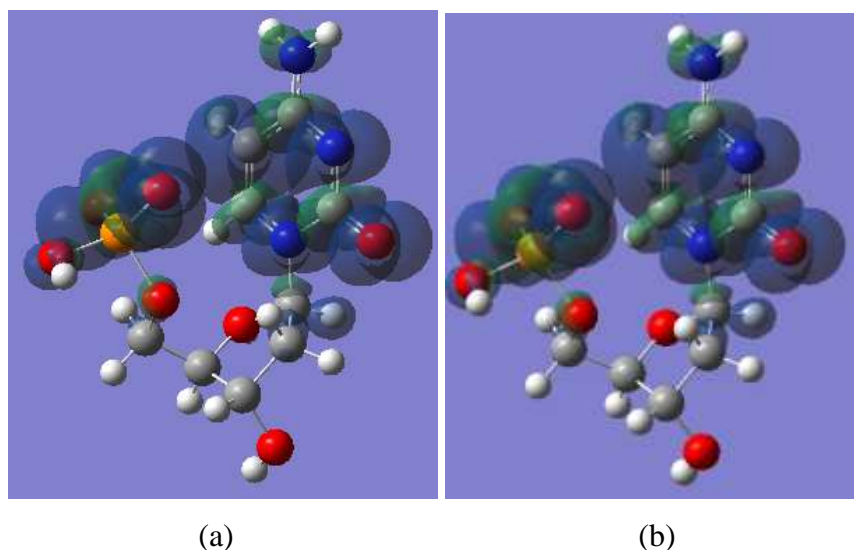


Figure. 24 The calculated spin density distribution of the isolated 5'-dCMP cation radical extracted from 5'-dCMP-Opt-2 optimized geometry. (isoval=0.0004) (a) Calculated at B3LYP/6-311+g(d,p) level of theory. (b) Calculated at M06-2X/6-311+g(d,p) level of theory.

5'-dCMP	N1	C2	N3	C4	C5	C6	O2	N4	C1'	C2'	OI	OII	OIII	P
Experiment	0.3					0.6		0.17						
Wetmore			0.24			0.33		0.45						
ub3lyp/6-311+g(d,p)	0.11	-0.07	0.11	-0.06	0.24	-0.04	0.21	-0.01	-0.03	0.01	0.32	0.02	0.26	-0.07
um052x/6-311+g(d,p)	0.20	-0.12	0.13	-0.08	0.41	-0.10	0.28	-0.01	-0.04	0.01	0.25	0.01	0.13	-0.08
um062x/6-311+g(d,p)	0.12	-0.07	0.09	-0.07	0.27	-0.08	0.19	-0.01	-0.03	0.01	0.41	0.02	0.29	-0.15

Model 1 5'dCMP	N1		N3		N4		N4-H1		N4-H2		C5-H		N1-C1'-H		P	
	isotropic	dipolar	isotropic	dipolar	isotropic	dipolar	isotropic	dipolar	isotropic	dipolar	isotropic	dipolar	isotropic	dipolar	isotropic	dipolar
Experiment																
							-12.40	-4.00	-14.50	2.30	-41.20	-1.70	41.90	-2.40		
								10.20		12.30		23.10		4.80		
Wetmore								-1.30		-1.90		20.40		-3.40		
							-0.90	-1.00	0.10	-1.80	-32.90	-1.40	40.60	0.70		
								2.30		3.70		21.80		4.10		
ub3lyp/6-311+g(d,p)		-5.06		-4.37		-1.34		-1.11		-1.54		-8.01		-1.44		-12.87
	4.48	-4.95	2.59	-4.34	-0.63	0.60	0.47	-0.48	0.55	-0.66	-12.24	-0.44	14.89	-0.21	-103.03	5.02
		10.01		8.70		0.74		1.59		2.20		8.45		1.65		7.84
um052x/6-311+g(d,p)		-8.82		-5.22		-1.68		-1.19		-2.21		-13.59		-2.00		-9.55
	12.49	-8.60	4.07	-5.08	-0.96	0.71	0.60	-0.72	0.93	-1.11	-24.25	-1.74	21.89	-0.42	-102.13	4.25
		17.42		10.30		0.97		1.91		3.32		15.34		2.41		5.30
um062x/6-311+g(d,p)		-5.18		-3.59		-1.39		-1.08		-1.68		-7.82		-1.39		-17.43
	8.86	-5.11	5.05	-3.44	-0.94	0.60	0.66	-0.38	0.85	-0.61	-14.40	-1.12	13.57	-0.24	-151.89	7.02
		10.29		7.03		0.78		1.47		2.29		8.93		1.63		10.41

Table 36. The calculated Mulliken spin population (a) and the calculated HFCCs (b) on the isolated 5'-dCMP cation radical extracted from 5'-dCMP-Opt-2 optimized geometry.

As would be expected from previous sections, in the gas phase calculation, the experimentally determined spin densities and hyperfine couplings are poorly predicted in all the tested jobs as listed in Table 35 and Table 36. Instead of the experimentally determined main

spin density sites of C5, N1 and N4 on the radical's cytosine base, large spin densities are calculated on the OI and OIII sites at the radical's phosphate group. OI and OIII are the two phosphate oxygen atoms without proton. The isotropic hyperfine couplings at the P atom given by M05/6-2X functionals are over 200 MHz on the 5'-dCMP-Opt-1 geometry, and over 100 MHz on the 5'-dCMP-Opt-2 geometry. The Mulliken spin population at C5 site and the iHFCCs at C5-H and C1'-H are closer to the experimental values as calculated on the radical optimized in a less complete environment (5'-dCMP-Opt-1) than those values calculated on the radical optimized in a more complete environment (5'-dCMP-Opt-2). These differences indicate the influences of different geometries on the spin density and HFCC calculations. The spin density delocalization errors from the radical's cytosine base to its phosphate group at both B3LYP and M05/6-2X level of theories are serious in the isolated calculations. In the next step, all the H-bonding effects of the radical are simulated by water molecules as shown in Figure. 25.

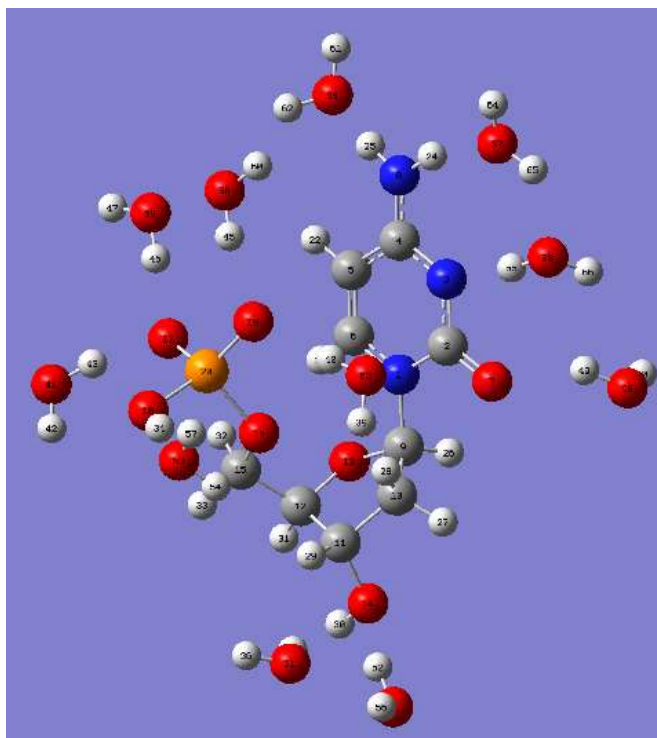


Figure. 25 All the radical's H-bonds are simulated by using water molecules. All the geometric parameters of the H-bonds remain unchanged from the optimized system.

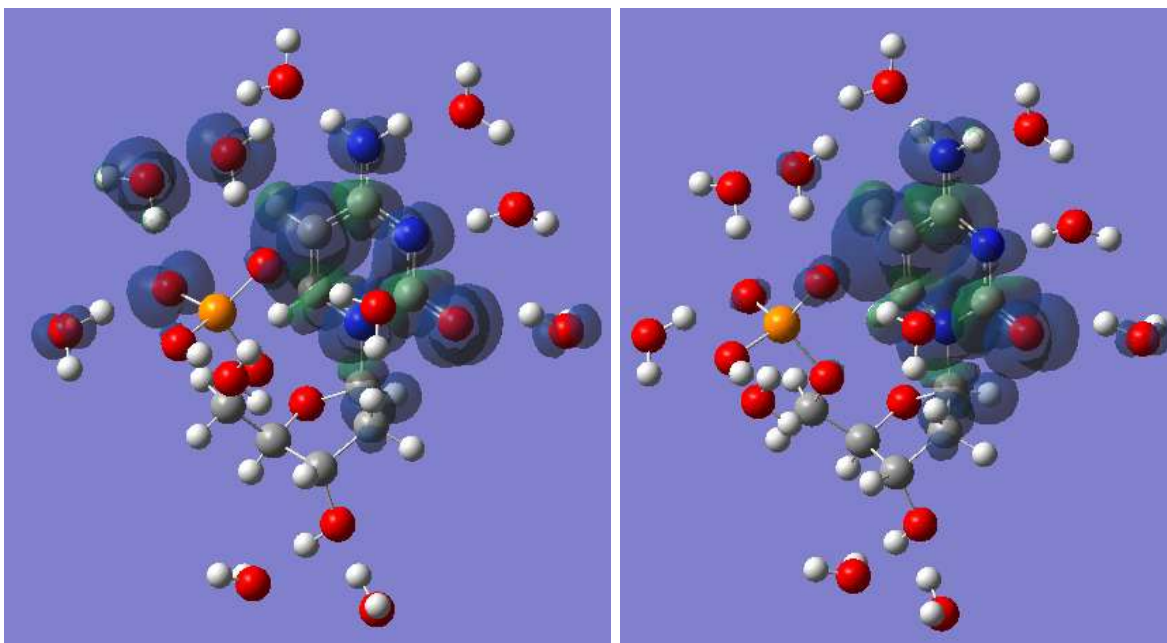


Figure. 26 The calculated spin density distribution on the system shown in Figure. 25, where the radical's geometry and all the H-bond's geometric parameters are extracted from the 5'-dCMP-Opt-1 optimization (isoval=0.0004) (a) Calculated at B3LYP/6-311+g(d,p) level of theory. (b) Calculated at M06-2X/6-311+g(d,p) level of theory.

5'-dCMP	N1	C2	N3	C4	C5	C6	O2	N4	C1'	OI	OII	OIII	P	W-H...OIII	W-H...OI
Experiment	0.3					0.6		0.17							
Wetmore			0.24		0.33		0.45								
ub3lyp/6-311+g(d,p)	0.21	-0.07	0.06	-0.06	0.36	-0.01	0.25	0.03	-0.03	0.05	0.00	0.01	-0.01	0.08	0.13
um052x/6-311+g(d,p)	0.33	-0.10	0.02	-0.05	0.54	-0.08	0.24	0.12	-0.03	0.01	0.00	0.01	-0.01	0.00	0.00
um062x/6-311+g(d,p)	0.33	-0.11	0.02	-0.07	0.57	-0.08	0.27	0.09	-0.04	0.00	0.00	0.00	-0.01	0.00	0.00

(a)

5'dCMP	N1		N3		N4		N4-H1		N4-H2		C5-H		N1-C1'-H		P	
	isotropic	dipolar	isotropic	dipolar	isotropic	dipolar	isotropic	dipolar	isotropic	dipolar	isotropic	dipolar	isotropic	dipolar	isotropic	dipolar
Experiment									-6.20	-10.00			-21.40		-2.40	
								-12.40	-4.00	2.30	-41.20	-1.70	41.90		-2.40	
									10.20	12.30		23.10		4.80		
Wetmore									-1.30	-1.90		20.40		-3.40		
								-0.90	-1.00	0.10	-32.90	-1.40	40.60		0.70	
									2.30	3.70		21.80		4.10		
ub3lyp/6-311+g(d,p)		-9.95		-2.04		-1.27		-1.54	-1.51		-13.56		-2.10		-0.38	
	8.92	-9.63	0.82	-1.97	0.76	-1.05	-1.88	-0.37	-2.45	-1.06	-21.62	-1.65	25.52	-0.65	-7.77	-0.14
		19.58		4.01		2.32		1.91		2.57		15.22		2.75		0.53
um052x/6-311+g(d,p)		-15.15		-0.42		-5.18		-3.68		-6.39		-20.25		-2.70		-0.41
	19.78	-14.61	-0.24	-0.01	7.03	-4.84	-9.38	-3.00	-10.53	-2.54	-40.47	-3.59	34.19	-1.28	-2.43	-0.15
		29.76		0.43		10.02		6.67		8.93		23.84		3.98		0.56
um062x/6-311+g(d,p)		-14.58		-0.61		-3.88		-3.19		-4.86		-19.70		-2.73		-0.34
	23.42	-14.17	0.62	-0.38	6.71	-3.58	-6.68	-1.94	-7.77	-2.16	-40.55	-3.79	35.77	-1.22	-2.24	-0.13
		28.74		0.98		7.46		5.13		7.02		23.49		3.95		0.47

(b)

Table 36. (a) The calculated Mulliken spin population with the last two columns showing the oxygen spin populations on two water molecules H-bonded to P-OI and P-OIII and (b) the

calculated HFCCs on the system shown in Figure. 25 extracted from 5'-dCMP-Opt-1 optimized geometry.

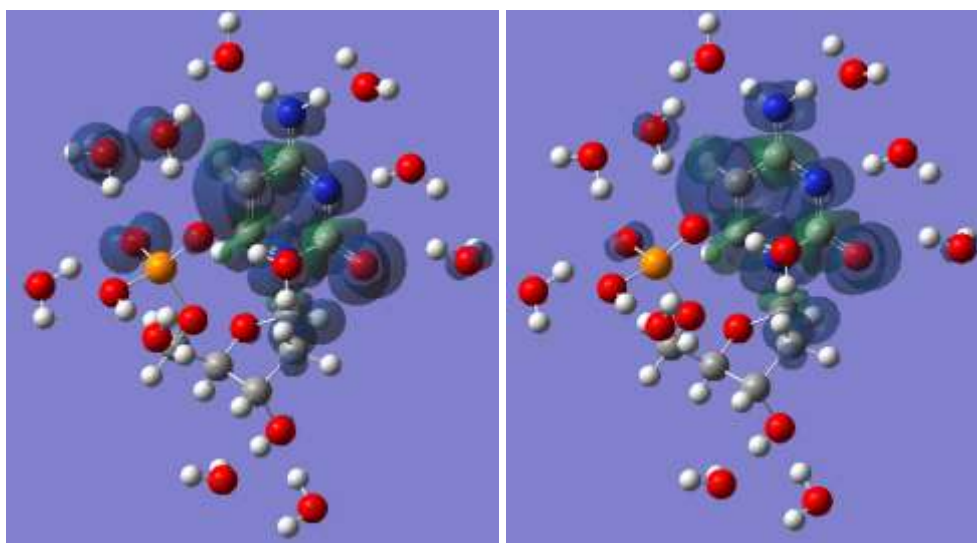


Figure. 27 The calculated spin density distribution on the system shown in Figure. 25, where the radical's geometry and all the H-bond's geometric parameters are extracted from the 5'-dCMP-Opt-2 optimization (isoval=0.0004) (a) Calculated at B3LYP/6-311+g(d,p) level of theory. (b) Calculated at M06-2X/6-311+g(d,p) level of theory.

5'-dCMP	N1	C2	N3	C4	C5	C6	O2	N4	C1'	C2'	OI	OII	OIII	P	OW-H...OI	OW-H...OIII
Experiment	0.3					0.6		0.17								
Wetmore			0.24		0.33		0.45									
ub3lyp/6-311+g(d,p)	0.24	-0.09	0.07	-0.07	0.41	-0.02	0.27	0.03	-0.04	0.02	0.04	0.00	0.01	0.00	0.09	0.06
um052x/6-311+g(d,p)	0.34	-0.11	0.04	-0.05	0.56	-0.10	0.26	0.07	-0.04	0.02	0.01	0.00	0.00	0.00	0.00	0.01
um062x/6-311+g(d,p)	0.34	-0.12	0.05	-0.07	0.58	-0.10	0.29	0.05	-0.05	0.02	0.01	0.00	0.00	0.00	0.00	0.01

(a)

Model 2 5'dCMP	N1		N3		N4		N4-H1		N4-H2		C5-H		N1-C1'-H		P	
	isotropic	dipolar	isotropic	dipolar	isotropic	dipolar	isotropic	dipolar	isotropic	dipolar	isotropic	dipolar	isotropic	dipolar	isotropic	dipolar
Experiment																
							-12.40	-4.00	-14.50	2.30	-41.20	-1.70	41.90	-2.40		
							10.20			12.30		23.10		4.80		
Wetmore							-1.30			-1.90		20.40		-3.40		
							-0.90	-1.00	0.10	-1.80	-32.90	-1.40	40.60	0.70		
										2.30		21.80		4.10		
ub3lyp/6-311+g(d,p)										-1.64		-15.47		-2.39		-0.31
	10.76	-11.42	1.20	-2.63	0.60	-0.98	-1.50	-0.63	-2.14	-1.24	-24.96	-2.07	34.51	-0.67	-4.93	-0.06
		23.14		5.17		1.71		2.27		2.32		17.54		3.06		0.37
um052x/6-311+g(d,p)																
		-15.71		-1.17		-3.07		-2.92		-3.65		-20.50		-2.81		-0.37
	20.84	-15.25	0.82	-1.15	4.39	-2.72	-5.53	-0.99	-6.57	-1.97	-40.43	-3.58	39.54	-1.14	-1.43	-0.23
		30.96		2.32		5.79		3.92		5.62		24.09		3.94		0.61
um062x/6-311+g(d,p)																
		-15.08		-1.71		-2.05		-2.59		-2.49		-19.87		-2.81		-0.36
	24.43	-14.71	2.36	-1.55	3.72	-1.72	-3.53	-0.62	-4.66	-1.68	-40.65	-3.75	41.32	-1.09	-1.53	-0.25
		29.79		3.26		3.77		3.21		4.17		23.63		3.91		0.61

(b)

Table 37. . (a) The calculated Mulliken spin population with the last two columns showing the oxygen spin populations on two water molecules H-bonded to P-OI and P-OIII and (b) the calculated HFCCs on the system shown in Figure. 25 extracted from 5'-dCMP-Opt-2 optimized geometry.

As shown in Table 36 and Table 37, by using water molecules to fulfill all the radical's H-bonding sites, the M05/6-2X calculated spin populations and HFCCs become much closer to experimental values when compared with the gas phase calculations. M05/6-2X calculated a localized spin density distribution upon the cytosine base, with small amounts extending onto the C1'-H sites in correspondence with the experimentally observed iHFCC at this site. On both the 5'-dCMP-Opt-1 and 5'-dCMP-Opt-2 optimized geometry, M05/6-2X give iHFCC values of -40.5 MHz at C5-H, which is in excellent agreement with the experimental value, -41.2 MHz at C5-H. Upon the 5'-dCMP-Opt-1 geometry, M05/6-2X underestimate the iHFCC at C1'-H about 6 MHz, also the iHFCCs at the N4-H1 and N4-H2 sites are underestimated. Meanwhile, upon the 5'-dCMP-Opt-2 geometry, M05/6-2X gives good iHFCC predictions on C1'-H sites, but give less satisfactory iHFCC predictions on the N4-H1 and N4-H2 sites. B3LYP functional delocalizes some amount of spin densities onto the radical's phosphate group and the two water molecules H-bonded with the radical's OI and OIII sites. Though water molecules can qualitatively simulate H-bonding effects on the radical, their H-bonding interactions are physically different from those in real crystalline molecular environment, which made the error contributions into HFCC calculations more indistinguishable. Besides, the long-pairs' directivity of the artificially assigned water molecules could also play a role in this simulation. Let's try to add the P-OIII protonated 5'-dCMP molecule into the single point calculations system, as shown in Figure. 28.

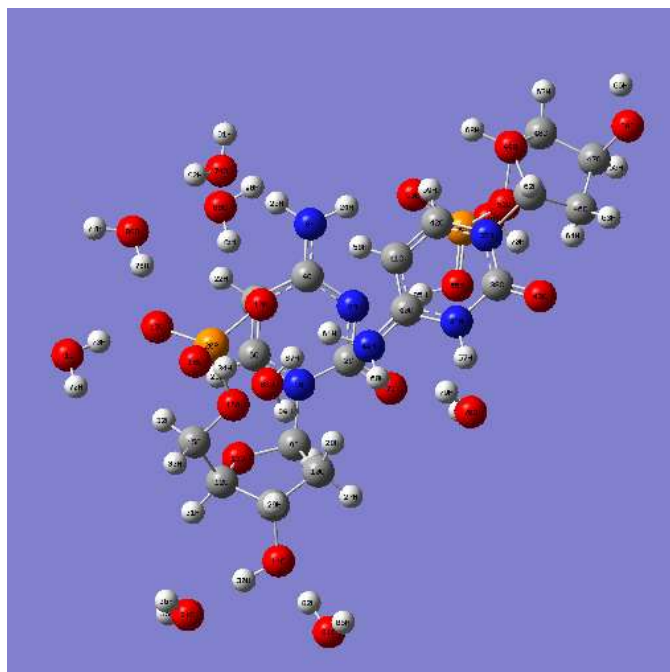


Figure. 28 The N3-deprotonated 5'-dCMP radical is H-bonded with the P-OIII protonated 5'-dCMP molecule and simulated water molecules.

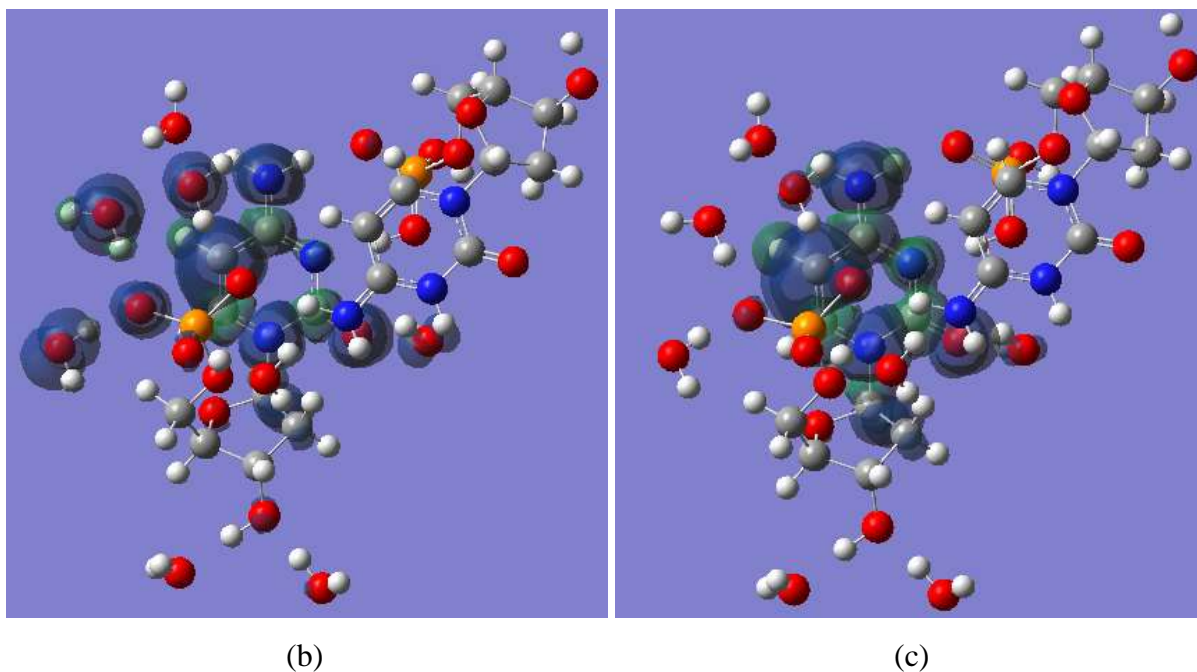


Figure. 29 The calculated spin density distribution on the system shown in Figure. 28, where the radical's geometry and all the H-bond's geometric parameters are extracted from the 5'-dCMP-

Opt-1 optimization (isoval=0.0004) (a) Calculated at B3LYP/6-311+g(d,p) level of theory. (b) Calculated at M06-2X/6-311+g(d,p) level of theory.

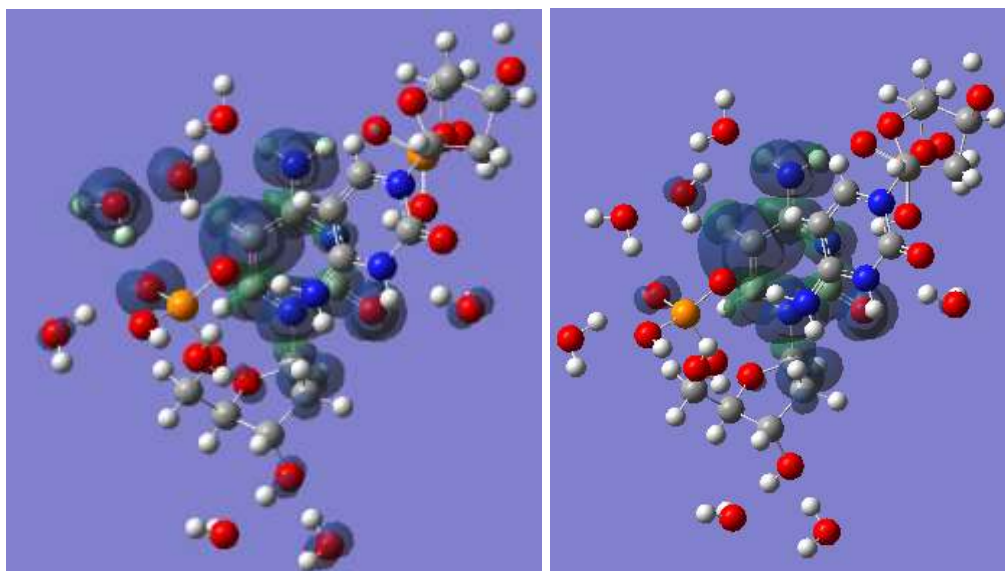
5'-dCMP	N1	C2	N3	C4	C5	C6	O2	N4	C1'	C2'	O1	OII	OIII	P	W-H...OIII	W1-H...OI	W2-H...OI	W-H...O2
Experiment	0.3				0.6			0.17							88	71	89	78
Wetmore			0.24		0.33		0.45											
ub3lyp/6-311+g(d,p)	0.19	-0.05	0.00	-0.07	0.31	0.00	0.12	0.11	-0.02	0.01	0.05	0.00	0.00	-0.01	0.06	0.12	0.20	0.01
um052x/6-311+g(d,p)	0.33	-0.08	-0.02	-0.06	0.55	-0.08	0.15	0.23	-0.03	0.02	0.01	0.00	0.01	-0.01	0.00	0.00	0.00	0.00
um062x/6-311+g(d,p)	0.34	-0.10	-0.02	-0.12	0.60	-0.07	0.16	0.23	-0.03	0.02	0.00	0.00	0.00	0.00	0.00	0.00	0.00	0.00

(a)

5'dCMP	N1		N3		N4		N4-H1		N4-H2		C5-H		N1-C1'-H		P	
	isotropic	dipolar	isotropic	dipolar	isotropic	dipolar	isotropic	dipolar	isotropic	dipolar	isotropic	dipolar	isotropic	dipolar	isotropic	dipolar
Experiment							-12.40	-4.00	-14.50	2.30	-41.20	-1.70	41.90	-2.40		
								10.20		12.30		23.10		4.80		
Wetmore							-0.90	-1.00	0.10	-1.80	-32.90	-1.40	40.60	0.70		
								2.30		3.70		21.80		4.10		
ub3lyp/6-311+g(d,p)		-8.78		-0.77		-4.45		-3.64		-5.48		-11.51		-1.70		-0.78
	8.06	-8.46	-0.53	0.31	3.11	-4.25	-6.23	-1.81	-6.84	-1.64	-18.81	-1.51	26.88	-0.70	-7.44	0.30
		17.24		0.46		8.70		5.45		7.13		13.02		2.40		0.49
um052x/6-311+g(d,p)		-15.12		-3.13		-9.97		-8.48		-12.42		-19.93		-2.73		-0.41
	19.75	-14.53	-1.71	1.46	12.93	-9.62	-18.16	-5.09	-19.50	-3.96	-41.40	-4.03	38.53	-1.38	-2.07	-0.17
		29.66		1.67		19.59		13.57		16.39		23.96		4.11		0.57
um062x/6-311+g(d,p)		-14.78		-3.27		-9.26		-7.97		-11.80		-19.62		-2.67		-0.32
	23.82	-14.32	-2.34	1.55	15.28	-8.92	-15.90	-4.88	-17.05	-3.74	-41.76	-4.30	41.20	-1.41	-2.08	-0.14
		29.10		1.72		18.17		12.84		15.54		23.92		4.08		0.46

(b)

Table 38. (a) The calculated Mulliken spin population with the last four columns showing the oxygen spin populations on four water molecules H-bonded to the radical's P-OI, P-OIII and C-O2 sites; (b) the calculated HFCCs on the system shown in Figure. 28 extracted from 5'-dCMP-Opt-1 optimized geometry.



(a)

(b)

Figure. 30 The calculated spin density distribution on the system shown in Figure. 28, where the radical's geometry and all the H-bond's geometric parameters are extracted from the 5'-dCMP-Opt-2 optimization (isoval=0.0004) (a) Calculated at B3LYP/6-311+g(d,p) level of theory. (b) Calculated at M06-2X/6-311+g(d,p) level of theory.

5'-dCMP	N1	C2	N3	C4	C5	C6	O2	N4	C1'	C2'	OI	OII	OIII	P
Experiment		0.3				0.6			0.17					
Wetmore			0.24			0.33		0.45						
ub3lyp/6-311+g(d,p)		0.24	-0.06	0.00	-0.08	0.40	-0.02	0.12	0.15	-0.03	0.02	0.04	0.00	0.00
um052x/6-311+g(d,p)		0.35	-0.09	-0.01	-0.06	0.56	-0.09	0.13	0.21	-0.03	0.02	0.01	0.00	0.00
um062x/6-311+g(d,p)		0.36	-0.10	-0.02	-0.12	0.61	-0.08	0.14	0.21	-0.03	0.01	0.01	0.00	0.00

OW-H...OI	OW-H...OIII	OI	OII	OIII	P
0.18	0.06	0.00	0.00	0.00	0.00
0.00	0.00	0.00	0.00	0.00	0.00
0.00	0.00	0.00	0.00	0.00	0.00

(a)

Model 3 5'dCMP	N1		N3		N4		N4-H1		N4-H2		C5-H		N1-C1'-H		P	
	isotropic	dipolar	isotropic	dipolar	isotropic	dipolar	isotropic	dipolar	isotropic	dipolar	isotropic	dipolar	isotropic	dipolar	isotropic	dipolar
Experiment																
Wetmore																
ub3lyp/6-311+g(d,p)																
	10.72	-11.42		-1.28		-6.02		-4.79		-7.12		-14.13		-2.15		-0.45
		-11.06	-0.75	0.58	4.37	-5.78	-8.35	-2.61	-8.95	-2.20	-23.67	-2.07	40.64	-0.87	-4.63	0.05
		22.47		0.70		11.79		7.41		9.32		16.19		3.02		0.39
um052x/6-311+g(d,p)																
		-15.90		-2.77		-9.23		-7.45		-11.14		-20.15		-2.87		-0.36
	21.12	-15.37	-1.57	1.31	12.25	-8.87	-16.63	-4.85	-17.69	-3.75	-41.68	-4.17	45.30	-1.29	-1.88	-0.22
		31.27		1.46		18.11		12.30		14.89		24.32		4.17		0.58
um062x/6-311+g(d,p)																
		-15.53		-2.92		-8.66		-7.09		-10.70		-19.88		-2.77		-0.34
	25.22	-15.09	-2.13	1.40	14.62	-8.32	-14.71	-4.70	-15.70	-3.59	-42.40	-4.41	48.47	-1.35	-2.02	-0.24
		30.62		1.51		16.98		11.79		14.29		24.29		4.13		0.57

(b)

Table 39. (a) The calculated Mulliken spin population (the second section of the table shows the oxygen spin populations on the radical's phosphate group and on two water molecules H-bonded to the radical's P-OI, P-OIII and C-O2 sites); and (b) the calculated HFCCs on the system shown in Figure. 28 extracted from 5'-dCMP-Opt-2 optimized geometry.

After the P-OIII protonated 5'dCMP molecule is included into the single point calculation (Figure. 28), the radical forms Hydrogen bonds at its N3 and N4-H2 sites with the protonated phosphate group. For the 5'-dCMP-Opt-1 optimized geometry as shown in Figure. 29 (a), B3LYP functional still spreads spin densities to three water molecules that are H-bonded to the radical's phosphate group, which results in a systematic underestimation of the spin density and hyperfine couplings on the radical's cytosine ring, as shown in Table 38. For the M05/6-2X calculated spin densities in Figure. 29 (b), a migration of spin density (when compare Table 38 (a) with Table 36 (a)) from the radical's O2 to N4 site leads to an overestimation of the spin density at the radical's N4 about 30%. In consequence, the experimentally unreported hyperfine couplings at N4 and a 3 to 5MHz overestimation of N4-H1, N4-H2 hyperfine couplings are predicted, as shown in Table 38. Whereas, as shown in Table 38 (a), the M05/6-2X calculated iHFCCs at the primary sites, C5-H and N1-C1'-H, are in excellent agreement with the experimental values. For the 5'-dCMP-Opt-2 optimized geometry, the M05/6-2X calculated spin population levels at N4 is lower and N1 higher than in the 5;-dCMP-Opt-1 case. By comparing the B3LYP calculated results in Table 39 and Table 38, one can see that both the spin and hyperfine coupling properties calculated by B3LYP functional are sensitive to the geometric parameters from different optimization jobs, when compared with the M05/6-2X results.

In the following two single point calculation models, shown in Figure. 31 and Figure. 34, serious delocalization errors presents with M05/6-2X functionals. This indicates that before the delocalization errors originated from the approximated exchange-correlation functionals could be effectively diminished or suppressed within molecular cluster, the idea is not always followed by DFT methods that more realistic iHFCCs can be calculated by imbedding the target radical within more complete molecular environment. Among the tested single point cluster calculations, one can see that a third neutral DNA constituent, introduced into the deprotonation-protonation coupled system, will usually bear the delocalized spin densities.

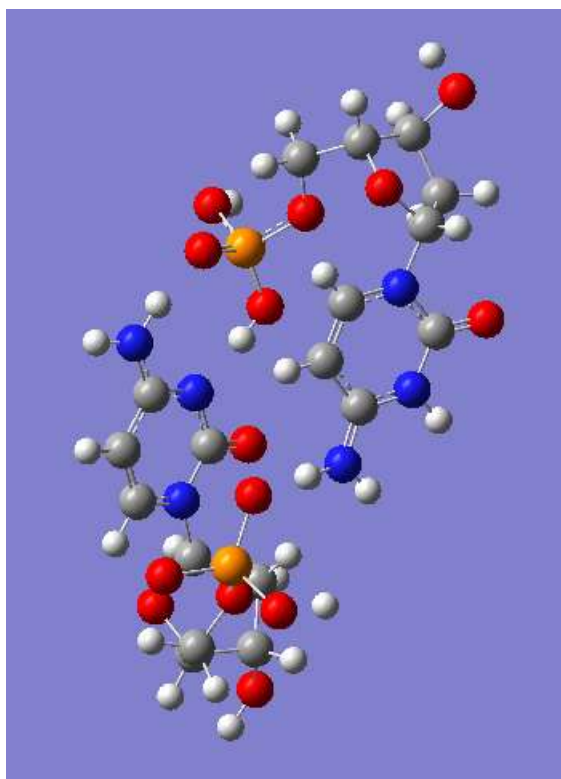
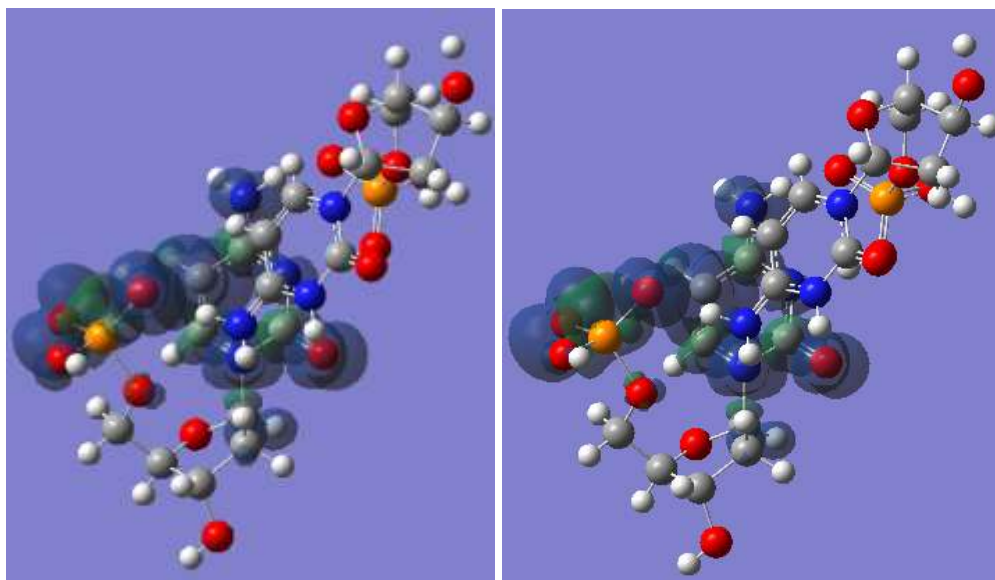


Figure. 31 The N3-deprotonated 5'-dCMP radical is H-bonded with the P-OIII protonated 5'-dCMP molecule, all the simulated water molecules in Figure. 28 are eliminated in this system.



(a)

(b)

Figure. 32 The calculated spin density distribution on the system shown in Figure. 31, where the radical's geometry and all the H-bond's geometric parameters are extracted from the 5'-dCMP-Opt-1 optimization (isoval=0.0004) (a) Calculated at B3LYP/6-311+g(d,p) level of theory. (b) Calculated at M06-2X/6-311+g(d,p) level of theory.

5'-dCMP	N1	C2	N3	C4	C5	C6	O2	N4	C1'	C2'	OI	OII	OIII	P
Experiment	0.3				0.6			0.17						
Wetmore			0.24		0.33		0.45							
ub3lyp/6-311+g(d,p)	0.15	-0.06	0.03	-0.05	0.28	-0.04	0.15	0.04	-0.02	0.01	0.37	0.02	0.18	-0.07
um052x/6-311+g(d,p)	0.32	-0.13	0.04	-0.06	0.56	-0.10	0.26	0.09	-0.03	0.02	0.05	0.00	0.01	-0.02
um062x/6-311+g(d,p)	0.14	-0.07	0.02	-0.05	0.28	-0.08	0.12	0.04	-0.01	0.01	0.57	0.02	0.13	-0.14

(a)

5'dCMP	N1		N3		N4		N4-H1		N4-H2		C5-H		N1-C1'-H		P	
	isotropic	dipolar	isotropic	dipolar	isotropic	dipolar	isotropic	dipolar	isotropic	dipolar	isotropic	dipolar	isotropic	dipolar	isotropic	dipolar
Experiment									-6.20	-10.00		-21.40		-2.40		
								-12.40	-4.00	-14.50	2.30	-41.20	-1.70	41.90	-2.40	
									10.20	12.30		23.10		4.80		
Wetmore								-1.30	-1.90			20.40		-3.40		
								-0.90	-1.00	0.10	-1.80	-32.90	-1.40	40.60	0.70	
									2.30		3.70		21.80		4.10	
ub3lyp/6-311+g(d,p)		-6.94		-0.81		-1.71		-1.49		-2.08		-9.65		-1.52		-9.23
	6.35	-6.71	0.18	-0.78	1.23	-1.53	-2.59	-0.57	-2.81	-0.93	-15.35	-0.46	20.29	-0.46	-93.66	3.57
		13.65		1.59		3.24		2.07		3.01		10.11		1.98		5.66
um052x/6-311+g(d,p)		-14.40		-0.70		-4.29		-3.32		-5.19		-20.22		-2.70		-0.73
	19.12	-13.89	0.36	-0.62	6.01	-3.92	-7.76	-2.12	-8.78	-2.29	-39.77	-3.39	36.64	-1.04	-14.41	0.13
		28.29		1.32		8.21		5.44		7.48		23.60		3.73		0.60
um062x/6-311+g(d,p)		-6.00		-0.38		-1.81		-1.60		-2.33		-8.31		-1.32		-10.83
	10.34	-5.87	0.48	-0.32	3.16	-1.65	-3.07	-0.61	-3.44	-0.99	-16.09	-1.21	15.82	-0.46	-137.42	5.04
		11.87		0.71		3.46		2.21		3.33		9.52		1.78		5.79

(b)

Table 40. (a) The calculated Mulliken spin population at the radical and (b) the calculated HFCCs on the system shown in Figure. 31 extracted from 5'-dCMP-Opt-1 optimized geometry.

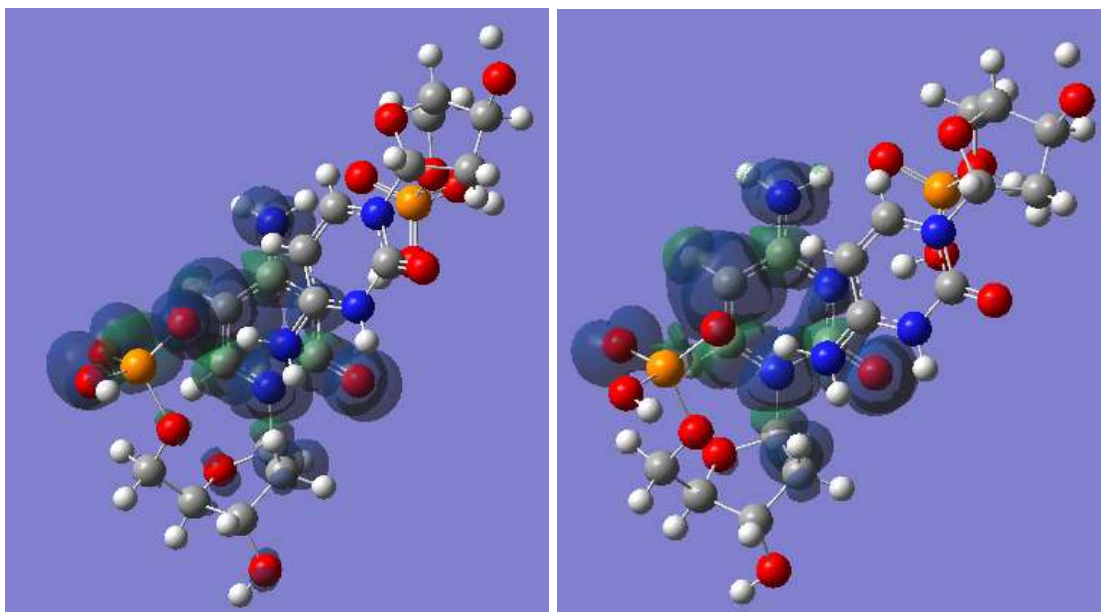


Figure. 33 The calculated spin density distribution on the system shown in Figure. 31, where the radical's geometry and all the H-bond's geometric parameters are extracted from the 5'-dCMP-Opt-2 optimization (isoval=0.0004) (a) Calculated at B3LYP/6-311+g(d,p) level of theory. (b) Calculated at M06-2X/6-311+g(d,p) level of theory.

5'-dCMP	N1	C2	N3	C4	C5	C6	O2	N4	C1'	C2'	O1	OII	OIII	P
Experiment	0.3					0.6			0.17					
Wetmore			0.24			0.33		0.45						
ub3lyp/6-311+g(d,p)	0.19	-0.07	0.03	-0.06	0.36	-0.05	0.16	0.06	-0.03	0.02	0.34	0.01	0.08	-0.03
um052x/6-311+g(d,p)	0.33	-0.12	0.02	-0.06	0.57	-0.11	0.22	0.10	-0.04	0.02	0.06	0.00	0.00	-0.01
um062x/6-311+g(d,p)	0.33	-0.14	0.03	-0.06	0.54	-0.09	0.23	0.09	-0.04	0.02	0.09	0.01	0.01	-0.02

(a)

Model 4 5'dCMP	N1		N3		N4		N4-H1		N4-H2		C5-H		N1-C1'-H		P	
	isotropic	dipolar	isotropic	dipolar	isotropic	dipolar	isotropic	dipolar	isotropic	dipolar	isotropic	dipolar	isotropic	dipolar	isotropic	dipolar
Experiment							-12.40	-6.20	-10.00	-14.50	2.30	-41.20	-1.70	41.90	-2.40	-2.40
								10.20	12.30			23.10			4.80	
Wetmore								-1.30	-1.90			20.40			-3.40	
							-0.90	-1.00	0.10	-1.80	-32.90	-1.40	40.60	0.70		
								2.30		3.70		21.80			4.10	
ub3lyp/6-311+g(d,p)		-8.71		-0.80		-2.62		-2.02	-3.04		-12.24		-1.85		-5.95	
	8.11	-8.46	0.20	-0.71	2.05	-2.40	-3.93	-1.10	-4.14	-1.34	-20.19	-1.50	31.02	-0.51	-66.67	2.19
		17.17		1.51		5.03		3.12	4.38		13.74			2.36		3.76
um052x/6-311+g(d,p)		-14.91		-0.33		-4.76		-3.49	-5.64		-20.63		-2.76		-0.63	
	20.11	-14.46	0.07	-0.26	6.82	-4.39	-8.50	-2.41	-9.43	-2.42	-40.68	-3.55	43.41	-1.03	-15.56	0.14
		29.37		0.59		9.14		5.90	8.07		24.18			3.78		0.49
um062x/6-311+g(d,p)		-13.96		-0.48		-4.00		-3.20	-4.84		-19.60		-2.63		-1.56	
	23.14	-13.63	0.60	-0.38	7.13	-3.67	-6.80	-1.90	-7.65	-2.17	-39.61	-3.97	44.24	-0.98	-20.37	0.62
		27.59		0.86		7.67		5.10	7.01		23.57			3.61		0.95

(b)

Table 41. (a) The calculated Mulliken spin population at the radical and (b) the calculated HFCCs on the system shown in Figure. 31 extracted from 5'-dCMP-Opt-2 optimized geometry.

In the system shown in Figure. 31, only the N3-deprotonated radical and the protonated 5'dCMP cation molecule are included. For both 5'-dCMP-Opt-1 and 5'-dCMP-Opt-2 optimized radicals within this model, M05-2X functional gives both reasonably close primary sites (C5-H and N1-C1'-H) iHFCC results to the experimental values. The M06-2X functional also gives good iHFCC results and only a small amount of spin density delocalization at the radical's phosphate site for 5'-dCMP geometry, but, as listed in Table 40, it predicts a large iHFCC (-137.4 MHz) at the radical's phosphorus based on the 5'-dCMP-Opt-1 geometry, and its spin density delocalization in this case is worse than B3LYP's performance. Ironically, one should recall that the radical geometry of the 5'-dCMP-Opt-1 type is optimized within a more complete single crystalline environment (eleven surrounding 5'-dCMP molecules) than that of the 5'-dCMP-Opt-2 optimization (four surrounding 5'-dCMP molecules). This might indicate the underlying error cancellations among the less accurate molecular geometry (the external potential for the electron system), the delocalization error and the static correlation error. In other words, the non-linear energy behavior on both the fractional charges and on the degenerate or quasi-degenerate states might be partially compensated by a perturbation from the external potential, which is due to the calculated displacement of the nuclei from their positions in real situation.

If this unexpected failure is only a piece of dark cloud that worries people, then the following M05/6-2X's complete failures on the system shown in Figure. 34, which is a more complete model system, indicate clearly the vulnerability of M05/6-2X functionals being a reliable method in predicting HFCCs in larger systems (beyond 70 heavy atoms for the three-5'-dCMP system here, shown in Figure. 34).

In the single point calculation system shown in Figure. 34, a third 5'-dCMP molecule is included as in the single crystalline structure. This 5'-dCMP is H-bonded to the radical's N4-H1 site with its phosphate OIII site and to the radical's phosphate OI and OIII sites with its N4-H2 and N3-H sites. A migration of the delocalized spin density from the radical's phosphate group to the third neutral 5'-dCMP molecule's phosphate group is observed from all the tested calculations. Recall that M05/6-2X calculations on the system in Figure. 28 for both 5'-dCMP-

Opt-1 and 5'-dCMP-Opt-2 geometries have already given spin densities and hyperfine couplings that match the experimental results very well (Table 38, 39). The slightly overestimated spin densities at the radical's N4 site, so as to the slightly overestimated hyperfine couplings at N4-H1 and N4-H2 sites, in Figure. 28, are expected to be improved for the system in Figure. 34 since the radical's amino group is now experiencing a more realistic environment effect. However, along with B3LYP functional, M05/6-2X delocalizes a great amount of spin densities onto the phosphate group of the third 5'-dCMP molecule (upper left in the Figures). As shown in Table 42, for the 5'-dCMP-Opt-1 geometry, negligible spin densities are predicted by M05/6-2X at the radical's base atoms, which predicts the iHFCCs at both the C5-H and N1-C1'-H sites are less than 2 MHz. Under the same case in Table 42, B3LYP functional gives -11.3 MHz and 16.9 MHz at the radical's C5-H and N1-C1'-H. For the 5'-dCMP-Opt-2 geometry, M05/6-2X's performance on iHFCCs is improved to give about half the experimental values at the primary sites. Again, the external potential perturbation is thought to play a role in this situation.

As shown in Figure. 37, if we use a H atom to replace the third 5'-dCMP's phosphate – OPO_3H^- group, which bears the major delocalized spin densities in Figure. 34, and fulfill the H-bond vacancy with a water molecule, then M05/6-2X gives good results (Table 43) resembling to those from the system in Figure. 25 (Table 36, 37). Specifically, this indicates that it is the inclusion of the third phosphate group that causes this delocalization. Meanwhile, the spin density delocalization of B3LYP functional transfers to water molecules and the radical's sugar group. This delocalization phenomenon can also result in unphysical ground-state energy discontinuity as reported by Pauwels et al. for their spin density delocalization problem with PM3 level of theory.²⁴

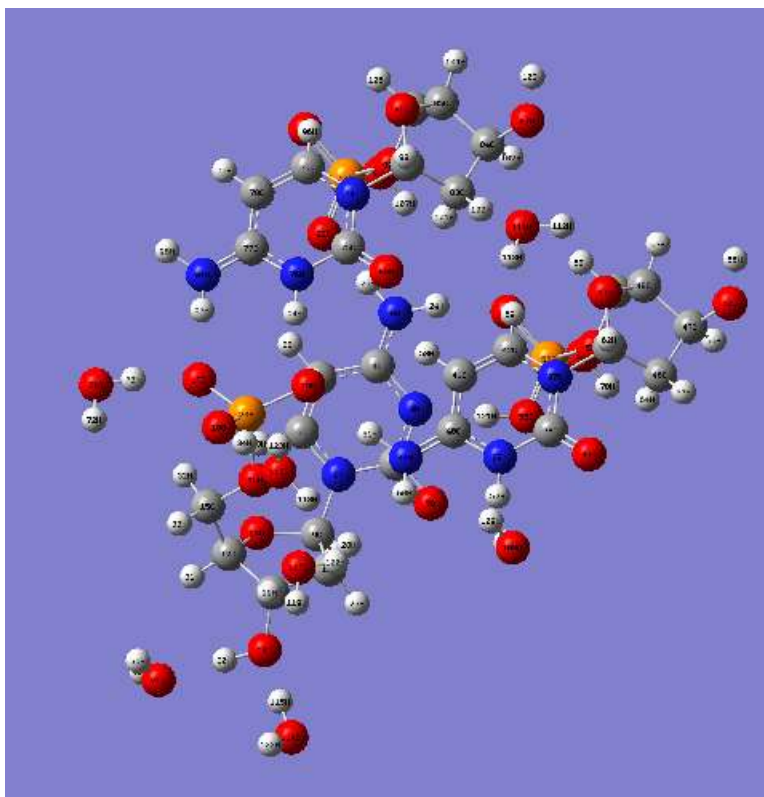


Figure. 34 The N3-deprotonated 5'-dCMP radical is H-bonded with the P-OIII protonated 5'-dCMP molecule, a neutral 5'-dCMP molecule and simulated water molecules. (A third 5'-dCMP molecule is added on the system in Figure. 28)

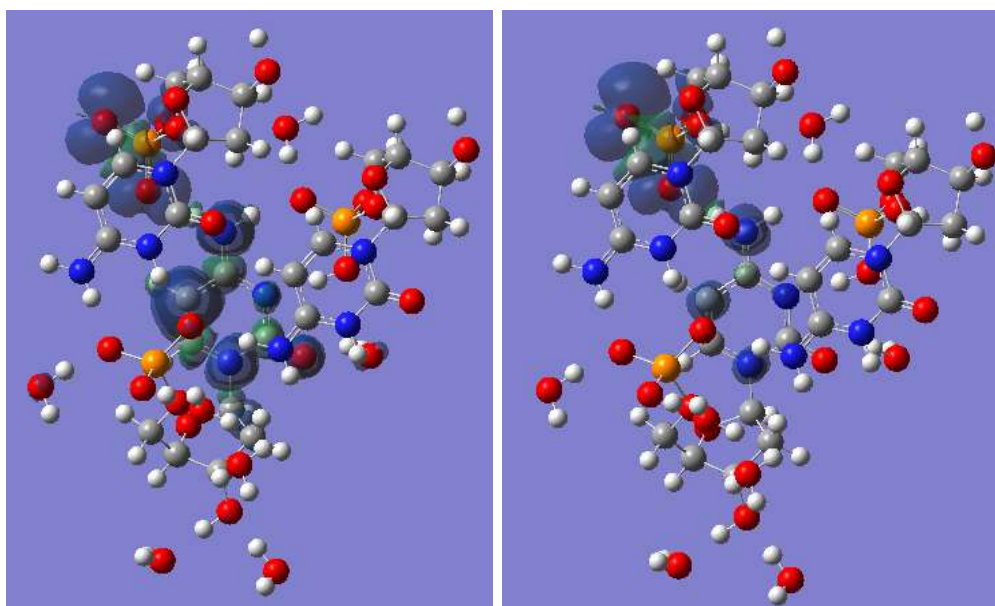


Figure. 35 The calculated spin density distribution on the system shown in Figure. 34, where the radical's geometry and all the H-bond's geometric parameters are extracted from the 5'-dCMP-Opt-1 optimization (isoval=0.0004) (a) Calculated at B3LYP/6-311+g(d,p) level of theory. (b) Calculated at M06-2X/6-311+g(d,p) level of theory.

5'-dCMP	N1	C2	N3	C4	C5	C6	O2	N4	C1'	C2'	OI	OII	OIII	P
Experiment	0.3				0.6			0.17						
Wetmore			0.24			0.33		0.45						
ub3lyp/6-311+g(d,p)	0.12	-0.03	-0.01	-0.03	0.18	-0.01	0.04	0.13	-0.01	0.00	0.00	0.00	0.00	0.00
um052x/6-311+g(d,p)	0.00	0.00	0.00	0.01	0.00	0.00	0.00	0.02	0.00	0.00	0.00	0.00	0.00	0.00
um062x/6-311+g(d,p)	0.01	0.00	0.01	0.00	0.01	0.00	0.00	0.05	0.00	0.00	0.00	0.00	0.00	0.00

Third 5'dCMP	N1	C2	N3	C4	C5	C6	O2	N4	C1'	C2'	OI	OII	OIII	P
	0.00	-0.02	-0.01	0.01	0.00	0.00	0.00	0.00	0.01	-0.01	0.41	0.03	0.24	-0.07
	0.00	-0.01	0.00	0.01	0.00	0.00	0.00	0.00	0.01	-0.01	0.75	0.03	0.32	-0.14
	0.00	-0.03	0.00	0.01	0.01	-0.01	0.00	0.00	0.01	-0.01	0.70	0.04	0.38	-0.18

(a)

5'dCMP	N1		N3		N4		N4-H1		N4-H2		C5-H		N1-C1'-H		P	
	isotropic	dipolar	isotropic	dipolar	isotropic	dipolar	isotropic	dipolar	isotropic	dipolar	isotropic	dipolar	isotropic	dipolar	isotropic	dipolar
Experiment									-6.20	-10.00	-21.40	-2.40				
								-12.40	-4.00	-14.50	2.30	-41.20	-1.70	41.90	-2.40	
									10.20		12.30		23.10		4.80	
Wetmore								-1.30		-1.90		20.40		-3.40		
								-0.90	-1.00	0.10	-1.80	-32.90	-1.40	40.60	0.70	
									2.30		3.70		21.80		4.10	
ub3lyp/6-311+g(d,p)		-5.68		-0.89		-5.61			-9.02		-6.39		-6.01		-1.04	-0.17
	5.27	-5.44	-0.50	0.40	4.20	-5.52	-8.90	-6.41	-7.54	-2.17	-11.26	-1.72	16.93	-0.56	-0.76	-0.07
		11.11		0.50		11.13		15.43		8.55		7.73		1.60		0.24
um052x/6-311+g(d,p)		-0.20		-0.12		-0.92		-6.34		-1.50		-1.25		-0.13		-0.07
	0.28	-0.15	0.16	-0.05	2.19	-0.89	-3.45	-5.56	-0.28	-0.44	-0.28	-0.96	0.38	-0.11	-0.01	-0.06
		0.35		0.17		1.81		11.90		1.94		2.21		0.24		0.12
um062x/6-311+g(d,p)		-0.61		-0.15		-1.71		-7.96		-2.23		-1.53		-0.20		-0.07
	1.04	-0.55	0.26	-0.08	4.02	-1.56	-7.07	-6.70	-1.29	-0.81	-1.15	-0.91	1.43	-0.14	-0.05	-0.06
		1.16		0.22		3.27		14.67		3.04		2.44		0.34		0.13

(b)

Table 42. (a) The calculated Mulliken spin population at the radical and the neutral third 5'-dCMP (upper left) and (b) the calculated HFCCs on the system shown in Figure. 34 extracted from 5'-dCMP-Opt-1 optimized geometry.

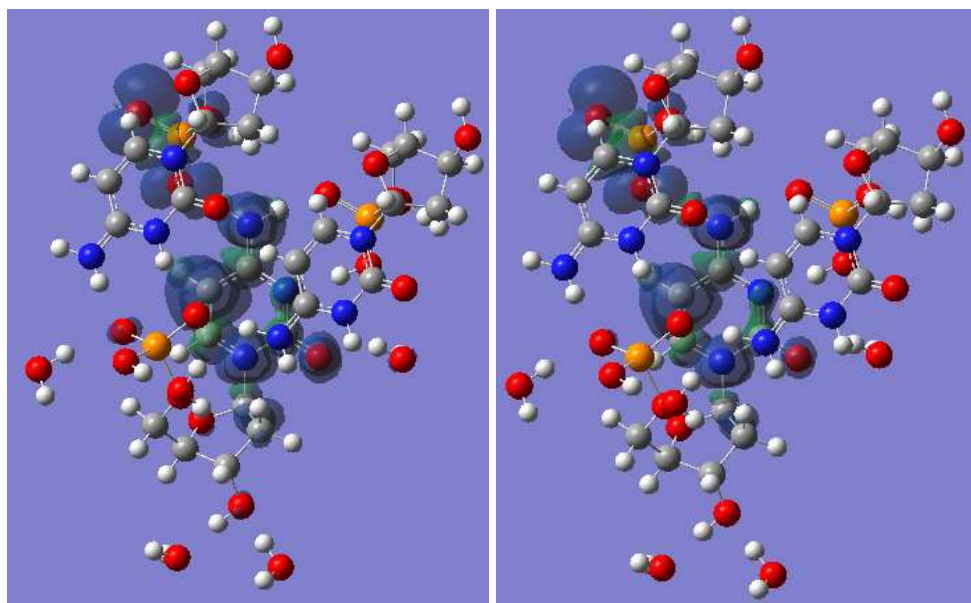


Figure. 36 The calculated spin density distribution on the system shown in Figure. 34, where the radical's geometry and all the H-bond's geometric parameters are extracted from the 5'-dCMP-Opt-2 optimization (isoval=0.0004) (a) Calculated at B3LYP/6-311+g(d,p) level of theory. (b) Calculated at M06-2X/6-311+g(d,p) level of theory.

cyto1		N1	C2	N3	C4	C5	C6	O2	N4	C1'	C2'	C3'	C4'	O4'	O3'	C5'	O5'	OI	OII	OIII	P
5'-dCMP																					
Experiment		0.3					0.6			0.17											
Wetmore				0.24			0.33		0.45												
ub3lyp/6-311+g(d,p)		0.17	-0.04	-0.01	-0.03	0.24	-0.03	0.04	0.16	-0.01	0.01	0.00	0.00	0.00	0.00	0.00	0.00	0.00	0.00	0.00	0.00
um052x/6-311+g(d,p)		0.20	-0.05	0.00	-0.02	0.28	-0.06	0.03	0.21	-0.01	0.00	0.00	0.00	0.00	0.00	0.00	0.00	0.00	0.00	0.00	0.00
um062x/6-311+g(d,p)		0.13	-0.04	0.00	-0.02	0.17	-0.03	0.01	0.16	0.00	0.00	0.00	0.00	0.00	0.00	0.00	0.00	0.00	0.00	0.00	0.00

cyto3		N1	C2	N3	C4	C5	C6	O2	N4	C1'	C2'	C3'	C4'	O4'	O3'	C5'	O5'	OI	OII	OIII	P
5'-dCMP																					
Experiment		0.3					0.6			0.17											
Wetmore				0.24			0.33		0.45												
ub3lyp/6-311+g(d,p)		0.00	-0.02	-0.01	0.02	0.00	0.00	0.00	0.00	0.01	-0.01	0.00	0.00	0.00	0.00	0.00	0.00	0.36	0.02	0.19	-0.06
um052x/6-311+g(d,p)		0.01	-0.02	-0.02	0.02	0.00	0.00	0.00	0.00	0.01	-0.01	0.00	0.00	0.00	0.00	0.00	0.00	0.34	0.02	0.19	-0.10
um062x/6-311+g(d,p)		0.01	-0.04	-0.01	0.02	0.00	-0.01	0.01	-0.01	0.01	-0.01	0.00	0.00	0.00	0.00	0.00	0.01	0.49	0.03	0.27	-0.15

(a)

Model 5 5'dCMP	N1		N3		N4		N4-H1		N4-H2		C5-H		N1-C1'-H		P	C6-H		Cyt3-P		
	isotropic	dipolar	isotropic	dipolar	isotropic	dipolar	isotropic	dipolar	isotropic	dipolar	isotropic	dipolar	isotropic	dipolar	isotropic	dipolar	isotropic	dipolar	isotropic	dipolar
Experiment									-12.40	-6.20	-10.00	-21.40	41.90	-2.40						
									10.20	-4.00	2.30	-41.20	-1.70	-2.40						
									10.20	10.20	12.30	23.10	4.80							
Wetmore									-1.30	-1.90	-1.90	20.40	-3.40							
									-0.90	-1.00	0.10	-1.80	-32.90	-1.40	40.60	0.70				
									2.30	3.70	21.80	4.10								
ub3lyp/6-311+g(d,p)		-7.69		-1.07		-6.81		-9.35		-7.54		-7.89		-1.41		-0.18		-2.08		-8.39
	7.28	-7.43	-0.60	0.47	4.37	-6.67	-10.54	-6.84	-9.40	-2.59	-14.59	-2.17	26.03	-0.65	-0.54	-0.12	1.42	-0.35	-74.93	1.85
		15.12		0.60		13.48		16.19		10.13		10.06		2.06		0.30		2.43		6.54
um052x/6-311+g(d,p)		-9.10		-1.25		-9.10		-11.42		-10.39		-9.33		-1.68		-0.23		-2.45		-11.11
	13.17	-8.77	-0.63	0.54	10.73	-8.84	-16.43	-8.10	-16.36	-3.69	-19.48	-2.89	25.13	-0.77	-0.62	-0.13	1.89	-0.74	-102.45	4.32
		17.87		0.71		17.95		19.51		14.08		12.22		2.45		0.36		3.19		6.79
um062x/6-311+g(d,p)		-5.73		-0.75		-6.42		-10.71		-7.30		-5.05		-1.05		-0.15		-1.63		-14.18
	10.03	-5.53	-0.40	0.28	10.13	-6.27	-13.71	-8.11	-10.28	-2.85	-11.84	-2.49	16.81	-0.56	-0.48	-0.09	0.07	-0.46	-124.50	3.77
		11.26		0.47		12.68		18.82		10.15		7.54		1.61		0.25		2.09		10.41

(b)

Table 43. (a) The calculated Mulliken spin population at the radical and the neutral third 5'-dCMP (upper left) and (b) the calculated HFCCs on the system shown in Figure. 34 extracted from 5'-dCMP-Opt-2 optimized geometry, with the last two columns giving the HFCCs on the phosphorus atom on the third 5'-dCMP molecule.

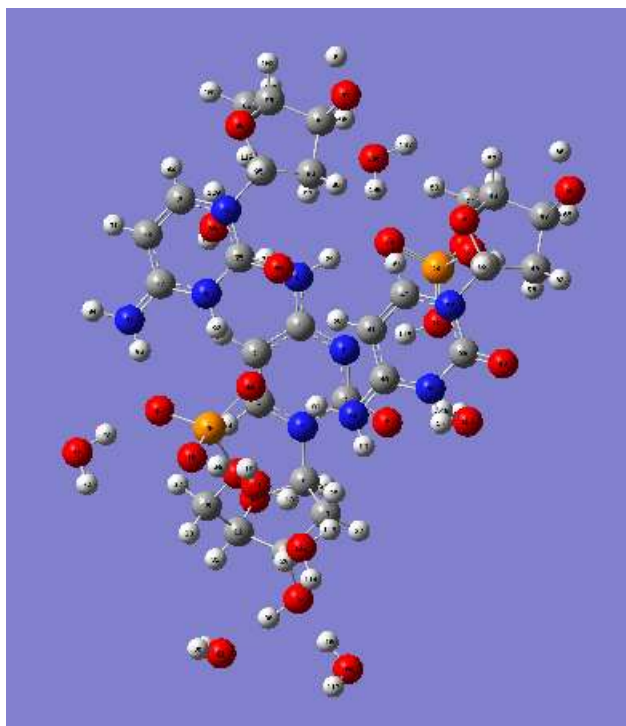


Figure. 37 The major spin density delocalization site in the system of Figure. 34 is removed (using an H atom to replace the third 5'-dCMP's phosphate $-\text{OPO}_3\text{H}^-$ group).

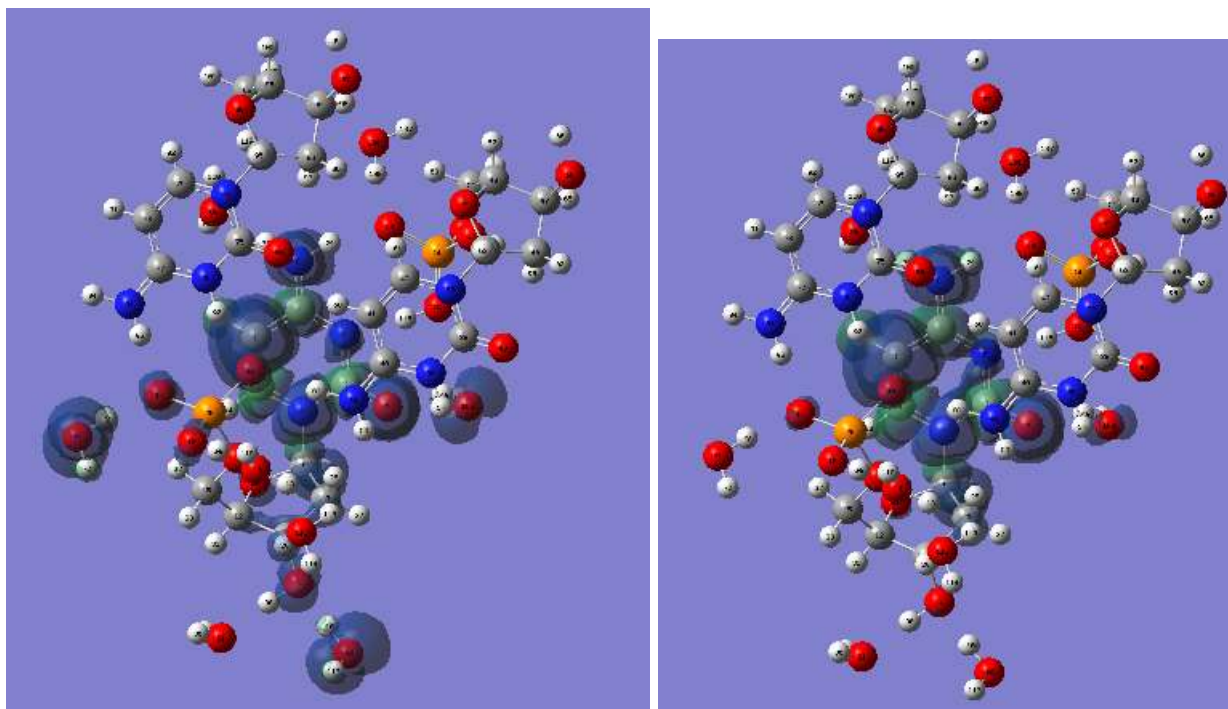


Figure. 38 The calculated spin density distribution on the system shown in Figure. 37, where the radical's geometry and all the H-bond's geometric parameters are extracted from the 5'-dCMP-Opt-1 optimization (isoval=0.0004) (a) Calculated at B3LYP/6-311+g(d,p) level of theory. (b) Calculated at M06-2X/6-311+g(d,p) level of theory.

5'-dCMP	N1	C2	N3	C4	C5	C6	O2	N4	C1'	C2'	C3'	C4'	O4'	O3'	C5'	O5'	OI	OII	OIII	P	W-H...OI	W-H...O2	W-H...O3'
Experiment	0.3				0.6			0.17															
Wetmore			0.24		0.33		0.45																
ub3lyp/6-311+g(d,p)	0.20	-0.06	0.02	-0.05	0.32	-0.04	0.16	0.07	-0.02	0.00	0.01	0.00	0.01	0.02	0.01	0.00	0.01	0.01	0.01	-0.01	0.16	0.06	0.14
um052x/6-311+g(d,p)	0.36	-0.12	0.01	-0.03	0.55	-0.15	0.23	0.14	-0.03	0.02	0.00	0.00	0.00	0.00	0.01	0.00	0.00	0.00	0.01	-0.01	0.00	0.01	0.00
um062x/6-311+g(d,p)	0.37	-0.14	0.01	-0.08	0.61	-0.14	0.26	0.13	-0.04	0.03	0.00	0.00	0.00	0.00	0.01	0.00	0.00	0.00	0.00	0.00	0.00	0.01	0.00

(a)

5'dCMP Sub 22	N1		N3		N4		N4-H1		N4-H2		C5-H		N1-C1'-H		P	
	isotropic	dipolar	isotropic	dipolar	isotropic	dipolar	isotropic	dipolar	isotropic	dipolar	isotropic	dipolar	isotropic	dipolar	isotropic	dipolar
Experiment																
										-6.20		-10.00		-2.40		-2.40
									-12.40	-4.00	-14.50	2.30	-41.20	-1.70	41.90	-2.40
										10.20		12.30		23.10		4.80
Wetmore										-1.30		-1.90		20.40		-3.40
										-0.90	-1.00	0.10	-1.80	-32.90	-1.40	40.60
										2.30		3.70		21.80		4.10
ub3lyp/6-311+g(d,p)										-2.24		-3.74		-11.37		-1.90
	8.41	-8.93	-0.10	-0.25	2.29	-3.01	-4.48	-1.81	-5.06	-1.41	-18.83	-1.57	33.36	-0.46	-5.59	-0.04
		18.13		0.55		6.20		4.05		5.15		12.94		2.36		0.52
um052x/6-311+g(d,p)										-4.37		-7.66		-20.34		-3.07
	20.94	-15.43	-0.65	0.38	8.35	-5.87	-11.11	-3.76	-12.42	-2.82	-40.04	-3.21	46.20	-1.14	-2.06	-0.15
		31.40		0.55		12.08		8.12		10.47		23.55		4.20		0.53
um062x/6-311+g(d,p)										-3.77		-6.56		-19.75		-3.00
	24.90	-14.96	-0.39	0.25	8.83	-4.94	-8.93	-3.21	-10.04	-2.49	-40.78	-3.38	48.68	-1.09	-1.92	-0.14
		30.30		0.39		10.17		6.98		9.06		23.13		4.09		0.41

(b)

Table 43. (a) The calculated Mulliken spin population at the radical and (b) the calculated HFCCs on the system shown in Figure. 37 extracted from 5'-dCMP-Opt-1 optimized geometry.

Chapter 5 Conclusions

The advantages of M05/6-2X functional over B3LYP functional in HFCC calculations are observed when including H-bonding effects. But the advantage of using EPR-II/III basis set over 6-311+g(d,p) basis set in HFCC calculations is not obvious for the tested jobs in the present work of study. For small radicals like the N1-deprotonated cytosine cation radical and the native guanine cation radical, an inclusion of another one or two bases (and extra water molecules if necessary) can allow M05/6-2X functional to produce results that can be rated as “Excellent”. If a local symmetric ionic environment exists for the radical within the crystalline structure (like the chloride ions in the guanine radical case), the complete symmetry pattern need be included in the single point calculations. An incomplete inclusion of the symmetric ionic environment may lead to poorer calculated HFCC results than those calculated without including the ionic components at all. For larger radical systems, like the N3-deprotonated 5'-dCMP cation radical, simulating the H-bonding effects by using water molecules can give excellent iHFCC results at primary HFCC sites using M05/6-2X functional. The real H-bonds environment is needed to reproduce good iHFCC results at secondary HFCC sites. H-bond substitution strategies may be further explored to simulate the electrostatic environment effects in HFCC calculations for large radical systems.

No noticeable spin density delocalization errors are observed for dimer systems including only the deprotonated radical and its protonated counterpart. It is the introduction of a third native neutral molecule into the single point calculation that could give rise to serious delocalization errors for both B3LYP and M05/6-2X functionals. And it is the third molecule the major site of bearing the delocalized spin densities.

Due to the delocalization errors in spin density calculations, the simple idea is not always true that one will always obtain better iHFCC results if the calculation includes more complete environment effects. In order to include a relatively complete environment while avoiding the delocalization errors, a temporary solution may be to substitute the major “delocalization bearing” sites with proper substituents, for example, water molecules, as subjected in the 5'-dCMP case study.

The optimized geometry plays an important role in HFCC calculations. If we consider the geometric effects on the DFT calculation as equivalent to effects of external potential

perturbations, then it may be easier in analyzing the delocalization and static correlation errors in DFT calculations by relating the geometric effects with functional approximations. For large systems, error cancellations become complicated and it is hard to trace different contributions to HFCC calculation errors. The spin density delocalization error roots deeply from the DFT exchange-correlation functional approximations. Further study in improving the expression of DFT exchange-correlation functional is the way to provide fundamental solutions for the accurate hyperfine coupling calculation.

References

1. Close, D. M., Model calculation of radiation induced damage in DNA constituents using density functional theory. In *Computational Chemistry, Review of Current Trends*, Leszczynski, J., Ed. World Scientific: Singapore, 2002; Vol. 8, p in press.
2. Capelle, K., A bird's-eye view of density-functional theory. *Brazilian Journal of Physics* **2006**, 36, 1318-1343.
3. Burke, K., Perspective on density functional theory. *The Journal of Chemical Physics* **2012**, 136, (15), 150901.
4. Cohen, A. J.; Mori-Sánchez, P.; Yang, W., Challenges for Density Functional Theory. *Chemical Reviews* **2011**, 112, (1), 289-320.
5. Cohen, A. J.; Mori-Sánchez, P.; Yang, W., Insights into Current Limitations of Density Functional Theory. *Science* **2008**, 321, (5890), 792-794.
6. Sherrill, C. D., An Introduction to Configuration Interaction Theory. **1995**.
7. Mok, D. K. W.; Neumann, R.; Handy, N. C., Dynamical and Nondynamical Correlation. *The Journal of Physical Chemistry* **1996**, 100, (15), 6225-6230.
8. Carrington, A.; McLachlan, A. D., *Introduction to Magnetic Resonance: With Applications to Chemistry and Chemical Physics*. Harper & Row: New York, 1967.
9. Fau, S.; Bartlett, R. J., Gaussian Basis Sets for Highly Accurate Calculations of Isotropic Hyperfine Coupling Constants at Hydrogen. *The Journal of Physical Chemistry A* **2003**, 107, (34), 6648-6655.
10. Improtà, R.; Barone, V., Interplay of Electronic, Environmental, and Vibrational Effects in Determining the Hyperfine Coupling Constants of Organic Free Radicals. *Chemical Reviews* **2004**, 104, (3), 1231-1254.
11. Chipman, D. M., The spin polarization model for hyperfine coupling constants. *Theoretical Chemistry Accounts: Theory, Computation, and Modeling (Theoretica Chimica Acta)* **1992**, 82, (1), 93-115.
12. Liang, L.; Rassolov, V. A., Fermi Contact Spin Density Calculations of Aromatic Radicals†. *The Journal of Physical Chemistry C* **2010**, 114, (48), 20648-20658.
13. Barone, V., Structure, Magnetic Properties and Reactivities of Open-Shell Species From Density Functional and Self-Consistent Hybrid Methods. In *Recent Advances in Density Functional Methods, Part I*, Chong, D. P., Ed. World Scientific Publishing Co. Pte. Ltd. : Singapore, 1995; Vol. Recent Advances in Computational Chemistry - Vol. 1, pp 287-334.
14. Hiller, J.; Sucher, J.; Feinberg, G., New techniques for evaluating parity-conserving and parity-violating contact interactions. *Physical Review A* **1978**, 18, (6), 2399-2411.
15. Rassolov, V. A.; Chipman, D. M., New operators for electronic density calculation. I. Derivations and formal analysis. *The Journal of Chemical Physics* **1996**, 105, (4), 1470-1478.
16. Wetmore, S. D.; Boyd, R. J.; Eriksson, L. A., Comparison of Experimental and Calculated Hyperfine Coupling Constants. Which Radicals are Formed in Irradiated Guanine? *J. Phys. Chem. B* **1998**, 102, 9332-9343.
17. Wetmore, S. D.; Himo, F.; Boyd, R. J.; Eriksson, L. A., Effects of ionizing radiation on crystalline cytosine monohydrate. *J. Phys. Chem. B* **1998**, 102, 7484-7491.
18. Wetmore, S. D.; Boyd, R. J.; Eriksson, L. A., Radiation products of thymine, 1-methylthymine, and uracil investigated by density functional theory. *J. Phys. Chem. B* **1998**, 102, 5369-5377.

19. Wetmore, S. D.; Boyd, R. J.; Eriksson, L. A., Theoretical Investigation of Adenine Radicals Generated in Irradiated DNA Components. *J. Phys. Chem. B* **1998**, 102, 10602-10614.
20. Close, D. M., Model Calculations of Radiation Induced Damage in DNA Constituents Using Density Functional Theory. In *Computational Chemistry: Reviews of Current Trends*, Leszczynski, J., Ed. World Scientific: Singapore, 2003; Vol. 8.
21. Zhao, Y.; Truhlar, D. G., Design of Density Functionals That are Broadly Accurate for Thermochemistry, Thermochemical Kinetics, and Nonbonded Interactions. *J. Phys. Chem. A* **2005**, 109, 5656-5667.
22. Zhao, Y.; Schultz, N. E.; Truhlar, D. G., Design of Density Functionals by Combining the Method of Constraint Satisfaction with Parametrization for Thermochemistry, Thermochemical Kinetics, and Noncovalent Interactions. *Journal of Chemical Theory and Computation* **2006**, 2, (2), 364-382.
23. Zhao, Y.; Truhlar, D. G., A new local density functional for main-group thermochemistry, transition metal bonding, thermochemical kinetics, and noncovalent interactions. *The Journal of Chemical Physics* **2006**, 125, (19), 194101.
24. Pauwels, E.; Van Speybroeck, V.; Waroquier, M., Evaluation of Different Model Space Approaches Based on DFT to Examine the EPR Parameters of a Radiation-Induced Radical in Solid-State α -Glycine. *The Journal of Physical Chemistry A* **2004**, 108, (51), 11321-11332.
25. O'Malley, P. J., Hybrid Density Functional Study of the p-Benzosemiquinone Anion Radical: The Influence of Hydrogen Bonding on Geometry and Hyperfine Couplings. *The Journal of Physical Chemistry A* **1997**, 101, (35), 6334-6338.
26. Jeffrey, G. A.; Kinoshita, Y., The crystal structure of cytosine monohydrate. *Acta Crystallographica* **1963**, 16, (1), 20-28.
27. Sagstuen, E.; Hole, E. O.; Nelson, W. H.; Close, D. M., Protonation state of radiation-produced cytosine anions and cations in the solid state: EPR/ENDOR of cytosine monohydrate single crystals x-irradiated at 10 K. *The Journal of Physical Chemistry* **1992**, 96, (21), 8269-8276.
28. Sagstuen, E.; Hole, E. O.; Nelson, W. H.; Close, D. M., Protonation state of radiation-produced cytosine anions and cations in the solid state: EPR/ENDOR of cytosine monohydrate single crystals x-irradiated at 10 K. *J. Phys. Chem.* **1992**, 96, (21), 8269-76.
29. McConnell, H. M.; Heller, C.; Cole, T.; Fessenden, R. W., Radiation damage in organic crystals. I. CH(COOH)₂ in malonic acid. *J. Amer. Chem. Soc.* **1960**, 82, 766-775.
30. Rowlands, J. R., The electron spin resonance spectrum of NH(SO₃⁻) in γ -irradiated potassium sulphamate. *Molecular Physics* **1962**, 5, (6), 565-571.
31. Broomhead, J., The structures of pyrimidines and purines. IV. The crystal structure of guanine hydrochloride and its relation to that of adenine hydrochloride. *Acta Crystallographica* **1951**, 4, (2), 92-100.
32. Maixner, J.; Zachova, J., Redetermination of the structure of guanine hydrochloride monohydrate. *Acta Crystallographica Section C* **1991**, 47, (11), 2474-2476.
33. Close, D. M.; Sagstuen, E.; Nelson, W. H., ESR study of the guanine cation. *J. Chem. Phys.* **1985**, 82, (9), 4386-8.
34. Viswamitra, M. A.; Reddy, B. S.; Lin, G. H. Y.; Sundaraligam, M., Stereochemistry of nucleic acids and their constituents. XVII. Crystal and molecular structure of deoxycytidine 5'-phosphate monohydrate. Possible puckering for the furanoside ring in B-deoxyribonucleic acid. *Journal of The American Chemical Society* **1971**, 93, (18), 4565-4573.

35. Close, D. M.; Hole, E. O.; Sagstuen, E.; Nelson, W. H., EPR and ENDOR Studies of X-Irradiated Single Crystals of Deoxycytidine 5'-Phosphate Monohydrate at 10 and 77 K. *J. Phys. Chem. A* **1998**, 102, (34), 6737-6744.
36. Emerson, J.; Sundaralingam, M., Zwitterionic character of guanosine 5'-monophosphate (5'-GMP): redetermination of the structure of 5'-GMP trihydrate. *Acta Crystallographica Section B* **1980**, 36, (6), 1510-1513.
37. Frisch, M. J. T., G. W.; Schlegel, H. B.; Scuseria, G. E.; Robb, M. A.; Cheeseman, J. R.; Scalmani, G.; Barone, V.; Mennucci, B.; Petersson, G. A.; Nakatsuji, H.; Caricato, M.; Li, X.; Hratchian, H. P.; Izmaylov, A. F.; Bloino, J.; Zheng, G.; Sonnenberg, J. L.; Hada, M.; Ehara, M.; Toyota, K.; Fukuda, R.; Hasegawa, J.; Ishida, M.; Nakajima, T.; Honda, Y.; Kitao, O.; Nakai, H.; Vreven, T.; Montgomery, Jr., J. A.; Peralta, J. E.; Ogliaro, F.; Bearpark, M.; Heyd, J. J.; Brothers, E.; Kudin, K. N.; Staroverov, V. N.; Kobayashi, R.; Normand, J.; Raghavachari, K.; Rendell, A.; Burant, J. C.; Iyengar, S. S.; Tomasi, J.; Cossi, M.; Rega, N.; Millam, J. M.; Klene, M.; Knox, J. E.; Cross, J. B.; Bakken, V.; Adamo, C.; Jaramillo, J.; Gomperts, R.; Stratmann, R. E.; Yazyev, O.; Austin, A. J.; Cammi, R.; Pomelli, C.; Ochterski, J. W.; Martin, R. L.; Morokuma, K.; Zakrzewski, V. G.; Voth, G. A.; Salvador, P.; Dannenberg, J. J.; Dapprich, S.; Daniels, A. D.; Farkas, Ö.; Foresman, J. B.; Ortiz, J. V.; Cioslowski, J.; Fox, D. J. *Gaussian 09*, Revision A.1; Gaussian, Inc.: Wallingford CT, 2009.
38. Malkin, V. G.; Malkina, O. L.; Eriksson, L. A.; Salahub, D. R., Theoretical and Computational Chemistry: Vol. 2, Modern Density Functional Theory-A Tool for Chemistry. In Politzer, P.; Seminario, J. M., Eds. Elsevier: Amsterdam, 1995; pp 273-346.
39. Barone, V., Recent Advances in Density Functional Theory. In Chong, D. P., Ed. World Scientific: Singapore, 1995; Vol. 1, pp 287-334.
40. Jeffrey, G. A.; Kinoshita, Y., The crystal structure of cytosine monohydrate. *Acta Cryst* **1963**, 16, 20-28.
41. Viswamitra, M. A.; Reddy, B. S.; Lin, G. H.-Y.; Sundaralingam, M., Stereochemistry of nucleic acids and their constituents. XVII. Crystal and molecular structure of deoxycytidine 5'-phosphate monohydrate. A possible puckering for the furanoside ring in B-deoxyribonucleic acid. *J. Am. Chem. Soc.* **1971**, 93, (18), 4565-4573.
42. Close, D. M.; Eriksson, L. A.; Hole, E. O.; Sagstuen, Experimental and Theoretical Investigation of the Mechanism of Radiation-Induced Radical Formation in Hydrogen-Bonded Cocrystals of 1-Methylcytosine and 5-Fluorouracil. *J. Phys. Chem. B* **2000**, 104, (39), 9343-9350.
43. Farkas, O.; Schlegel, H. B., Methods for optimizing large molecules. Part III. An improved algorithm for geometry optimization using direct inversion in the iterative subspace (GDIIS). *Physical Chemistry Chemical Physics* **2002**, 4, (1), 11-15.
44. Stewart, J., Optimization of parameters for semiempirical methods V: Modification of NDDO approximations and application to 70 elements. *Journal of Molecular Modeling* **2007**, 13, (12), 1173-1213.
45. Cerny, J.; Hobza, P., The X3LYP extended density functional accurately describes H-bonding but fails completely for stacking. *Physical Chemistry Chemical Physics* **2005**, 7, (8), 1624-1626.
46. Zhao, Y.; Truhlar, D. G., Density Functionals for Noncovalent Interaction Energies of Biological Importance. *Journal of Chemical Theory and Computation* **2006**, 3, (1), 289-300.

47. Hohenstein, E. G.; Chill, S. T.; Sherrill, C. D., Assessment of the Performance of the M05-2X and M06-2X Exchange-Correlation Functionals for Noncovalent Interactions in Biomolecules. *Journal of Chemical Theory and Computation* **2008**, 4, (12), 1996-2000.
48. Polo, V.; Kraka, E.; Cremer, D., Electron correlation and the self-interaction error of density functional theory. *Molecular Physics* **2002**, 100, (11), 1771-1790.
49. Bartha, F.; Kapuy, O.; Kozmutza, C.; Van Alsenoy, C., Analysis of weakly bound structures: hydrogen bond and the electron density in a water dimer. *Journal of Molecular Structure: THEOCHEM* **2003**, 666-667, (0), 117-122.
50. Zhao, Y.; Truhlar, D., The M06 suite of density functionals for main group thermochemistry, thermochemical kinetics, noncovalent interactions, excited states, and transition elements: two new functionals and systematic testing of four M06-class functionals and 12 other functionals. *Theoretical Chemistry Accounts: Theory, Computation, and Modeling (Theoretica Chimica Acta)* **2008**, 120, (1), 215-241.
51. Bally, T.; Sastry, G. N., Incorrect Dissociation Behavior of Radical Ions in Density Functional Calculations. *The Journal of Physical Chemistry A* **1997**, 101, (43), 7923-7925.
52. Lundberg, M.; Siegbahn, P. E. M., Quantifying the effects of the self-interaction error in DFT: When do the delocalized states appear? *The Journal of Chemical Physics* **2005**, 122, (22), 224103.
53. Martin, J.; Baker, J.; Pulay, P., Comments on the molecular geometry of ferrocene: The dangers of using quantum chemistry programs as black boxes. *Journal of Computational Chemistry* **2009**, 30, (6), 881-883.
54. Mantz, Y. A.; Gervasio, F. L.; Laino, T.; Parrinello, M., Charge Localization in Stacked Radical Cation DNA Base Pairs and the Benzene Dimer Studied by Self-Interaction Corrected Density-Functional Theory. *The Journal of Physical Chemistry A* **2006**, 111, (1), 105-112.
55. Van Lenthe, J. H.; Zwaans, R.; Van Dam, H. J. J.; Guest, M. F., Starting SCF calculations by superposition of atomic densities. *Journal of Computational Chemistry* **2006**, 27, (8), 926-932.
56. Frisch, J. B. F. a. A., *Exploring Chemistry with Electronic Structure Methods* Second ed.; Gaussian, Inc. : Pittsburgh, PA, 15106 USA, 1996.